University of Memphis
University of Memphis Digital Commons

Electronic Theses and Dissertations

1-1-2018

Contribution Towards Ideal Solid Contact Ion-Selective Electrodes: Mechanistic Studies, Optimization, and Characterization

Jennifer Marie Jarvis

Follow this and additional works at: https://digitalcommons.memphis.edu/etd

Recommended Citation
Jarvis, Jennifer Marie, "Contribution Towards Ideal Solid Contact Ion-Selective Electrodes: Mechanistic Studies, Optimization, and Characterization" (2018). *Electronic Theses and Dissertations*. 1894.
https://digitalcommons.memphis.edu/etd/1894

This Dissertation is brought to you for free and open access by University of Memphis Digital Commons. It has been accepted for inclusion in Electronic Theses and Dissertations by an authorized administrator of University of Memphis Digital Commons. For more information, please contact khggerty@memphis.edu.

CONTRIBUTION TOWARDS IDEAL SOLID CONTACT ION-SELECTIVE ELECTRODES: MECHANISTIC STUDIES, OPTIMIZATION, AND CHARACTERIZATION

by

Jennifer Marie Jarvis

A Dissertation

Submitted in Partial Fulfillment of the

Requirements for the Degree of

Doctor of Philosophy

Major: Biomedical Engineering

The University of Memphis

May 2018

Copyright © 2018 Jennifer Marie Jarvis
All rights reserved

DEDICATION

I dedicate this work to my amazing parents, Dale and Mary Jarvis, for their endless love and support. I am so incredibly thankful for you.

ACKNOWLEDGMENTS

I would like to acknowledge a number of people who have helped me get to where I am today and helped to make my graduate school career successful. First and foremost, I need thank my advisor, Dr. Ernő Lindner, for taking a chance on me and for introducing me to the world of chemical sensors. Through his stories and teachings, his obvious passion for the field became my own. He never stopped believing in me and he continued to encourage me when I would stumble and for that, I will be forever grateful. I thank my committee member, Dr. Bradford Pendley, for teaching me priceless skills and for pushing me to think about my future and set goals for myself. I would like to thank Dr. Esra Roan for her continued guidance on my graduate committee and for reminding me to be confident in my abilities. To my committee member, Professor Johan Bobacka, and his lab group at Åbo Akademi University where I spent several amazing months researching, I thank you for sharing your expertise and for making my short time in Finland something I will never forget.

Additionally, I must thank my lab mates – Dr. Marcin Guzinski, Brad Hambly, and Dr. Jim Atherton - for your support and encouragement and for making the lab an enjoyable and productive space. I thank Marcin, additionally, for his invaluable help throughout my studies and his hard work that helped to bring about multiple exciting publications. I am very thankful for the help from Dr. Felio Perez with the SEM and XPS, and the friendship that we formed while anxiously waiting for many experiments to finish. I would also like to thank Melanie James and Hope Clippinger for their moral support and for making paperwork a little less painful and Mark Farrar and Martha Harrell for their encouragement, technical expertise with computers, and for printing

many conference posters for me throughout the years. I also thank John Davison for his electrical engineering support.

Thank you, to my family and friends, for loving me so well. Thank you to my parents, Dale and Mary Jarvis, for the hours spent on the phone laughing, crying, and sometimes sitting in silence, and knowing it was just what I needed. To my brother, Steve Jarvis, for his endless support and willingness to help in whatever way possible, even from hundreds of miles away. I am so thankful for my grandmothers, who called and wrote me so many letters throughout the past six years and to my late grandfathers, who encouraged me throughout my earlier years. I want to thank Corey Holt for continually committing to calm me down before a big meeting, exam, or presentation, even if he thought I was being ridiculous. Additionally, I would like to thank my friends in Memphis who have become my family. Thank you for cheering me on and for helping to make this city my home. Finally, I need to thank my boyfriend, J Pallme, for believing that I could do anything and for celebrating each victory with me, large and small.

PREFACE

This dissertation contains several manuscripts that have been published in peer-reviewed journals. Chapter 3 contains information related to an article entitled "Equilibration time of solid contact ion-selective electrodes", which has been published in *Analytical Chemistry* (2015). Chapter 4 contains information from an article published in *Analytical Chemistry* entitled "PEDOT(PSS) as solid contact for ion-selective electrodes: the influence of the PEDOT(PSS) film thickness on the equilibration times" (2017). Chapter 5 contains information related to an article entitled "Differences in electrochemically deposited PEDOT(PSS) films on Au and Pt substrate electrodes: a quartz crystal microbalance study", which has been published in *Electroanalysis* (2017). The work reported in Chapter 6 is related to an article entitled "Poly(3-octylthiophene) as solid contact for ion-selective electrodes: contradictions and possibilities", which has been published in *Journal of Solid State Electrochemistry* (2016). Chapter 7 contains information related to an article entitled "Solid contact pH sensor without CO_2 interference with a superhydrophobic PEDOT-C_{14} as solid contact: the ultimate "water layer" test" (2017), which was published in *Analytical Chemistry*. The work in this dissertation was supported by the FedEx Institute of Technology through the Sensor Institute of the University of Memphis (SENSORIUM) and Instrumentation Laboratory.

ABSTRACT

Solid contact (SC) ion-selective electrodes (ISEs) utilizing conductive polymers (CPs) as ion-to-electron transducers are plagued with poor potential stability, sensor-to-sensor standard potential reproducibility, and long equilibration times which hinders their use as minimal calibration or calibration-free sensors for clinical diagnostics. Some imperfections in the SC sensor performance are thought to be due to the presence of an undesired water layer beneath the ion-selective membrane; a result of the unsatisfactory hydrophobicity of the CP layer. The time-dependent change in the redox potential of the CP layer is the other major factor. To address these issues, in this work, the benefits of the implementation of highly hydrophobic CP layers with controlled redox potentials are investigated.

ISEs built with PEDOT(PSS) as SC on Au and GC had short equilibration times while those on Pt had sluggish equilibration. These results were among the first to suggest that the substrate electrode|CP interface plays a significant role in the electrochemical behavior of the SC ISE.

Due to the hydrophilicity and hydrogel-like properties of PEDOT(PSS), pH ISEs with PEDOT(PSS) as SC showed significant CO_2 interference, which limits its use as a universal SC. To minimize the CO_2 interference, PEDOT(PSS) was replaced by POT and PEDOT-C_{14}(TPFPhB) as ion-to-electron transducers in SC ISEs. SC ISEs with POT as SC had unacceptable potential reproducibility partly due to the significant light sensitivity of the POT film. However, the performance characteristics of the POT-based sensors were significantly improved through the incorporation of a TCNQ/$TCNQ^{\bullet-}$ redox couple into the POT film along with adjusting the TCNQ/$TCNQ^{\bullet-}$ ratio.

In contrast to the POT-based SC ISEs, electrodes with the superhydrophobic PEDOT-C_{14}(TPFPhB) as SC exhibited short equilibration times, excellent potential stability, and no light sensitivity. In addition, the PEDOT-C_{14}(TPFPhB) film eliminated CO_2 interference, which has been experienced with PEDOT(PSS) as SC. Consequently, the pH sensors with PEDOT-C_{14}(TPFPhB) as SC allow accurate pH determination in whole blood samples with fluctuating CO_2 levels. In summary, the data collected with PEDOT-C_{14}(TPFPhB)-based SC K^+, Na^+, and pH sensors suggest that PEDOT-C_{14}(TPFPhB) may be the ideal SC for SC ISEs which may lead to ISEs requiring minimal to no calibration.

TABLE OF CONTENTS

LIST OF TABLES

LIST OF FIGURES

KEYS TO SYMBOLS OR ABBREVIATIONS

Abbreviation	Meaning	Page
a_i	ion activity	2
Δf	change in frequency	73
AFM	atomic force microscopy	9
Ag|AgCl	silver|silver chloride	3
Au	gold	3
Au:Pd	gold:palladium	73
c_i	ion concentration	2
Ca^{2+}	calcium ion	1
CO_2	carbon dioxide	4
CP	conductive polymer	5
CV	cyclic voltammetry	85
CWE	coated wire electrode	4
DI	deionized	12
E	potential	2
E^0	standard potential	2
$E^{0'}$	formal potential	2
EQCM	electrochemical quartz crystal microbalance	69
FTIR-ATR	Fourier transform infrared spectroscopy-attenuated total reflectance	84
GC	glassy carbon	3
IFS	inner filling solution	2
IMFP	inelastic mean free path	62

ISE	ion-selective electrode	1
ISM	ion-selective membrane	2
K^+	potassium ion	1
KCl	potassium chloride	12
LiOAc	lithium acetate	13
mV	millivolts	3
Na^+	sodium ion	1
NaCl	sodium chloride	12
OCP	open circuit potential	162
PEDOT-C_{14}(TPFPhB)	poly(2-n-tetradecyl-2,3-dihydrothieno-[3,4b] [1,4]dioxine):(tetrakis(pentafluorophenyl) borate)	5
PEDOT(PSS)	poly(3,4-ethylenedioxythiophene) (polystyrenesulfonate)	5
POT	poly(3-octylthiophene)	5
Pt	platinum	3
QCM	quartz crystal microbalance	9
SC	solid contact	3
S.D.	standard deviation	24
SEM	scanning electron microscopy	9
SR-XPS	synchrotron radiation-X-ray photoelectron spectroscopy	9
WCA	water contact angle	5
XPS	X-ray photoelectron spectroscopy	9

CHAPTER 1

INTRODUCTION

Ion-selective electrodes (ISEs) are valuable tools used to measure the concentration of ions in medical and environmental applications. These chemical sensors are the analytical technique of choice in a variety of applications due to their small size, portability, low cost, and low energy consumption [1]. In clinical diagnostics, they are used to determine the pH and the concentrations of e.g., K^+, Na^+, Ca^{2+} ions in whole blood, serum, saliva, etc. These ions are essential in the metabolic and homeostatic functions of the body including the nerve signal conduction, muscle contraction, and maintenance of acid-base equilibrium [2]. In healthy individuals, physiological ion concentration levels are tightly regulated. Therefore, any deviation from the normal concentration ranges can be an indication of a disease or an irregular physiological condition. For example, K^+ concentrations outside the normal serum concentration range (3.5 - 5 mM), i.e., hypokalemia ($c_{K+} < 3.5$ mM) or hyperkalemia ($c_{K+} > 5$ mM), may result in various degrees of impaired muscular contraction and cardiac arrhythmias, depending on the severity [2]. For the diagnosis and management of hypo- and hyperkalemia, physicians utilize ISEs. Patients whose blood electrolyte levels require monitoring would benefit from a simple at-home test. Such a test for the measurement of ion concentrations in whole blood by non-professionals is not yet realized. The difficulties will be discussed below.

The analytical method in which ISEs are utilized for the measurement of ion concentrations is known as potentiometry. In potentiometry, the potential difference between the ISE and a reference electrode (RE) is measured in a sample solution (e.g.

whole blood) [3]. The correlation between the measured potential (cell voltage) (E) and ion concentration (c_i) is described by the Nernst equation (Eq. 1.1-1.4). In this equation, E^0 is the standard potential of the electrochemical cell, a_i is the activity of the primary ion (i.e. the ion being measured), γ_i is the activity coefficient, R is the universal gas constant (8.314 J/K mol), T is the absolute temperature (298 K at room temperature or 310 K at body temperature), z is the charge of the ion (in the case of K^+, z = 1), and F is the Faraday constant (96485 C/mol). Though E is originally related to a_i, as shown in Eq. 1.1, it can be seen through Eq. 1.2-1.4 that this can be written instead in terms of c_i. The clinically relevant information is given as a concentration so the Nernst equation is often modified to reflect the relationship between E and c_i, as shown in Eq. 1.4. In this equation, $E^{0\prime}$ is the formal potential and is assumed to be constant.

$$E = E^0 + \frac{RT}{zF} ln a_i \tag{1.1}$$

$$E = E^0 + \frac{RT}{zF} ln \gamma_i c_i \tag{1.2}$$

$$E = E^0 + \frac{RT}{zF} ln \gamma_i + \frac{RT}{zF} ln c_i \tag{1.3}$$

$$E = E^{0\prime} + \frac{RT}{zF} ln c_i \tag{1.4}$$

Conventional ISEs contain an ion-selective membrane (ISM) sandwiched between a sample solution and an inner filling solution (IFS), which is involved in the ion-to-electron transduction. A cross sectional figure of a conventional ISE is shown on the left-hand side of Figure 1.1. The IFS makes the utilization of conventional ISEs in certain applications challenging. For example, measuring small sample volumes requires miniaturized ISEs and simply decreasing the volume of the IFS to miniaturize the sensor brought along unexpected disadvantages for the once robust ISEs [4].

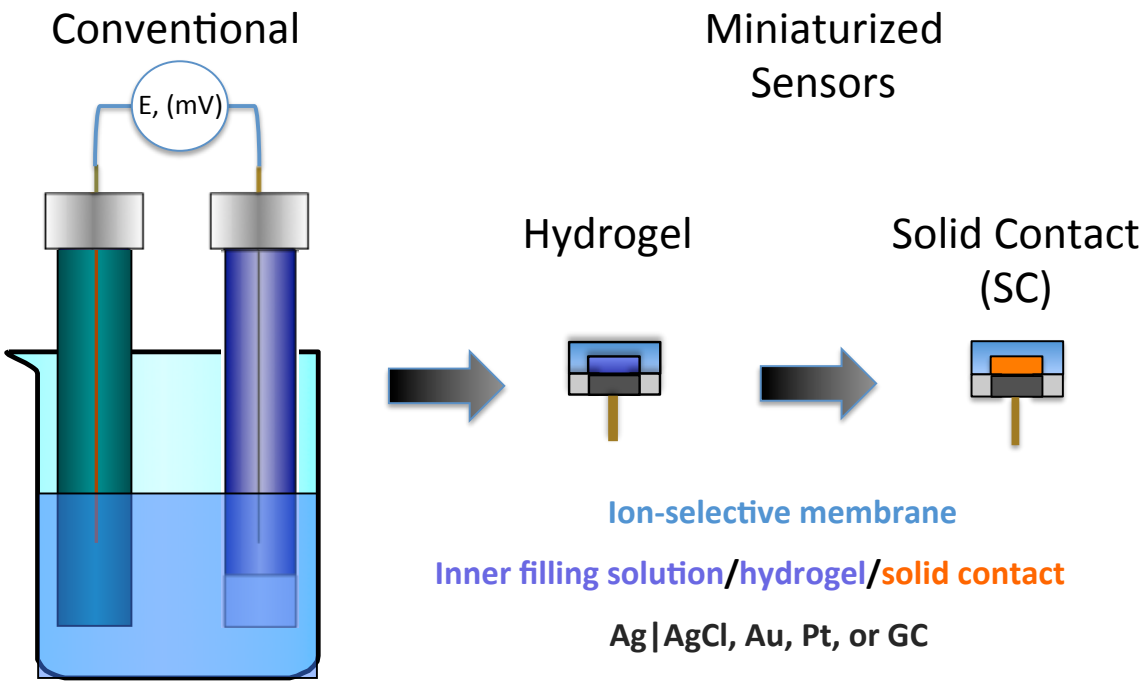

Figure 1.1. Schematic cross-sectional figures of ISEs including a conventional ISE in a beaker with a reference electrode (far left), a miniature hydrogel-based ISE (middle), and a solid contact ISE (right).

Initial works to miniaturize ISEs involved the reduction of the volume and the complete removal of the IFS. ISEs without an IFS are termed as coated wire electrodes (CWEs), in which the ISM is deposited directly on top of an electron-conducting substrate (e.g. Au, Pt, or glassy carbon, denoted as GC) [5]. CWEs have poor potential stability and sensor-to-sensor reproducibility, which is attributed to a blocked interface between the ion-conducting ISM and the electron-conducting substrate. Sensors with inadequate potential stability and sensor-to-sensor potential reproducibility require frequent calibrations; a significant disadvantage compared to conventional ISEs.

ISEs with reduced IFS volume, hydrogel-based ISEs (Figure 1.1, middle), maintain the ion-to-electron transduction present in conventional ISEs. However, the ISEs with hydrogel inner contact were sensitive to transport of water and small neutral molecules (e.g., CO_2) across the ISM [1]. These ISEs require a long equilibration process, which is a disadvantage in certain applications (e.g. single-use or at-home sensors and short turnaround time (STAT) point of care testing (POCT) devices). The need for simple, robust, single-use ISEs for on-site and at-home measurements, as well as for long-term monitoring of ion concentrations is the drive behind the significant efforts for the development of calibration-free ISEs that have short equilibration times and negligible potential drift [1, 4, 6].

To improve the performance characteristics of CWEs, and address the concerns with hydrogel-based ISEs, various materials with ion-to-electron transduction properties were sandwiched between the electron-conducting substrate and the ion-sensing membrane. The new ion sensors are called solid contact ISEs (SC ISEs) (Figure 1.1, right). The role of the solid contact (SC) layer is to provide well-defined interfacial

potentials between the substrate electrode and the ISM. The materials used as solid contact layers include self-assembled monolayers (SAMs) [7], organic compounds [8], special carbon materials [9], and conductive polymers (CPs). In this dissertation, various CPs were studied as SCs to understand the role of the CP|substrate and CP|membrane interfaces on the equilibration time, potential drift, and standard potential reproducibility of SC ISEs. To reveal the importance of the CP hydrophobicity on the responses of SC ISEs, CPs with significantly different water contact angles (WCAs) were tested as SCs (PEDOT(PSS)[1] (55°), POT[2] (103°), and PEDOT-C_{14}(TPFPhB)[3] (136°)) and the performance characteristics of the corresponding SC ISEs were compared. The chemical structures of these CPs are shown in Figure 1.2.

[1] poly(3,4-ethylenedioxythiophene):poly(4-styrenesulfonate)

[2] poly(3-octylthiophene)

[3] poly(2-n-tetradecyl-2,3-dihydrothieno-[3,4-b][1,4]dioxine):(tetrakis(pentafluorophenyl) borate)

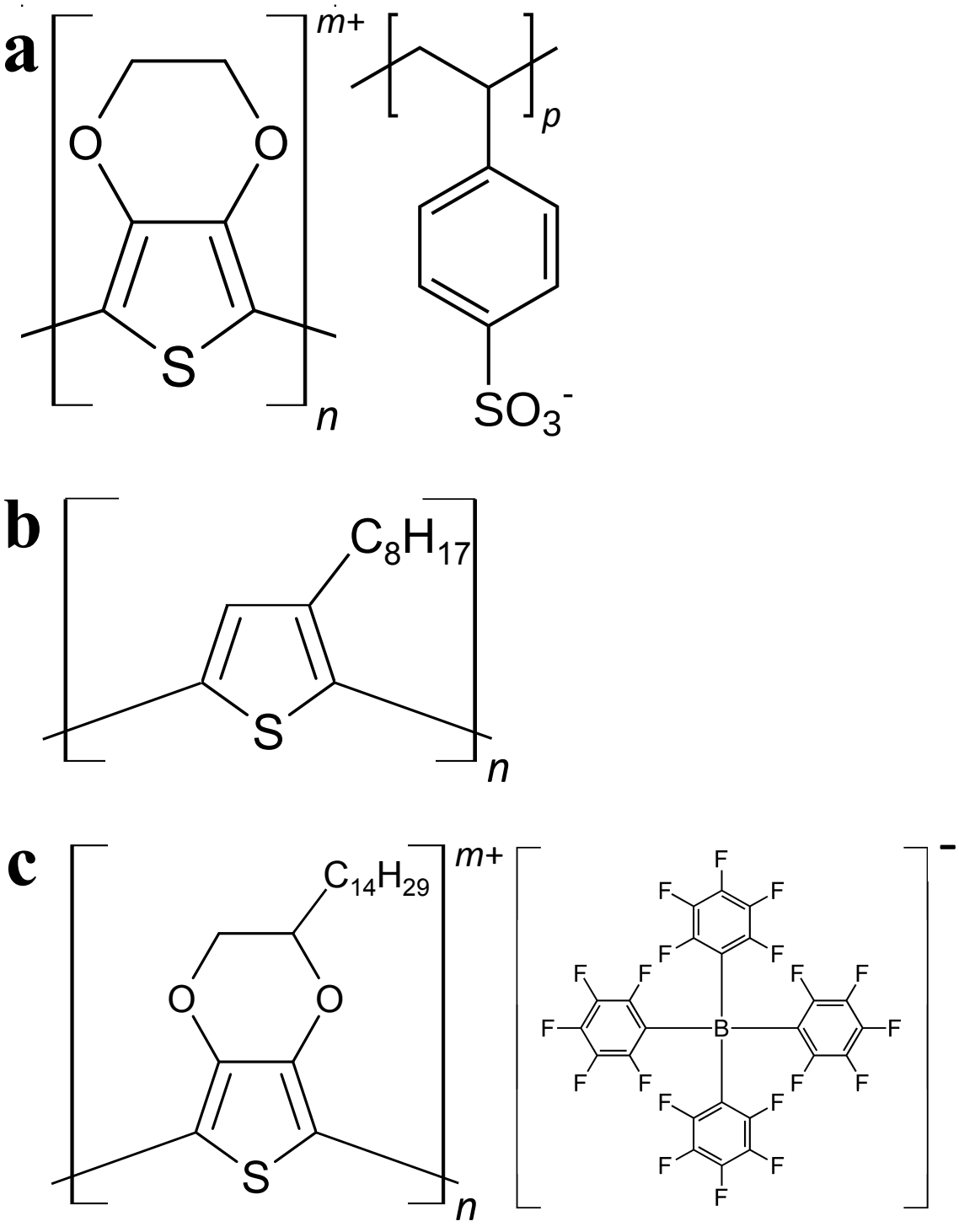

Figure 1.2. Chemical structures of (a) PEDOT(PSS), (b) POT*, and (c) PEDOT-C_{14}(TPFPhB). *The counter anion used during polymerization of POT (Sigma Aldrich) was not obtainable due to proprietary information.

Despite decades of research, SC ISEs with short equilibration time and both excellent potential stability and standard potential reproducibility are still not realized. However, the benefits of hydrophobic SC materials are generally accepted since they deter the formation of a water layer between the SC and the ISM, one of the reasons for poor potential stability of SC ISEs [10, 11]. Once such a water layer is formed under the ISM, the ISE should not be considered a SC ISE. Due to the extremely small volume of such a water layer, even miniscule transport of ions or neutral molecules (e.g. CO_2, NH_3) across the ISM would induce significant concentration changes in the water layer and lead to drifting potentials. The response characteristics of such non-genuine SC ISEs are similar to the responses of ISEs with small volume hydrogel contact (Figure 1.1, middle). Consequently, most new materials tested as SCs in ISEs are highly hydrophobic [11]. In this work, the performance characteristics of ISEs with a highly hydrophobic PEDOT derivative, PEDOT-C_{14}, and POT as SCs (hydrophobic CPs) are compared to the performance of SC ISEs utilizing the hydrophilic PEDOT(PSS) as SC.

CHAPTER 2

SPECIFIC AIMS AND MOTIVATION

The purpose of this work is to understand how the substrate electrode and CP affect the equilibration time, potential stability, and sensor-to-sensor standard potential reproducibility of SC ISEs and to optimize these electrochemical parameters. It is hypothesized that by enhancing these parameters, after decades of research, SC ISEs will become real alternatives of conventional electrodes and will be utilized in a variety of medical applications.

This dissertation focuses on three specific aims:

1) Decrease the equilibration time of SC ISEs.
2) Study the chemical composition and morphology of CP films on different substrate electrodes by surface analytical methods and determine their influence on the equilibration times.
3) Improve the potential stability and sensor-to-sensor standard potential reproducibility of SC ISEs.

This project began after our lab group was approached with a problem related to the long equilibration times of ISEs implemented in critical care whole blood analyzers that are used in hospitals, specifically in intensive care units (ICUs) and emergency rooms. Critical care whole blood analyzers commonly contain a sensor card, comprising over a dozen sensors, each selective for a particular analyte, including ions (ISEs). These analyzers are often used for the initial tests that physicians will run to determine the course of action to be taken regarding the patient's care. Based on the current ISE construction within the sensor card, similar to that represented in Figure 1.1 (middle), the

sensors require approximately 60 minutes of equilibration until they can be used for sample measurement. In a hospital setting, especially in a critical care unit, 60 minutes is too long of a wait time before a decision on patient care can be made.

Specific aim one is related to the reduction of the equilibration times of ISEs from 60 minutes down to 15 minutes. In this effort, we changed the configuration of the ISEs in the sensor card from a hydrogel-based inner contact to a solid contact (SC). The equilibration time is defined as the time it takes for a sensor from its initial contact with solution until it reaches a threshold drift value. In this work, we have arbitrarily set the threshold drift value to 0.3 mV/min to allow for direct comparison of the equilibration times of the various SC ISEs. The equilibration time is discussed in Chapter 3 and Chapter 7.

The second specific aim of this work is related to the utilization of various surface characterization techniques (SEM, SR-XPS, XPS, and AFM) and quartz crystal microbalance (QCM) studies to understand the chemical and morphological differences of the CP films in order to relate them to the electrochemical performance of the SC ISEs. By understanding the correlation between the chemical composition and surface morphology and the electrochemical performance of SC ISEs, we may be able to tune the CP properties for optimal ISE performance. Surface analysis and QCM studies are discussed in Chapters 4 and 5.

The third specific aim of this work is related to the improvement of both the potential stability and sensor-to-sensor standard potential reproducibility of SC ISEs to 0.1 mV/h and ±1 mV, respectively. An SC ISE even with very short equilibration time is of little practical use, particularly for at-home testing, without excellent potential stability and

sensor-to-sensor potential reproducibility, as well. Towards SC ISEs with high stability and good sensor-to-sensor reproducibility, a redox mediator was implemented into the CP-based SC and the oxidized to reduced ratio of the CP and redox mediator was potentiostatically set to achieve a maximum redox buffer capacity. This goal is discussed in Chapter 6.

CHAPTER 3

EQUILIBRATION TIME OF SOLID CONTACT ION-SELECTIVE ELECTRODES

INTRODUCTION

PEDOT(PSS) is considered one of the most successful CPs used in SC ISEs. Though the performance characteristics of PEDOT(PSS)-based SC ISEs were reported in several studies [12-15], no research had been done to determine the equilibration time of this class of sensors. The objective of this study was to characterize the equilibration time of K^+, Na^+, and pH ISEs with PEDOT(PSS) as SC. Since very little information was available in the literature regarding the selection of the substrate electrode and the influence of the substrate electrode on the electrochemical performance of SC ISEs [16], all commonly used substrate electrodes (Au, Pt, and GC) were coated with PEDOT(PSS). To investigate the influence of the substrate electrode on the potentiometric response of SC ISEs, first, we recorded the potential changes of these PEDOT(PSS)-coated Au, Pt, and GC electrodes, with an ISM coating, following their initial contact with aqueous solution and found significant differences in the equilibration times. Since PEDOT(PSS) was deposited under the same conditions (same solutions, same charge) on all three electrode substrates, the significant differences in the transients during the equilibration process suggested that the electrode substrate|PEDOT(PSS) interface plays an important role on the equilibration time. Beyond the equilibration times of fully assembled SC ISEs, we were interested in the role of the individual interfaces and transport processes on the equilibration rate of SC ISEs. To further investigate the equilibration process related to the electrode substrate|PEDOT(PSS) interface, we electrochemically deposited

PEDOT(PSS) onto Au, Pt, and GC electrodes and repeated the equilibration experiments without an ISM coating, i.e., recorded the potential vs. time transients during their equilibration. Again, there were significant differences in the recorded transients, which support the assumption that the electrode substrate|PEDOT(PSS) interface has a significant influence on the electrochemical behavior of SC ISEs.

EXPERIMENTAL

Chemicals

All chemicals used for the ISM preparation, i.e., poly(vinyl chloride) (PVC, high molecular weight), bis(2-ethylhexyl) sebacate (DOS), potassium tetrakis(*p*-chlorophenyl)borate (KTpClPB), sodium tetrakis[3,5-bis(1,1,1,3,3,3-hexafluoro-2-methoxy-2-propyl)phenyl]borate trihydrate (NaTHFPB), sodium ionophore X (4-tert-Butylcalix[4]arene-tetraacetic acid tetraethyl ester), potassium ionophore I (Valinomycin), hydrogen ionophore I (tridodecylamine, TDDA) and tetrahydrofuran (THF) were purchased from Sigma Aldrich. For the electrochemical polymerization of PEDOT(PSS), we used 3,4-ethylenedioxythiophene (EDOT) from Sigma-Aldrich and poly(sodium 4-styrenesulfonate) (NaPSS) from Acros Organics. The aqueous solutions were prepared with 18.2 MΩcm resistivity deionized (DI) water from Millipore Mili-Q A10 system. The potentiometric responses of the solid contact electrodes were tested using citrate-phosphate universal buffer solutions (pH electrodes), KCl, and NaCl standard solutions (K^+ and Na^+ electrodes) prepared by serial dilution and in blood serum-like electrolyte solution BSE-1 and BSE-2 (pH, K^+, and Na^+ electrodes). The pH 7.384 BSE-1 solution contained 140 mM Na^+, 5 mM K^+, 1 mM Ca^{2+}, and 119 mM Cl^-.

The pH 6.840 BSE-2 solution contained 100 mM Na^+, 2 mM K^+, 3 mM Ca^{2+}, and 81 mM Cl^-.

Electrodes and apparatus

The potentiometric measurements were performed at room temperature using a 16-channel high input impedance data acquisition system (Lawson Lab, Malvern, PA), which has been connected to computer equipped with the EMF Suite version 2.0 program. As a reference electrode, an Orion model 900200 double junction Ag|AgCl reference electrode (Thermo Scientific, USA) was used with 3 M KCl and 0.1 M LiOAc as inner and outer filling solutions, respectively. The solid contact electrodes were built on commercially available 3 mm diameter glassy carbon, 1.6 mm diameter gold and 1.6 mm diameter platinum BASi electrodes (Bioanalytical System, Inc. USA). The outer diameter of the BASi electrodes was 6.4 mm. In addition to the commercial electrodes, we also used homemade glassy carbon electrodes in which 1.0 mm diameter glassy carbon rods were secured in 9.8 mm diameter PVC electrode bodies. The glassy carbon rod for the homemade electrodes was purchased from CH Instruments, Inc (USA). For the electrochemical deposition of PEDOT(PSS) over the GC, Au, and Pt substrates, a Reference 600 Potentiostat/Galvanostat (Gamry Instruments, Warminster, PA) was used.

PEDOT(PSS) deposition onto GC, Au, and Pt electrodes

The electrodes were polished stepwise on wet microcloth pads using Al_2O_3-based slurry with gradually decreasing grain sizes (1 μm, 0.3 μm, and 0.05 μm) (Buehler, Lake Bluff, IL). Between the individual polishing steps, the electrodes were rinsed with DI water. The polished electrodes were cleaned by sonication in DI water for 15 min before use. The EDOT solution (0.015 mol/dm^3) was prepared in the deaerated DI water

(saturated with argon for 30 min) and stirred overnight to allow for EDOT to completely dissolve. The appropriate amount of NaPSS was dissolved in the EDOT solution to set its concentration to 0.1 mol/dm^3. PEDOT(PSS) was deposited over the polished electrode surfaces by galvanostatic polymerization in a three-electrode electrochemical cell. The electrochemical cell was filled with deaerated EDOT/NaPSS solution in which a platinum coil and a single junction Ag|AgCl|KCl(0.1M) reference electrode served as auxiliary and reference electrodes, respectively. The electrosynthesis of PEDOT(PSS) was performed at 0.2 mA/cm^2 current density for 714 s [17]. After electropolymerization, the electrodes were rinsed with DI water and left to dry overnight in a solid KOH-filled desiccator.

Table 3.1. Composition of the ion-selective membranes tested in combination with PEDOT(PSS)-based solid contact electrodes

Electrode	Ionophore (wt%)	PVC (wt%)	Plasticizer DOS (wt %)	Ion-exchanger KTpClPB (wt%)
Potassium	potassium ionophore I (2.05)	32.5	65	0.45
Sodium	sodium ionophore X (0.8)	33	66	0.2
Sodium*	sodium ionophore X (0.8)	32.9	65.8	0.5*
Hydrogen	hydrogen ionophore I (1.0)	33.0	65.5	0.5

*NaTHFPB as ion-exchanger

Membrane cocktails and drop-casting

The composition of the ion-selective membranes is provided in Table 3.1. The membrane components (200 mg dry mass) were dissolved in 1.5 mL of THF to prepare a

membrane cocktail for drop-casting. The amount of the drop-cast membrane cocktail was proportional to the surface area of the PEDOT(PSS)-coated electrodes to have membrane coating of very similar thicknesses over the different sizes of electrodes: 5.0 µL for 1.0 mm diameter electrodes, 11.0 µL for 1.6 mm diameter electrodes, and 40.0 µL for 3.0 mm diameter electrodes. After deposition of the membrane cocktails, the electrodes were kept under the protective glass cover for at least 8 hours, i.e., until the complete evaporation of THF.

Measurements of equilibration time

The equilibration times for each electrode were determined twice. In the first experiment, we used freshly prepared electrodes that have never been in contact with an aqueous solution (generally BSE-1 but for Na^+ and K^+ electrodes 0.1 M KCl or 0.1 M NaCl was also used). In the second experiment, we used electrodes that were "hydrated" once but after the "hydration" they were completely dried prior to the second hydration testing to mimic the dry storage conditions of commercial sensors. To dry the electrodes, they were flushed with dry argon gas for 3 minutes and then kept in a solid KOH-filled desiccator for at least 48 hours. The equilibration times were determined from the potential-time transients recorded following the exposure of the electrodes to aqueous solutions (conditioning). In our protocol, the data acquisition started immediately after the freshly prepared or dried electrodes were exposed to BSE-1 solution (t=0 min) and the electrode potentials were recorded for 24 hours. The equilibration time in this work is defined as the time elapsed from the exposure of the electrode to an aqueous solution until the potential drift of the tested electrodes dropped below ±0.3 mV/min and remained

below this threshold value. The equilibration times measured in 0.1 M KCl (K^+ electrodes) or 0.1 M NaCl (Na^+ electrodes) were the same as those measured in BSE-1.

At the end of equilibration, the potentiometric response of the electrodes was tested using BSE-1 and BSE-2 solutions. BSE-1 and BSE-2 were used for equilibration and calibration because the most important application of the Na^+, K^+, and pH electrodes is the analysis of blood electrolytes and these solutions closely match the electrolyte composition of human serum.

RESULTS AND DISCUSSION

Figure 3.1 shows potential vs. time transients that were recorded with K^+-selective SC electrodes following their first exposure to an aqueous solution, i.e., during their initial conditioning or hydration. All three electrodes were freshly prepared and immersed in the same solution (BSE-1) at the same time. The electrodes were prepared with the same PEDOT(PSS) inner contact and the same ion-selective membrane (same composition, same thickness). The only difference between the electrodes was the electron-conducting substrate. As seen in Figure 3.1, the K^+ SC electrode on a Pt substrate had significantly longer equilibration time than the K^+ SC electrodes formed on GC and Au substrates. Very similar transients were recorded by placing the freshly prepared SC ISEs in 0.1 M KCl or 0.001 M KCl solutions.

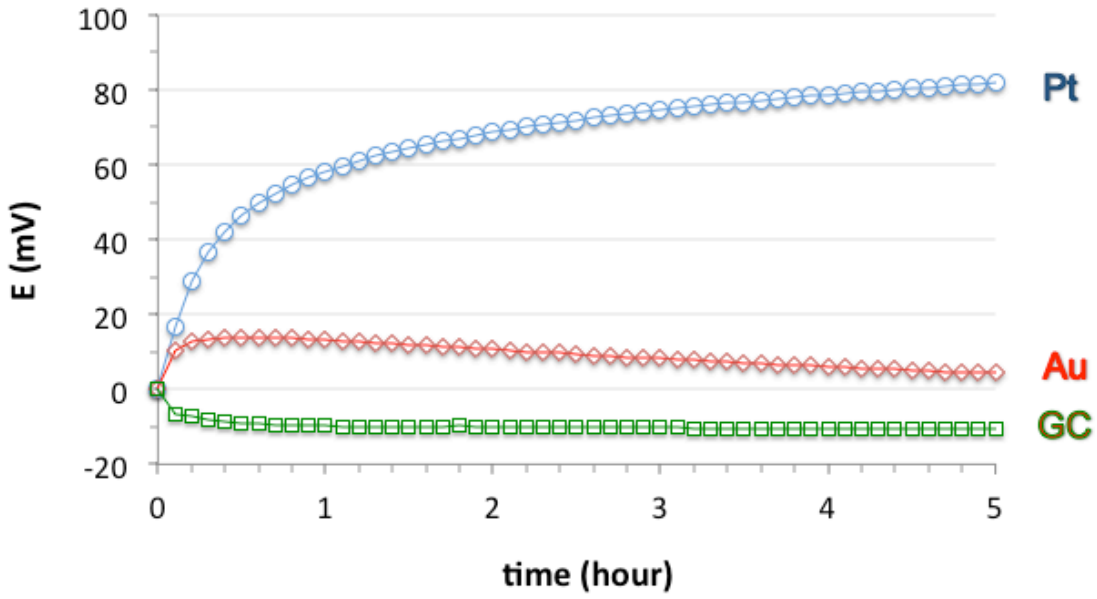

Figure 3.1. Potential-time transients recorded with three freshly prepared solid contact potassium-selective electrodes during conditioning in blood serum-like electrolyte solution (BSE-1). The electrodes had the same ISM and PEDOT(PSS)-based SC. The only difference between the three electrodes was the electron-conducting substrate; i.e., Pt, Au, and GC. For better comparison, the individual transients were shifted along the potential axis to have the same potential at time t=0 (0.0 mV).

After the first equilibration experiment (24 hours long), the SC electrodes were dried (in a solid KOH-filled desiccator for 48 hours) and the equilibration test was repeated. The potential vs. time transients for this 2nd equilibration experiment are shown in Figure 3.2. As it can be seen in Figure 3.2, the significant difference between the transients recorded with the K^+ SC electrodes on Pt, Au, and GC substrates remained. Again, the SC K^+ electrode constructed on the Pt substrate had a much longer equilibration time compared to the electrodes constructed on Au or GC substrates. However, after 24 hours of equilibration, the drifts were very similar.

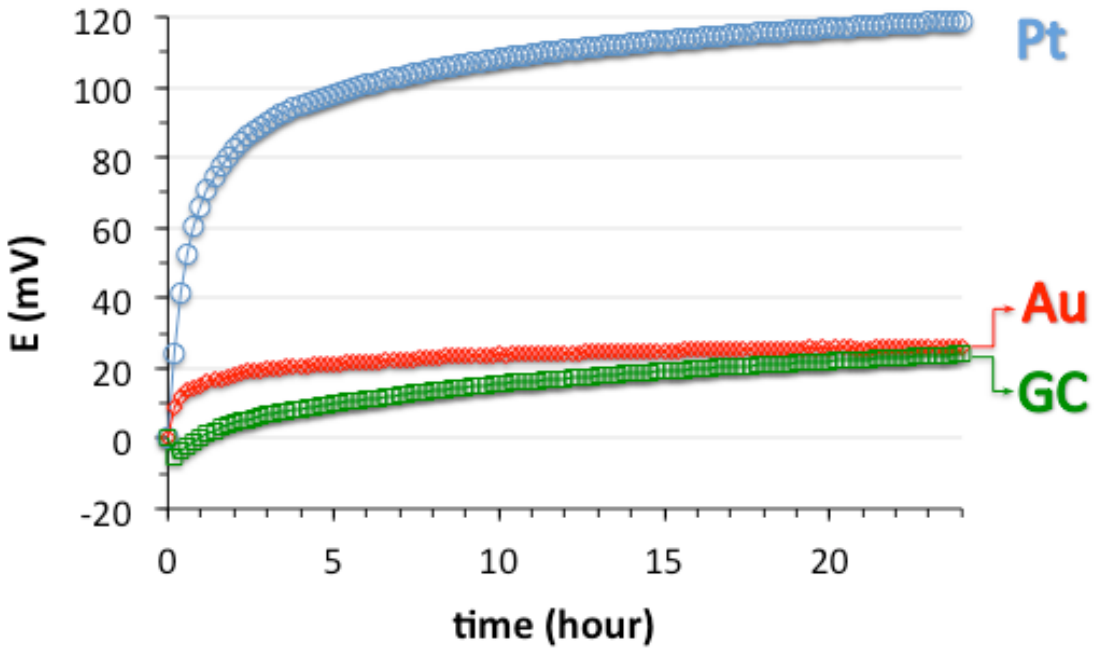

Figure 3.2. The potential transients recorded with SC K^+ ISEs during their 2nd equilibration in blood serum-like electrolyte solution (BSE-1). The electrodes were completely dried prior to this 2nd equilibration. The electrodes had the same ISM and PEDOT(PSS)-based SC. The only difference between the three electrodes was the electron-conducting substrate; i.e., Pt, Au, and GC. For better comparison, the individual transients were shifted along the potential axis to have the same potential at time t=0 (0.0 mV).

In Figure 3.3, we compiled all the equilibration times determined during the 1st and 2nd equlibration experiments with the PEDOT(PSS)-based SC K^+ electrodes. In Table 3.2, we summarized the potential drifts recorded with the same electrodes after 15 minutes, 1 hour, and 2 hours of equilibration. Based on these results, it can be stated that the equilibration times of the electrodes constructed on GC and Au ($\leq$ 10 min) are significantly shorter ($p<<0.001$) than with the SC electrodes constructed on Pt as electrode substrate (~77 min). The relatively large standard deviation (15-20%) in the equilibration times is assumed to be a consequence of slight differences in the membrane thicknesses. Although we tried to make the membranes the same thickness, the deposition of small volumes of highly volatile membrane cocktails over various surface areas by drop-casting limited the attainable reproducibility in the membrane thickness.

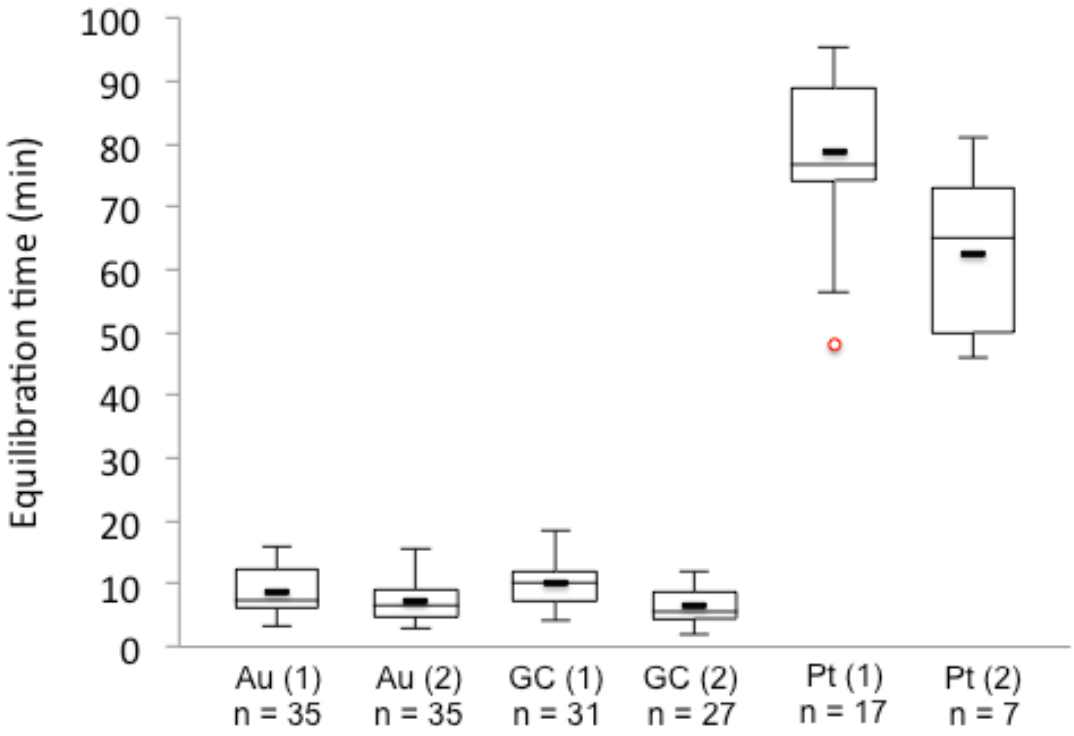

Figure 3.3. Box plot representation of the 1st (1) and 2nd (2) equilibration times measured in BSE-1 solution with PEDOT(PSS^-)-based SC K^+ electrodes built on Au, GC, and Pt substrates. The number of data points used for constructing the individual boxes (n) is indicated below each column. The bottom and top horizontal lines of the boxes represent the 1st and 3rd quartile of the data, respectively. The lines in the middle of the boxes represent median values, while the marks on the whiskers indicate the minimum and maximum equilibration time values in minutes. The short thick horizontal lines within the boxes represent the average values of the equilibration times. The circle below the Pt (1) column (the first hydration times of the electrodes on Pt substrates) represents a medium outlier (a point that is greater than 1.5 times the range of the 1st and 3rd quartiles of data either above the 3rd quartile or below the 1st quartile).

Table 3.2. Drift values of SC K^+-selective electrodes after 15 minutes, 1.0 hour, and 2.0 hours of equilibration in BSE-1 solution during the 1st and 2nd hydration experiments. The electrodes had the same ISM and PEDOT(PSS)-based SC but were prepared on different electron-conducting substrates (i.e. Au, GC, Pt).

	Drift (mV/min)					
	15 min		**1.0 hour**		**2.0 hours**	
Substrate	1st	2nd	1st	2nd	1st	2nd
Au	0.14	0.26	0.04	0.04	0.01	0.03
GC	0.11	0.15	0.04	0.05	0.02	0.02
Pt	1.3	1.7	0.27	0.33	0.14	0.12

To confirm these unexpected findings (shown in Figures 3.1-3.3 and Table 3.3), we performed identical equilibration experiments using SC Na^+ and pH electrodes. The layer structure of the SC Na^+ and pH electrodes was the same as with the K^+ electrodes. The same amount of PEDOT(PSS) was deposited over Pt, Au, and GC substrates; only the composition of the ISMs applied over the PEDOT(PSS) layers was different. The compositions of the membrane cocktails are provided in Table 3.1. The equilibration times compiled for the K^+, Na^+, and pH electrodes are shown in Table 3.3. In complete agreement with our findings with SC K^+ electrodes, the equilibration times for the Na^+ and pH electrodes are short when they are constructed over Au or GC as substrate ($\leq$ 13 min), but they are significantly longer when built over Pt substrate ($\leq$ 76 min). Only the 1st equilibration times for the SC Na^+ ISE on Pt substrate were unexpectedly short (~8

min). However, the 2nd equilibration times of these SC Na^+-selective sensors were again long (~58 min) and similar to the SC K^+ ISEs on Pt substrate.

The equilibration times for the SC Na^+-selective electrodes were determined with two different ISMs over the PEDOT(PSS) conductive polymer layer (Table 3.1); in one of the membranes, KTpClPB, while in the other, NaTHFPB was used as an ion-exchanger. When the ISM is prepared with KTpClPB, the K^+ ions are replaced by Na^+ ions during the 1st conditioning in a diffusion-controlled ion-exchange process. No such ion-exchange is necessary when the membranes are prepared with NaTHFPB. This means, that one may expect shorter 1st equilibration times when the membranes were prepared with NaTHFPB but no difference is expected in the 2nd equilibration times if we assume that all the K^+ ions in the membrane were replaced by Na^+ ions during the first hydration. In agreement with these expectations, the 1st equilibration times for the Na^+ electrodes prepared on Au and GC substrates were shorter when the membranes were prepared with NaTHFPB (Table 3.3). These results suggest that the rate of the K^+ / Na^+ ion-exchange is not negligible compared to other time-dependent processes during the hydration. We do not have a plausible explanation for the differences in the hydration times of the SC Na^+ electrodes made on a Pt substrate.

Table 3.3. Equilibration times measured with PEDOT(PSS)-based SC Na^+, K^+, and pH electrodes in BSE-1 solution. The data in the table are mean values calculated from (n) measurements and are represented with their S.D. The SC Na^+-selective electrodes were tested with two different ISMs: one with KTpClPB as ion-exchanger and another in which NaTHFPB was used (marked with *).

Substrate Electrode	**Equilibration**	**K^+ ISE, min (n)**	**Na^+ ISE, min (n)**	**H^+ ISE, min (n)**
GC	1st	$10._1\pm3._6$ (31)	$10._7\pm1._6$ (5) $6._1\pm1._9$ (5)*	$8._9\pm3._8$ (5)
	2nd	$6._5\pm2._8$ (27)	$5._4\pm2._2$ (5) $11._8\pm0._8$ (5)*	$6._2\pm1._4$ (5)
Au	1st	$8._8\pm3._7$ (35)	$11._1\pm3._2$ (16) $6._2\pm1._4$ (4)*	$11._8\pm3._1$ (16)
	2nd	$7._2\pm3._4$ (35)	$12._5\pm4._4$ (25) $13._2\pm0._8$ (4)*	$8._7\pm2._8$ (18)
Pt	1st	77±13 (18)	$7._8\pm2._8$ (5) 58±8 (5)*	76±12 (5)
	2nd	62±14 (7)	85±7 (5) 64±4 (5)*	82±11 (5)

The significant differences in the equilibration times of PEDOT(PSS)-based SC ISEs prepared on Pt and Au or GC substrates suggest that the processes at the electrode substrate|PEDOT(PSS) interface are rate-determining. To investigate this hypothesis, we have conducted equilibration experiments with PEDOT(PSS)-coated Pt, Au, and GC electrodes without ISM in 0.1 mol/dm^3 KCl. The results are shown in Figure 3.4.

As hypothesized, there were significant differences in the potential vs. time transients. The transients for the PEDOT(PSS)-coated Au and GC electrodes were very similar to each other. Both electrodes approached their equilibrium potential slowly with a large negative potential drift (~ -160 mV in 24 hours). In sharp contrast, the PEDOT(PSS)-coated Pt electrode approached its equilibrium potential quickly with only a small positive potential drift. These results can be understood if we assume that the rate of the potential change is dominated by the equilibration process at the substrate|PEDOT(PSS) interface. All other processes, which may influence the potential vs. time transients (e.g., equilibration of the aqueous solution|PEDOT(PSS) interface and transport in the bulk of the PEDOT(PSS) film) were the same for all three electrodes.

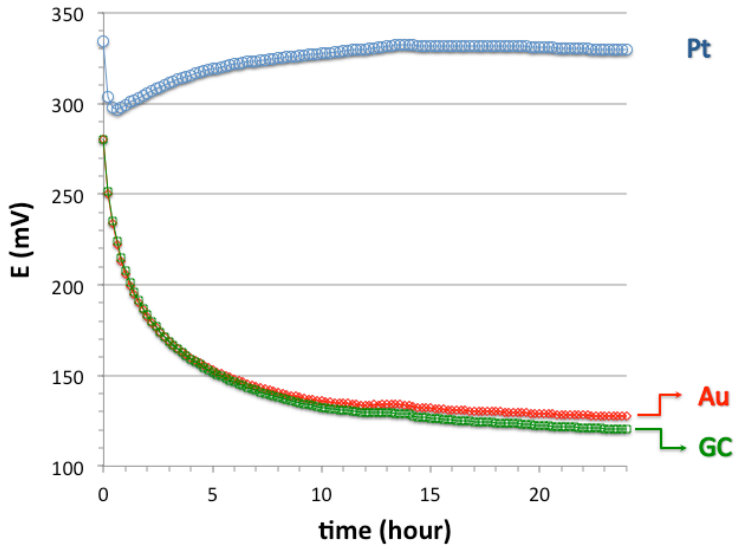

Figure 3.4. The potential-time transients recorded with freshly prepared bare PEDOT(PSS)-coated Pt, Au, and GC electrodes in 0.1 mol/dm^3 KCl. For better comparison, the transient recorded with the Pt electrode was shifted -20 mV along the potential axis.

The results shown in Figure 3.4 can help to deconvolute the individual contributions to the potential-time transients shown in Figures 3.1 and 3.2. The potential of the PEDOT(PSS)-coated Pt electrode (without ISM) rapidly approaches an equilibrium potential when the electrode is exposed to 0.1 M KCl (Figure 3.4). On the other hand, the PEDOT(PSS)-coated GC and Au electrodes approach an equilibrium potential quite slowly following a large negative drift. The potential-time transients recorded with GC|PEDOT(PSS) and Au|PEDOT(PSS) systems are in good agreement with earlier work shown by Vazquez [18] and Wagner [15], although the experimental conditions were quite different. Vazquez [18] recorded the potential transients after 2 minutes of prepolarization at 0.5 V and showed that the prepolarization has a significant effect on

the transients, while Wagner used a drop-cast PEDOT(PSS) ink instead of the electrochemically deposited PEDOT(PSS).

A comparison of the potential drifts recorded by the Pt|PEDOT(PSS) electrode with and without ISM (Figures 3.1 & 3.2 vs. Figure 3.4) suggests that a significant portion of the large positive drift recorded with a Pt|PEDOT(PSS)|ISM construct (Figures 3.1 & 3.2) is due to the ISM itself. However, it appears that this large positive drift induced by the ISM cancels out in combination with the same order of magnitude large negative drift of the PEDOT(PSS)-coated Au and GC electrodes (without ISM) (Figure 3.4). This compensation of the positive (membrane) and negative drifts (Au or GC|PEDOT(PSS)) could explain the fairly constant potential of the K^+-selective electrodes with PEDOT(PSS) SC on Au and GC substrates (Figures 3.1 and 3.2).

To reinforce this interpretation, following the experiment shown in Figure 3.4, the PEDOT(PSS)-coated Pt, Au, and GC electrodes were removed from the KCl solution, rinsed thoroughly with deionized water, dried in a solid KOH-filled desiccator for 48 hours, and coated with a K^+-selective membrane (as described in the experimental section). These membrane-coated electrodes were then placed in 0.1 M KCl solution for recording the potential vs. time transients during equilibration. These curves were very similar to the transients shown in Figures 3.1 & 3.2, which were recorded in BSE-1. Finally, to estimate the contribution of the ISM to the overall drift of the SC ISEs, the potential vs. time transients of the PEDOT(PSS)-coated Pt, Au, and GC electrodes (the transients shown in Figure 3.4) were subtracted from the potential vs. time transients recorded with the same electrodes but with ISM coating (curves similar to those shown in Figures 3.1 & 3.2). The obtained curves are shown in Figure 3.5.

As expected, the traces representing the contribution of the K^+-selective membrane to the overall drift of SC ISEs are similar although they were constructed from the potential vs. time transients of three SC electrodes with significantly different equilibration characteristics. However, to conclude that the traces shown in Figure 3.5 are representing the ISM contribution to the overall drift, one must assume that the potential drift of the substrate|PEDOT(PSS) would be the same after coverage by the ISM. We recognize that this assumption might not be true for two reasons: (1) because the substrate|PEDOT(PSS) construct is in quite a different environment in the two experiments (in aqueous KCl solution or in contact with the highly plasticized polymeric membrane) and (2) because in the SC ISE arrangement, the substrate electrode|PEDOT(PSS) construct becomes in contact with water with a delay related to the water diffusion across the PVC membrane. Consequently, despite the striking similarity of the transients in Figure 3.5, only qualitative conclusions can be drawn; namely that the drift recorded with SC ISEs following their first exposure to an aqueous solution is the consequence of several processes including bulk and interfacial processes in this multilayer system. It is assumed that a significant part of the drift is controlled by transport processes (primarily water transport) within the ISM, the equilibration of the PEDOT(PSS)|ISM interface and the hydration of the PEDOT(PSS) film [19]. The divergence of the transient recorded with the Pt|PEDOT(PSS)|ISM system from the other two traces recorded with similar electrodes but using GC or Au as substrate (especially at longer times, as shown in Figure 3.4 inset) suggests that processes at the substrate|PEDOT(PSS) interface could also be important.

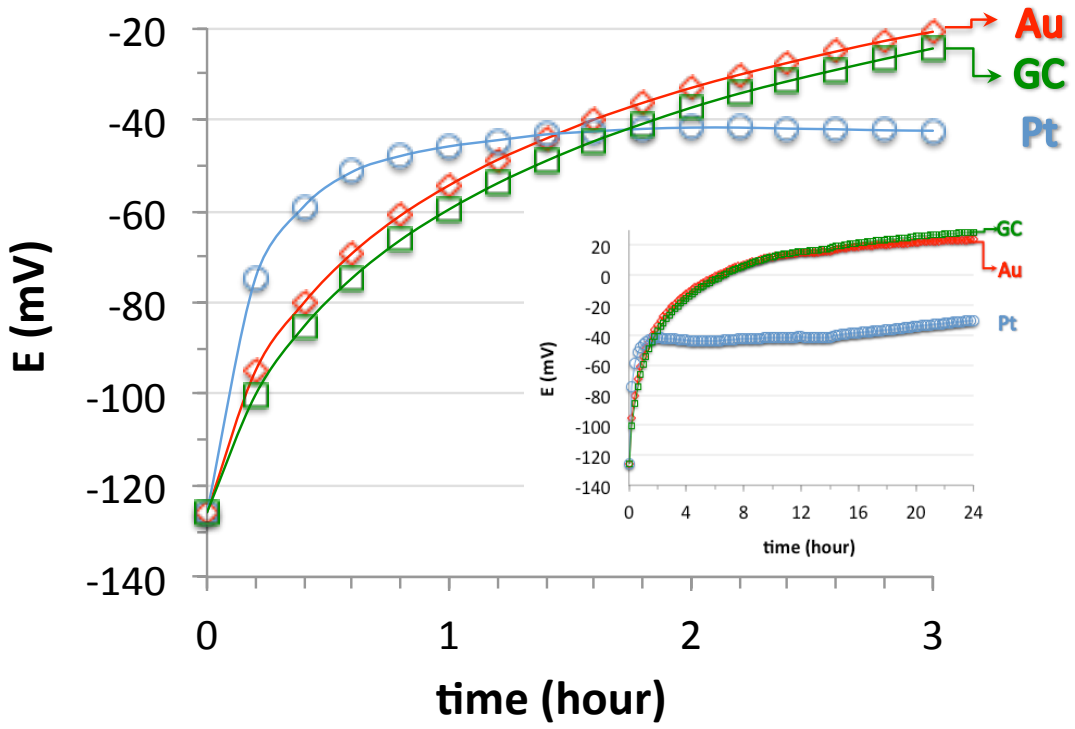

Figure 3.5. The potential vs. time transients of "K^+-selective membranes" following their first contact with an aqueous electrolyte solution shown at two time scales: 3h (full picture) and 24 h (inset). The membranes were cast over dried PEDOT(PSS) films. The traces were constructed by subtracting the potential vs. time transients of PEDOT(PSS)-coated Pt, Au, and GC electrodes (Figure 3.4) from the potential vs. time transients of the same electrodes with a K^+-selective membrane coating.

When a SC ISE is brought into contact with an aqueous solution, the ISM and SC become hydrated. The rate of the hydration is controlled by the diffusion coefficient of water. It appears that a dual-sorption model in which two diffusion coefficients are used to fit the experimental data best describes the water uptake. According to Lindfors, et al. [20] the fast diffusing water ($D=1.9\times10^{-7}$ cm^2/s) can be detected on the back-side of a ~100 μm thick membrane (similar to the membrane thicknesses used in this study) after only 10 minutes of solution contact and reaches saturation level within 2 hours. However, the complete hydration of the membrane may last over 24 hours, which is modeled by slow diffusing water ($D=8.7\times10^{-9}$ cm^2/s). The cause and effect-like correlation of the fast and slow diffusion of water on the potential vs. time transients recorded during the equilibration of SC ISEs has not been confirmed in this work but according to the data shown in this paper, the rate of the potential change is the largest in the first two hours of the hydration of the membrane.

CONCLUSIONS RELATED TO THE EQUILIBRATION TIME OF SC ISEs

Potential vs. time traces were recorded during the equilibration of SC K^+, Na^+, and H^+ ion-selective electrodes with PEDOT(PSS)-based SC. The SC electrodes were built over Pt, Au, and GC substrate electrodes. For ISEs constructed on Pt substrate, the equilibration times were long (> 60 minutes) but were short (between 5 and 13 minutes) with Au and GC as substrate electrodes. Significant differences in the equilibration times of SC ISEs built on different substrate electrodes are reported here for the first time.

By subtracting the potential vs. time transients recorded with PEDOT(PSS)-coated Pt, Au, and GC electrodes (without membrane) from the transients recorded with the SC ISEs (with ISM), the transients recorded with SC ISEs during their equilibration

with an aqueous electrolyte solution could be deconvoluted into two terms: (i) potential drifts at the substrate electrode|PEDOT(PSS) interface; and (ii) potential drifts related to the ISM, including the ISM|PEDOT(PSS) interface. The source of the significant differences in the equilibration times of the SC ISEs was traced back to the equilibration processes at the substrate electrode|PEDOT(PSS) interface.

CHAPTER 4

PEDOT(PSS) AS SOLID CONTACT FOR ION-SELECTIVE ELECTRODES: THE INFLUENCE OF THE PEDOT(PSS) FILM THICKNESS ON THE EQUILIBRATION TIMES

INTRODUCTION

In Chapter 3, we discussed the mechanism of the equilibration process of the multi-layered structure of SC ISEs. As these sensors become hydrated, the bulk and interfacial properties of both the ISM and the ion-to-electron transducer (SC) change, leading to a gradual change in the potential of the SC ISE [10, 21]. Compared to conventional electrodes, in which the ion-selective membrane is sandwiched between the inner filling solutions and the sample solution, the equilibration processes during conditioning of SC ISEs are more complex and tracing the contributions of the individual bulk and interfacial potential changes to the overall potential change of the sensor during conditioning is challenging.

Following the study in Chapter 3, it was assumed that the differences in the equilibration times of SC ISEs fabricated on different substrate electrodes are the result of the compensation of varying positive and negative drifts within the multi-layered sensor structure [22]. To support this explanation and isolate the sources of the differences in the equilibration times of PEDOT(PSS)-based K^+, Na^+, and H^+ electrodes constructed over Pt, Au, and GC substrates [22], we considered the following equilibration processes: (i) at the interface between the metal substrate electrode and PEDOT(PSS) ($\delta\varepsilon_{Metal|PEDOT}$); (ii) within the PEDOT(PSS) layer ($\delta\varepsilon_{diff(PEDOT}$)); (iii) at the interface between PEDOT(PSS) and the ISM ($\delta\varepsilon_{PEDOT|ISM}$); (iv) within the ISM

($\delta\varepsilon_{diff(ISM)}$); and (v) at the ISM and solution interface ($\delta\varepsilon_{ISM|KCl}$) from the first solution contact until complete equilibration (~24h). More so, the substrate|PEDOT(PSS) interface was investigated by using photon energy dependent SR-XPS depth profiling. These methods provided data on the NaPSS to PEDOT ratio of the PEDOT(PSS) layer in close proximity to the substrate electrode surface which is assumed to determine the hydrophilicity of the electrochemically deposited PEDOT(PSS) films and consequently influence the rate of equilibration of SC ISEs. This assumption is supported by the water uptake-related [23-26] potential drifts recorded during the equilibration of the SC electrodes built with different PEDOT(PSS) layer thicknesses on Au, Pt, and GC as substrate electrodes. The influence of the substrate electrode on the hydrophilicity of the PEDOT(PSS)|aqueous solution interface has been studied by water contact angle measurements over 0.1 μm, 1.0 μm, 2.0 μm, and 4.0 μm thick PEDOT(PSS) films coated on Pt, Au, and GC electrodes.

To assess the influence of activity changes in the ISM during its hydration on the overall drift of ISEs, the potential of a sandwich membrane has been recorded. The sandwich membrane has been assembled from one dry and one fully hydrated membrane (this is an adaptation of the sandwich membrane method [27] used to assess the stability constants of ionophore-ion complexes).

EXPERIMENTAL

Chemicals

All chemicals used for preparation of the K^+ ISM cocktail, PEDOT(PSS) deposition, and aqueous solutions can be found in the Experimental section in Chapter 3.

Potentiometric measurements and electrodes

The methods for potentiometric measurements, electrochemical deposition, and details of the electrodes used were previously described in Chapter 3. In the sandwich membrane method experiment, the dry and wet membranes were secured in an IS 561 (Moeller S.A., Zurich, Switzerland) type liquid membrane electrode body.

PEDOT(PSS)-coated Au, GC, and Pt electrodes

The electrodes were polished and prepared as described in Chapter 3. To polymerize PEDOT(PSS) films of different thicknesses (0.1 μm, 1.0 μm, 2.0 μm, and 4.0 μm), the electrolysis was performed at 0.2 mA/cm^2 current density with 72 s, 714 s, 1428 s, and 2856 s electrolysis times, respectively. The thicknesses were confirmed with an Alpha-Step 500 surface profiler (KLA Tencor, Milpitas, CA) for 1.0 μm and 2.0 μm-thick PEDOT(PSS) films.

Upon completing the current application necessary for PEDOT(PSS) polymerization, the resultant voltage that was produced during the current application decays as the PEDOT(PSS)-coated electrode equilibrates in the solution. This decay is the result in a change in the redox state of PEDOT(PSS). To follow these processes in time, the potential-time transients of PEDOT(PSS)-coated Pt, Au, and GC electrodes were recorded for 24 hours (i) immediately after their galvanostatic deposition in the same solution which has been used for the PEDOT(PSS) deposition (0.015 mol/dm^3 EDOT and 0.1 mol/dm^3 NaPSS); (ii) in 0.1 M KCl following a few seconds long rinsing with DI water; as well as (iii) in 0.1 M KCl solution after keeping the rinsed (with DI water) and dried (5 min in Ar stream) electrodes in a KOH-filled desiccator overnight.

Potassium-selective electrodes with PEDOT(PSS) solid contact

The potassium membrane preparation was previously described in Table 3.1 of Chapter 3. The potential vs. time transients of the PEDOT(PSS)-based SC K^+ electrodes over Au, GC, and Pt electrodes were recorded in 0.1 mol/dm^3 KCl solution for 24 h using the same protocol as for the PEDOT(PSS)-coated electrodes.

The modified sandwiched membrane method

Activity coefficients change in the ISM during its hydration and induce changes in the phase boundary potential at the PEDOT(PSS)|ISM and ISM|KCl interfaces and in the diffusion potential within the ISM. To determine the significance of these potential changes in the overall potential drift of a SC ISEs during their equilibration, the sandwich membrane method [27] has been modified.

The ISM cocktail used for drop-casting (200 mg dry mass in 1.5 mL THF) was cast into a glass ring secured on a glass plate. After evaporation of THF, an ~200 μm thick membrane remained on the glass plate. From this membrane, 6.8 mm diameter discs were punched out. Half of these membrane discs were conditioned in 0.1 mol/dm^3 KCl for 24 h while the other half were kept dry. To assemble a sandwich membrane, a fully hydrated and a dry membrane disc were layered over each other. This sandwich membrane was placed into the IS 561 electrode body with 0.1 mol/dm^3 KCl as inner filling solution, and the fully assembled electrode was placed into 0.1 mol/dm^3 KCl solution in combination with a reference electrode. The full procedure, from contacting the two membranes until insertion of the fully assembled electrode into the KCl solution was accomplished in less than 1 min, with the potential recordings commenced immediately after placement of the electrode in solution.

Water contact angle measurements

The completely dry PEDOT(PSS)-coated Pt, Au, and GC electrodes (BASi 3 mm diameter Pt (MF 1012), Au (MF 1002), and GC (MF 1000) electrodes) were placed onto the sample stage of the VCA Optima surface analysis system (AST Products, Inc., Billerica, MA). Next, one droplet of DI water (0.5 μL) was dispensed from a microsyringe onto the PEDOT(PSS) film and the image of the droplet was captured. The contact angles were evaluated from the captured images using the VCA Optima XE goniometry software. The average contact angles were calculated from 4 to 6 measurements performed on the surface of 4 to 6 PEDOT(PSS)-coated electrodes.

XPS surface analysis

XPS analysis of electrochemically polymerized PEDOT(PSS) samples was performed using a Thermo Scientific K-Alpha XPS system equipped with a monochromatic Al K_α X-ray source at 1486.6 eV. The X-ray power of 75 W at 12 kV was used for all experiments with a spot size of 400 μm^2. The base pressure of this instrument was 10^{-9} mbar. The instrument was calibrated to give a binding energy of 84.0 eV for Au $4f_{7/2}$ (also in SR-XPS studies) and 284.6 eV for the C 1s line of adventitious (aliphatic) carbon present on the non-sputtered samples. Photoelectrons were collected from a takeoff angle of 90° relative to the sample surface. The Pt, Au, and GC electrodes (BASi MF 1012, MF 1002 and MF 1000, respectively) coated with 100 nm thick (72 s electrolysis time) electrochemically deposited PEDOT(PSS) were sputtered with an Ar^+ gun to perform a depth profile analysis. A series of XPS spectra at 150 etching-levels were recorded in constant analyzer energy mode. Survey spectra were taken at each level with 200 eV pass energy, while the high resolution core level spectra of C 1s, O 1s, S 2p,

Na 1s, Pt 4f, and Au 4f were taken at a 40 eV pass energy with an energy step size of 0.1 eV using an average of 10 scans. The XPS data acquisition was performed using the "Avantage v5.932" software provided with the instrument.

SR-XPS surface analysis

Ar^+ and photon energy dependent SR-XPS surface analysis of electrochemically deposited PEDOT(PSS) (~100 nm thickness) was performed at the Australian Synchrotron (AS) soft X-ray (SXR) beamline, while photon energy dependent SR-XPS depth profiles of ~10 nm thick PEDOT(PSS) films were measured at both the AS SXR beamline and the Elettra Materials Science beamline (MSB) (Elettra – Synchrotron, Trieste, Italy).

Since the bending magnet Elettra MSB has a diminished beam brilliance and therefore lesser beam-induced damage compared to the high flux undulator SXR beamline at the AS, the Elettra MSB was the beamline of choice for this surface study of PEDOT(PSS).

Ion sputtering and beam induced damage of the PSS^- species in PEDOT(PSS) is highly problematic, as illustrated in the SR-XPS results section. Consequently, photon energy dependent SR-XPS depth profiling of thin films of PEDOT(PSS) at Elettra MSB were essential to the successful completion of this study.

SR-XPS surface analysis at Elettra – Synchrotron MSB

Photon energy dependent SR-XPS depth profiling of the S 2p core level at photon energies of 220, 320, 570, and 970 eV were recorded at the MSB at the Elettra synchrotron light source in Trieste, Italy. The MSB end-station comprises an ultrahigh vacuum instrument (10^{-10} mbar base pressure, and was maintained at 5×10^{-9} mbar or

better during measurements) that is equipped with a Specs Phoibos 150 multichannel electron energy analyzer along with an argon gas inlet and Ar^+ sputtering gun.

SR-XPS at the soft X-ray (SXR) beamline at the Australian Synchrotron (AS)

SR-XPS survey and high-resolution spectra were recorded on the AS SXR beamline in Melbourne, Australia. High-resolution S 2p spectra were recorded at photon energies of 220, 320, 570, 970, and 1487 eV, and all measurements were performed at an angle of 55° with respect to the sample normal. This beamline utilizes an insertion device based on an elliptically polarized undulator providing a flux between 5×10^{11} and 3×10^{12} photons/200 mA at the sample at 400 eV. The optimal energy range of the beamline is between 90 to 2000 eV with a resolution (E/ΔE) of 5,000 to 10,000 and a beam size of 0.6 mm×0.6 mm. The end-station was constructed by OmniVac and PreVac using a SPECS Phobios 150 hemispherical electron energy analyzer in conjunction with photodiode and drain current detectors. The analyzer chamber was maintained at 1×10^{-9} mbar or lower and the storage ring was operated in the decay mode.

Ion sputtering beam-induced damage of the PEDOT(PSS) film on Au was ascertained by sputtering the sample for 90 s (or a depth of 5.5 nm) at 600 V, 5 mA, and 5×10^{-6} mbar of Ar, noting that the sputter rate of this ion gun was previously found to be 3.7±0.4 nm/min [28].

CasaXPS was used to fit Gaussian/Lorentzian peaks together with a Shirley background correction, so as to deconvolute spectra comprising multiple components. Since the effect of photon energy on the Scofield photoabsorption cross-section and asymmetry parameter of the S 2p orbital together with the influence of electron kinetic energy on the spectrometer transmission function and inelastic mean free path of the

photoelectrons are similar on both the PEDOT and PSS components in the S 2p spectra, the ratio of PSS-to-PEDOT peak intensities is equivalent to the mole ratio of PSS-to-PEDOT.

RESULTS AND DISCUSSION

Measurement of the potential drift related to the hydration of an ISM: the modified "sandwich membrane" method

In our previous study [22], we showed that freshly prepared PEDOT(PSS)-coated Au and GC electrodes (half-cell I) had a significant negative potential drift during their equilibration in KCl solutions. Conversely, fully fabricated ISEs with PEDOT(PSS) as solid contact on Au and GC electrodes (half-cell II) had only a slight positive drift during their equilibration. These findings suggested that the negative drift related to PEDOT(PSS) has been compensated by a positive drift related to the ISM. To estimate this drift (see Equation 4.1), the potential transient of half-cell (I) has been subtracted from the potential transient of half-cell (II):

$$Pt, Au, or\ GC|PEDOT(PSS)|0.1\ M\ KCl \quad \text{(I)}$$

$$Pt, Au, or\ GC|PEDOT(PSS)|ISM|0.1\ M\ KCl \quad \text{(II)}$$

$$\Delta E(t) = \Delta E(t)_{half-cell(II)} - \Delta E(t)_{half-cell(I)} \quad (4.1)$$

By considering the individual interfacial and diffusion potential terms in half cells (I) and (II), one can write:

$$\Delta E(t) = \left(\delta\varepsilon_{Metal|PEDOT} + \delta\varepsilon_{diff(PEDOT)} + \delta\varepsilon_{PEDOT|ISM} + \delta\varepsilon_{diff(ISM)} + \delta\varepsilon_{ISM|KCl}\right) - \left(\delta\varepsilon_{Metal|PEDOT} + \delta\varepsilon_{diff(PEDOT)} + \delta\varepsilon_{PEDOT|KCl}\right) \quad (4.2)$$

In Equation 4.2, $\varepsilon_{Metal|PEDOT}$ represents the interfacial potential at the metal|PEDOT(PSS) interface, $\varepsilon_{diff(PEDOT)}$ the diffusion potential in the PEDOT(PSS) film, $\varepsilon_{PEDOT|ISM}$ the interfacial potential at the PEDOT(PSS)|ISM interface, $\varepsilon_{diff(ISM)}$ the diffusion potential in the ISM, $\varepsilon_{ISM|KCl}$ the interfacial potential at the ISM|KCl solution interface, and $\varepsilon_{PEDOT|KCl}$ the interfacial potential at the PEDOT(PSS)|KCl solution interface.

Equation 4.2 can be simplified with the assumption that the $\varepsilon_{Metal|PEDOT}$ and $\varepsilon_{diff(PEDOT)}$ potential terms are the same in half cells (I) and (II):

$$\Delta E(t) = \delta\varepsilon_{PEDOT|ISM} + \delta\varepsilon_{diff(ISM)} + \delta\varepsilon_{ISM|KCl} - \delta\varepsilon_{PEDOT|KCl} \quad (4.3)$$

The first three terms on the right hand side of Equation 4.3 are related to activity changes in the ISM during hydration. To estimate the magnitude of these potential changes, the so-called "sandwich membrane" method [27] has been modified. In the original sandwich membrane method, the potential vs. time transients recorded during the equilibration between an ionophore-loaded and an ionophore-free membrane (sandwich) are used to calculate the stability constants of ionophores in ISMs [27]. In the modified "sandwich membrane" method, a dry and a fully hydrated membrane with the same composition are layered upon each other. Upon assembling the sandwich, the originally dry side of the sandwich becomes hydrated until equilibrium is achieved. The potential transient recorded during the hydration of the "sandwich" is a consequence of activity changes within the dry membrane until it becomes fully hydrated. The experiment, with a representative example of the potential transients recorded during such experiments, is shown in Figure 4.

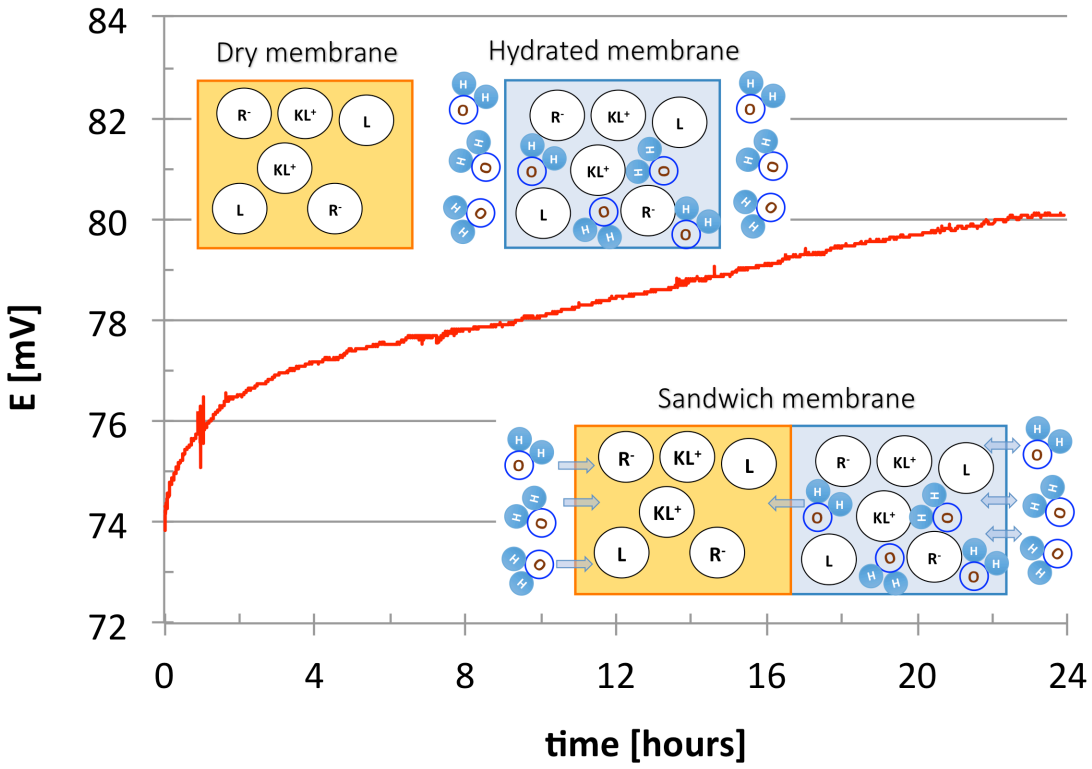

Figure 4.1. The protocol of the modified "sandwich membrane" method and an actual potential vs. time recording of the experiment. The potential recording started within one minute of assembling the "sandwich". The insets show the compositions of a dry and a fully hydrated membrane as well as the direction of water diffusion in the assembled "sandwich". L: Ionophore; R^-: lipophilic counter ion; KL^+: ion-ionophore complex; : water molecules.

As shown in Figure 4.1, the asymptotic potential change recorded during the first 24 h of hydration of a dry membrane is only ≈(5 ± 1) mV (n=8). This potential change is significantly smaller than the 80 to 120 mV potential difference calculated with Equation 4.1 with PEDOT(PSS)-based SC ISEs [22]. This result suggests that the significant negative potential drift observed during the equilibration of PEDOT(PSS)-coated Au and GC electrodes is compensated primarily by a potential drift of opposite sign at the PEDOT(PSS)|ISM interface in a SC ISE since the positive potential drift related to the hydration of the ISM is only a few mVs. This conclusion is consistent with the general experience that the drift during the conditioning of conventional or liquid inner contact electrodes is significantly smaller compared to SC ISEs.

During hydration [20, 29], ion-exchange processes are initiated and several parameters change in the ISM, e.g., dielectric constant, viscosity, membrane thickness, resistance, etc., until a new equilibrium is reached. These changes are accompanied by variations in the activities of the different species as well as the stability constants of ion-ionophore complexes in the membrane. The drift recorded during the equilibration of an ISE is a reflection of all of the changes in these physicochemical parameters. With symmetrically bathed ISMs as in conventional ISEs as represented in cell III, the drift is significantly smaller compared to SC ISEs (cell IV) because the phase boundary potentials on the two sides of the membrane in cell III cancel out. On the right-hand side of cells III and IV, Ag|AgCl represents a reference electrode in contact with 0.1 M KCl, which is the sample solution.

$$Ag|AgCl|0.1\ M\ KCl|ISM|0.1\ M\ KCl|AgCl|Ag \quad \text{(III)}$$

$$Pt, Au, or\ GC|PEDOT(PSS)|ISM|0.1\ M\ KCl|AgCl|Ag \quad \text{(IV)}$$

Potential vs. time transients recorded during the equilibration of PEDOT(PSS)-coated Pt, Au, and GC electrodes following the galvanostatic deposition of the PEDOT(PSS) films

In the introduction, we discussed that the overall drift of a fully fabricated ISE with PEDOT(PSS) as SC (Pt, Au, or GC|PEDOT(PSS)|ISM|KCl) is a consequence of time-dependent changes at three interfaces (Pt, Au, or GC|PEDOT(PSS), PEDOT(PSS)|ISM, and ISM|KCl) and within the bulk materials of PEDOT(PSS) and the ISM. Upon immersing a SC ISE into the aqueous solution, the ISM and consecutively the PEDOT(PSS) film become equilibrated, which is accompanied by diffusion-controlled activity changes in these phases. Since the phase boundary and diffusion potentials are related to the ion activities in the contacting phases, the potential drifts recorded during the equilibration of SC ISEs can be interpreted in part as water transport-related diffusion phenomena and ionic activity changes in the ISM and PEDOT(PSS) films. However, the deconvolution of the individual potential terms from the overall drift of the SC ISE during equilibration is not straightforward. With PEDOT(PSS)-based SC ISEs, beyond the ionic sensitivity, the redox sensitivity of the conducting polymer should also be considered [21, 30].

To follow changes in the redox state of the galvanostatically deposited PEDOT(PSS) films as function of time, the potentials of PEDOT(PSS)-coated Pt, Au, and GC electrodes were recorded for 24 hours immediately after completing the galvanostatic deposition of 1.0 μm or 0.1 μm-thick PEDOT(PSS)-films. The potential vs. time transients shown in Figure 4.2 were recorded with 1.0 μm thick PEDOT(PSS)-coated electrodes in the same solution which has been used for the PEDOT(PSS)

deposition (0.015 mol/dm^3 EDOT and 0.1 mol/dm^3 NaPSS). The shapes of the transients were very similar when the PEDOT(PSS) film over the Pt, Au, and GC electrode was only 0.1 μm thick but the rates of equilibration were higher on Au and GC, as they stabilized around 6 hours whereas the 1.0 μm thick PEDOT(PSS)-coated electrodes were still drifting negatively at 24 hours. More so, the potential values measured at the end of the experiment (after 24 hours of equilibration) were more positive with 0.1 μm-thick films (by 52 mV, 55 mV, and 26 mV for Pt, Au, and GC electrodes, respectively) than with the 1.0 μm-thick PEDOT(PSS)-coated electrodes. However, the significant differences between the Pt electrode and the Au and GC electrodes remained.

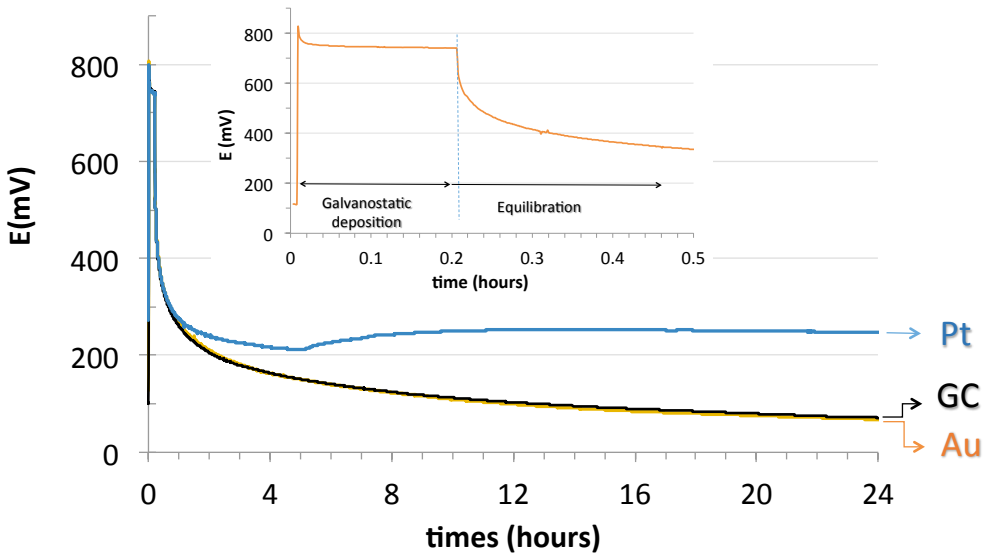

Figure 4.2. Potential vs. time transients recorded at two different time scales during the galvanostatic deposition (0-0.2 hours, inset) and consecutive equilibration (0.2-24 hours) of PEDOT(PSS)-coated Pt, GC, and Au electrodes in the solution used for the electrochemical deposition) (0.015 mol/dm^3 EDOT and 0.1 mol/dm^3 NaPSS). The layer thickness of the PEDOT(PSS) film was 1.0 μm for all three electrodes.

The equilibration is much faster when the PEDOT(PSS) film is formed on a Pt electrode compared to Au and GC electrodes. The potential of the 1.0 μm-thick PEDOT(PSS) layer-coated Pt, Au, and GC electrodes in the first 24 hours dropped from ~740 mV to 245±15 mV, 68±1 mV, and 67±3 mV, respectively. The steady state potentials were very similar if the electrodes were stored 24 hours in 0.1 M KCl after the electrochemical deposition (287±6 mV for Pt, 81±7 mV for Au, and 75±6 mV for GC). Apparently, the potential decay is slower when the PEDOT(PSS)-coated electrodes are stored dry. As a consequence, at the beginning of the equilibration experiments of dry PEDOT(PSS)-coated electrodes shown in Figures 4.3a, 4.4a, and 4.5a (see next section), the potentials of the PEDOT(PSS)-coated Pt electrodes (336 ± 20 mV) are about 60 mV more positive compared to the PEDOT(PSS)-coated Au and GC electrodes (277 ± 4 mV and 273 ± 5 mV, respectively). The significantly more positive potential values recorded with the PEDOT(PSS)-coated Pt electrodes compared to the PEDOT(PSS)-coated Au and GC electrodes (~180 mV after 24 hours wet storage and ~60 mV after dry storage) suggests that the ratio of the oxidized (n) and reduced (m) monomeric units ($EDOT_n^+ / EDOT_m^0$) in PEDOT(PSS) should also be significantly larger when deposited over Pt compared to Au and GC as substrates. In addition, these results are in accord with the conclusions of our previously published paper [22] that the interface between the supporting electrode and the conductive polymer (metal|PEDOT(PSS)) is critically important in understanding the responses of SC ISEs with PEDOT(PSS) as solid contact. In a more oxidized PEDOT film, the concentration of NaPSS is higher; consequently a PEDOT(PSS) film deposited over Pt is expected to be more hydrophilic than a PEDOT(PSS) film deposited over Au or GC as electrode substrate.

The complexity of the interpretation of the equilibration processes is easily understood by considering the potential vs. time traces of the PEDOT(PSS)-coated Pt electrode. As shown in Figure 4.2, after about 5.2±0.4 (n=3) hours of equilibration, the drift abruptly changes sign (from negative to positive) without any change in the composition of the solution, temperature, etc. With 0.1 μm thick PEDOT(PSS)-coating on the electrodes, the change in the sign of the drift becomes visible with all three electrode substrates, but the time instant when it happens is very different 3.6±0.1 (n=4) hours with Pt, 8±4 (n=3) hours with Au, and 14.4±2.6 (n=5) hours with GC electrodes.

Potential vs. time transients recorded during equilibration of PEDOT(PSS)-coated Au, GC, and Pt electrodes: Influence of the PEDOT(PSS) film thickness

Figures 4.3a, 4.4a, and 4.5a show potential vs. time transients recorded in 0.1 M KCl with PEDOT(PSS)-coated Au, GC, and Pt electrodes, respectively. The thicknesses of the electrochemically deposited PEDOT(PSS) films were 0.1 μm, 1.0 μm, 2.0 μm, and 4.0 μm. The thicknesses were calculated from the total charge used for the PEDOT(PSS) deposition, the electrode surface area, and the PEDOT(PSS) density. In agreement with the potential-time transients in the previous chapter, PEDOT(PSS)-coated GC electrodes were similar to the transients recorded with the PEDOT(PSS)-coated Au electrodes [22].

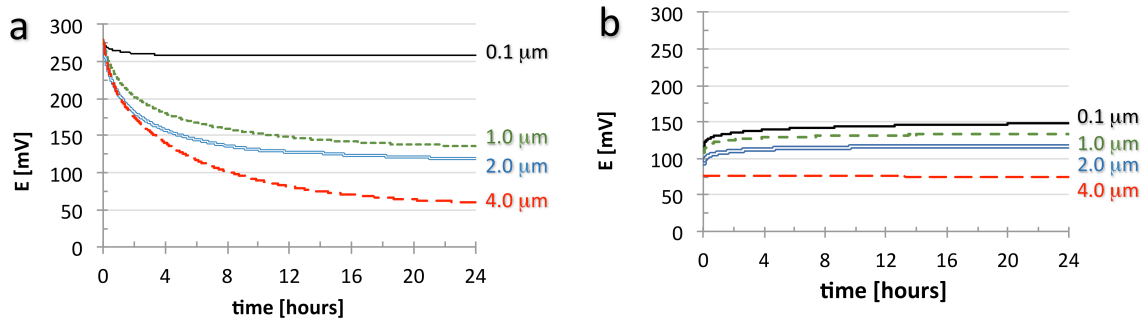

Figure 4.3. Potential vs. time transients recorded during the equilibration of PEDOT(PSS)-coated Au electrodes (a) and fully fabricated potassium-selective electrodes prepared on Au substrates with PEDOT(PSS) as solid contact (b) in 0.1 M KCl. The PEDOT(PSS) films (0.1 µm, 1.0 µm, 2.0 µm, and 4.0 µm) were deposited onto the Au electrodes electrochemically.

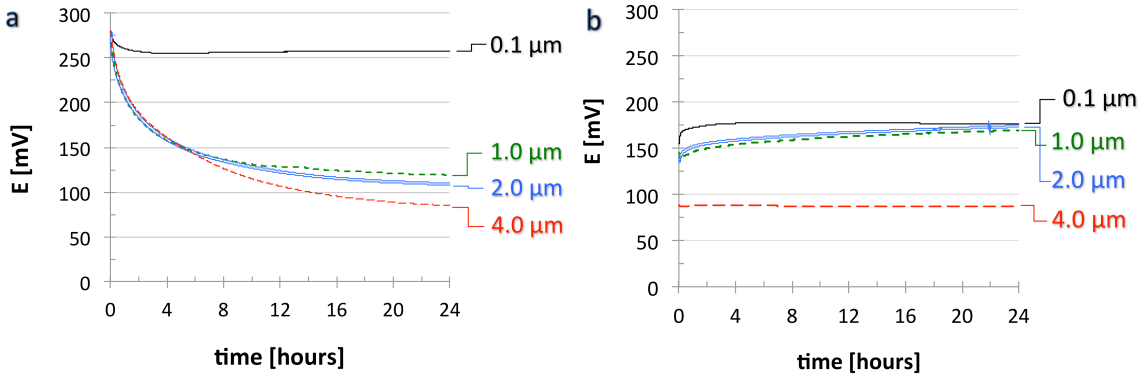

Figure 4.4. Potential vs. time transients recorded during the equilibration of PEDOT(PSS)-coated GC electrodes (a) and fully fabricated potassium-selective electrodes prepared on GC substrates with PEDOT(PSS) as solid contact (b) in 0.1 M KCl. The PEDOT(PSS) films (0.1 µm, 1.0 µm, 2.0 µm, and 4.0 µm) were deposited onto the GC electrodes electrochemically.

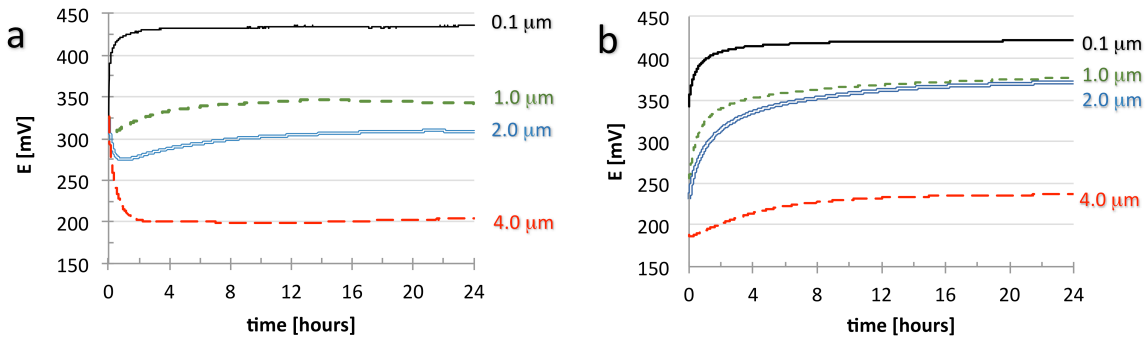

Figure 4.5. Potential vs. time transients recorded during the equilibration of PEDOT(PSS)-coated Pt electrodes (a) and fully fabricated potassium-selective electrodes prepared on Pt substrates with PEDOT(PSS) as solid contact (b) in 0.1 M KCl. The PEDOT(PSS) films (0.1 µm, 1.0 µm, 2.0 µm, and 4.0 µm) were deposited onto the Pt electrodes electrochemically.

The potential values recorded after 24 hours of conditioning decrease gradually with increasing film thickness for the PEDOT(PSS)-coated Au, GC, and Pt electrodes (Figures 4.3a, 4.4a, and 4.5a). It is assumed that the influence of the PEDOT(PSS) film thickness on the steady state potential values is related to the mixed ionic and electronic sensitivity of the PEDOT(PSS) film. The influence of redox processes on the measured potentials are expected to be more significant with thinner PEDOT(PSS) layers over the substrate electrodes [21, 30]. In line with this assumption, Bobacka et. al. reported a strong correlation between the PEDOT(PSS) layer thickness and the potentiometric response slope of PEDOT(PSS)-coated GC electrodes in KCl [17]. Moreover, the differences between the potentials measured with electrodes coated with 0.1 µm, 1.0 µm, 2.0 µm and 4.0 µm PEDOT(PSS) layers are also very similar for the Au and Pt electrodes

(see Table 4.1). This implies, that the ($EDOT_n^+/EDOT_m^0$) ratio and concomitant PEDOT(PSS) composition varies gradually with film thickness in a consistent manner regardless of the starting potential values measured with the different substrate electrodes. This conclusion is in agreement with the gradual changes in contact angles with increasing PEDOT(PSS) film thicknesses (Table 4.2).

As it is shown in Table 4.1, the steady state potential values of electrodes with 0.1 μm PEDOT(PSS) coatings are about ~200 mV more positive than with 4 μm thick coatings. This potential difference is assumed to be related to the differences in the redox sensitivities of the electrodes [21, 30] and differences in the $EDOT_n^+/EDOT_m^0$ ratios in thin and thick PEDOT(PSS) films. Unfortunately, the measured potentials do not provide information about whether the $EDOT_n^+/EDOT_m^0$ ratio has a gradient from the metal substrate towards the PEDOT(PSS)|KCl interface or can be considered homogeneous throughout the PEDOT(PSS) film. However, the SR-XPS data on the buried layer of PEDOT(PSS) at the metal substrate|PEDOT(PSS) interface (see the SR-XPS section below), as well as the water contact angle data of the outermost layers of PEDOT(PSS) at different PEDOT(PSS) layer thicknesses (Table 4.2), suggest a gradual change in the $EDOT_n^+/EDOT_m^0$ ratio from the metal|PEDOT(PSS) interface toward the PEDOT(PSS)|KCl interface.

Table 4.1. Potential changes recorded during the first 24 hours of equilibration with 0.1 μm, 1.0 μm, 2.0 μm, and 4.0 μm thick PEDOT(PSS)-coated electrodes.[a]

Substrate electrode	Potential differences	Potential differences (mV)			
		0.1 μm PEDOT(PSS)	1.0 μm PEDOT(PSS)	2.0 μm PEDOT(PSS)	4.0 μm PEDOT(PSS)
Au	$E^{t=0} - E^{24h}$	23±5 (n=8)	127±18 (n=8)	160±16 (n=8)	232±9 (n=6)
	$E_{0.1\mu m}^{24h} - E_{x\mu m}^{24h}$		100±18	136±17	200±9
GC	$E^{t=0} - E^{24h}$	20±9 (n=8)	155±15 (n=8)	168±9 (n=8)	193±6 (n=7)
	$E_{0.1\mu m}^{24h} - E_{x\mu m}^{24h}$		138±15	150±11	175±11
Pt	$E^{t=0} - E^{24h}$	-125±14 (n=8)	2±8 (n=8)	14±6 (n=6)	115±16 (n=6)
	$E_{0.1\mu m}^{24h} - E_{x\mu m}^{24h}$		124±9	127±11	225±27

[a] $E^{t=0} - E^{24h}$ is the potential difference between initial potential (potential at time t=0) and potential after 24h equilibration.

$E_{0.1\mu m}^{24h} - E_{x\mu m}^{24h}$ represents potential differences after 24 h equilibration between the electrode coated with a 0.1 μm thick PEDOT(PSS) film and the electrodes coated with x=1.0 μm, 2.0 μm, and 4.0 μm thick PEDOT(PSS) films on the same substrate.

Table 4.2. Water contact angles measured on the surface of electrochemically deposited 0.1 μm, 0.5 μm, 1.0 μm, 2.0 μm, and 4.0 μm thick PEDOT(PSS) films over Pt, Au, and GC substrate electrodes.[a]

Substrate electrode	PEDOT(PSS) layer thickness				
	0.1 μm[b]	0.5 μm[b]	1.0 μm[b]	2.0 μm	4.0 μm
Au	35.0±4.1 (n=5)	43.2±1.7 (n=4)	55.2±3.5 (n=6)	56.5±2.7 (n=4)	63.4±3.9 (n=5)
GC	32.2±2.2 (n=6)	36.3±1.5 (n=4)	49.0±7.8 (n=6)	56.3±2.6 (n=4)	57.0±2.8 (n=5)
Pt	30.1±3.0 (n=7)	36.0±7.2 (n=4)	48.8±1.9 (n=4)	56.3±1.7 (n=4)	62.8±1.0 (n=4)

[a]The measured values are provided with their S.D. [b]Statistically significant difference between contact angles of PEDOT(PSS) on Au vs. GC and Pt.

To interpret the significant differences in the shape of the potential vs. time transients of PEDOT(PSS)-coated Au and GC compared to Pt electrodes during their equilibration in aqueous KCl solutions, differences in the level of oxidation and the related hydrophobicity or hydrophilicity of the PEDOT(PSS) films over the Au, GC, and Pt substrate electrodes were considered. All the transients recorded with the PEDOT(PSS)-coated Au and GC electrodes are sluggish with an asymptotic negative drift (Figure 4.3a and 4.4a). Electrodes with thicker PEDOT(PSS) films needed more time to become fully equilibrated and had larger overall drifts. Apparently, the rate determining step of the response is the slow equilibration of the PEDOT(PSS) film, which appears to be layered from near to the electrode substrate (hydrophilic thin surface films) to the more hydrophobic bulk of the PEDOT(PSS) of thicker films. Veder et al. showed that PEDOT(PSS) has hydrogel-like properties with more significant water uptake than plasticized PVC membranes [19]. Compared to the PEDOT(PSS)-coated Au and GC electrodes (Figure 4.3a and 4.4a), the equilibration of the PEDOT(PSS)-coated Pt electrodes is fast (Figure 4.5a). All the PEDOT(PSS)-coated Pt electrodes approached their equilibrium potential values between 2 and 4 hours. The faster equilibration coincides with more positive potentials of the PEDOT(PSS)-coated Pt electrodes compared to Au and GC electrodes. The more positive potentials indicate a larger $EDOT_n^+/EDOT_m^0$ ratio, i.e., a more hydrophilic surface compared to Au and GC electrodes.

Potential vs. time transients recorded during equilibration of solid contact potassium-selective electrodes with PEDOT(PSS) as solid contact over Au, GC, or Pt as substrate electrodes: Influence of the PEDOT(PSS) film thickness

Figure 4.3b shows potential vs. time transients recorded during the equilibration of fully fabricated potassium-selective electrodes prepared on Au substrates with 0.1 μm, 1.0 μm, 2.0 μm, and 4.0 μm PEDOT(PSS) coatings and constant ISM thickness (~90 μm). The corresponding transients recorded with PEDOT(PSS)-based SC potassium-selective electrodes prepared on GC as substrate are very similar, as shown in Figure 4.4b. When the transients in Figures 4.3a and 4.3b (or similarly, 4.4a and 4.4b) are compared using the same potential scales in the plots, the most striking difference is the change in the sign and magnitude of the potential drift during equilibration as a consequence of layering an ISM onto the PEDOT(PSS) film. It is also noteworthy that the ~200 mV potential difference between the equilibrium potentials of the electrodes with 0.1 μm and 4.0 μm PEDOT(PSS) film thickness (Figure 4.2a) dropped to ~75 mV with the placement of an ISM layer onto the PEDOT(PSS) film (Figure 4.2b). The electrode with a 0.1 μm PEDOT(PSS) film thickness has the smallest drift for bare PEDOT(PSS) layers (see Figure 4.3a), but the largest potential change during equilibration when the PEDOT(PSS) film is coated by an ISM (see Figure 4.3b). In contrast, the electrode with 4.0 μm PEDOT(PSS) film thickness has the largest drift with the bare PEDOT(PSS) layer (see Figure 4.3a), but has almost no drift when the PEDOT(PSS) film is coated with an ISM (see Figure 4.3b). The transients for the electrodes with 1 μm and 2 μm thick PEDOT(PSS) films in Figures 4.3a and 4.3b fit into the expected trend, i.e., the drift rate increases with PEDOT(PSS) film thickness for bare

PEDOT(PSS) layers (see Figure 4.3a), but decreases with ISM coated PEDOT(PSS) layers (see Figure 4.2b). These differences between the transients in Figures 4.3a and 4.3b can be explained by acknowledging that the drift observed during conditioning of a fully fabricated SC ISE is the sum of multiple individual potential drifts related to the equilibration processes at interfaces and bulks of the multi-layered sensor system (metal|PEDOT(PSS)|ISM|KCl). Consistent with earlier work [22], the four PEDOT(PSS) thickness-based transients (see Figure 4.3b) show that the negative potential drift related to the equilibration of the PEDOT(PSS) film (see Figure 4.3a) is in part or completely (electrodes with 4.0 μm thick layer of PEDOT(PSS)) compensated by the positive potential drifts ($\delta\varepsilon_{diff(ISM)}$ and $\delta\varepsilon_{PEDOT|ISM}$) related to activity changes in the ISM. Due to the remarkable similarities between Figures 4.3 and 4.4 in the potential vs. time transients recorded during the equilibration for Au and GC-based PEDOT(PSS) SC potassium ISEs, it is clear that GC (Figure 4.4b) and Au (Figure 4.3b) substrate electrodes impose similar stabilities onto PEDOT(PSS)-based SC ISEs.

The drift behavior of fully fabricated potassium-selective electrodes prepared on Pt is different from those prepared on Au and GC as substrate electrode. Since the equilibration rate of the PEDOT(PSS) film over the Pt substrate is fast compared the equilibration of the ISM, the overall rate is dominated by the equilibration of the ISM and the interfacial potential between the PEDOT(PSS) and the ISM ($\delta\varepsilon_{diff(ISM)}$ and $\delta\varepsilon_{PEDOT|ISM}$). The sign of the drift (see Figure 4.5b) qualitatively follows the expectations i.e., the overall drift of the SC ISE is the sum of the potential drift related to the equilibration of the PEDOT(PSS) film (see Figure 4.5a) and the potential drifts related to activity changes in the ISM. However, there are significant differences in the measured

and expected drift values. For example, the drift with 0.1 μm PEDOT(PSS) solid contact is much smaller than expected. It is assumed that the discrepancy is in part related to the uncertainty in the subtraction procedure. Potentially significant differences in the interfacial potentials at the PEDOT(PSS)|0.1 M KCl and PEDOT(PSS)|ISM could not be taken into account because the activities in the ISM are not known. Additionally, in contrast to the PEDOT(PSS)-based ISEs on Au, coating the PEDOT(PSS) film with the ISM on Pt did not coincide with a decrease in the divergence of the equilibrium potentials between the electrodes with 0.1 μm and 4.0 μm PEDOT(PSS) film thicknesses (compare Figures 4.3 and 4.5). The equilibrium potential difference ($E_{0.1\mu m}^{t=24h} - E_{4.0\,\mu m}^{24h}$) of bare (Figure 4.5a) and ISM-coated PEDOT(PSS) films (Figure 4.4b) with 0.1 μm and 4.0 μm thicknesses on Pt substrate remained the same. The reason for the difference between the electrodes with Au and Pt as substrate electrodes is not abundantly clear, but it is assumed that it is related to the differences in the redox state of the PEDOT(PSS) film with different thicknesses, i.e., differences in the absolute value of the interfacial potential at the PEDOT(PSS)|ISM interface due probably to differences in the ionic and redox sensitivity of the PEDOT(PSS) films with increasing thicknesses and the differences in the ($EDOT_n^+ / EDOT_m^0$) ratio in the PEDOT(PSS) conductive polymer solid contact on Au and Pt.

Finally, we found that the drift decreased with increasing PEDOT(PSS) film thickness (especially for the solid contact ISEs with Au and GC as substrate electrode (Figures 4.3b and 4.4b). Similar findings were reported by Gyurcsanyi, et al. on the influence of the polypyrrole film thickness on the potential stability of SC K^+ electrodes [31] and Bobacka [17] on the long term stability of PEDOT(PSS)-based SC ISEs.

Bobacka claimed that the long-term stability of SC ISEs is directly related to the low-frequency capacitance (C_L) of the solid contact. According to Bobacka, increasing the thickness of the PEDOT(PSS) film beneath the ISM increases the C_L and consequently improves the long term stability of SC ISEs. However, above a certain film thickness (~1.0 μm), the C_L hardly changed and no significant improvement could be achieved in the long-term stability. Consequently, the improved stability of PEDOT(PSS)-based SC ISEs with thicker PEDOT(PSS) films is related to the C_L of the SC as well as to the surface composition (as determined by XPS in this work) and concomitant hydrophobicity of PEDOT(PSS) (as deduced from the results of contact angle measurements). As the PEDOT(PSS) film thickens during electropolymerization onto the substrate electrode, it acquires consistency and the influence of the substrate electrode|PEDOT(PSS) interface decreases.

Photon energy dependent SR-XPS depth profiling of PEDOT(PSS) films on Au, GC, and Pt

Figures 4.6 and 4.7 present the S 2p and O 1s SR-XPS spectra of the native PEDOT(PSS) surface after electropolymerization onto Au, as measured at the SXR beamline in Australia. The presence of a pair of S $2p_{3/2}$ and S $2p_{1/2}$ spin-orbit split component peaks at 163.7 and 164.9 eV together with 168.1 and 169.3 eV (see Figure 4.6) are consistent with sulfur in the PEDOT backbone of PEDOT(PSS) and the sulfonate functionality of the PSS^- counteranion, respectively [32]. Similarly, the presence of an O 1s peak at 533.2 eV is symbolic of oxygen in the ethoxy functionality of the PEDOT backbone, while the peak at 531.6 eV is ascribable to oxygen in the sulfonate functionality of the PSS^- counteranion [32] (see Figure 4.7). Note that the small pair of S

$2p_{3/2}$ and S $2p_{1/2}$ spin-orbit split peaks at 165.0 and 166.2 eV are indicative of the $PEDOT^+$ polaron in oxidized PEDOT. From the S 2p spectra (Figure 4.6), it is evident that the ratio of PSS_{tot}- to-PEDOT on Au is about 0.25, or 25%.

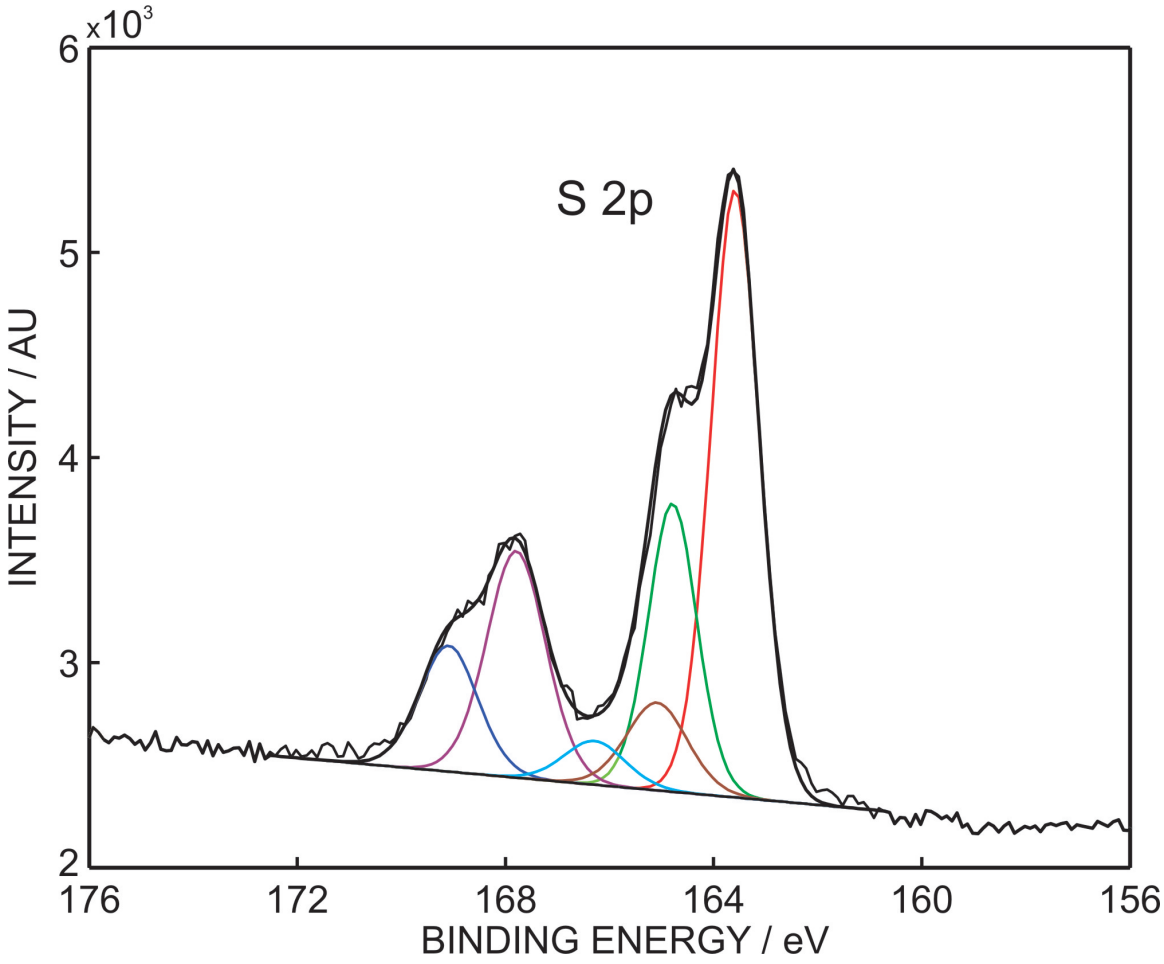

Figure 4.6. SR-XPS spectrum of the S 2p core level for electropolymerized PEDOT(PSS) on Au (approximate 10 nm film thickness) as measured on the SXR beamline at the Australian Synchrotron.

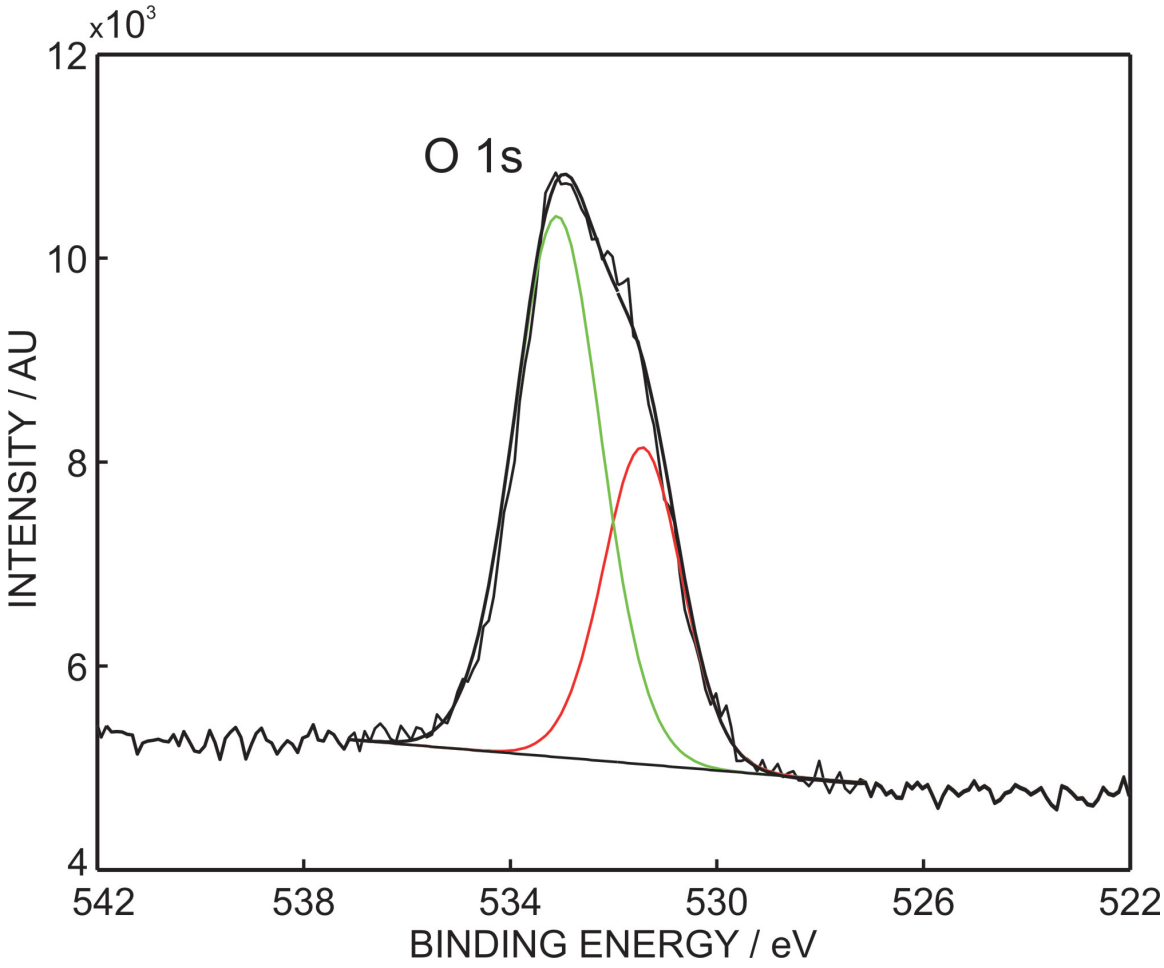

Figure 4.7. SR-XPS spectrum of the O 1s core level for electropolymerized PEDOT(PSS) on Au (approximate 10 nm film thickness) as measured on the SXR beamline at the Australian Synchrotron.

By curve fitting of the PEDOT and PSS^- S 2p components, Figure 4.8 presents the $PSS_{tot}/PEDOT$ (total PSS^--to-PEDOT) ratios deduced for the ~10 nm thick electropolymerized PEDOT(PSS) films on Au, GC, and Pt substrates, as measured on the bending magnet MSB at the Elettra Synchrotron in Italy. From Figure 4.8, it is evident that the degree of oxidation of PEDOT and its association with PSS^- is significantly different on the Pt, GC, and Au substrate electrodes.

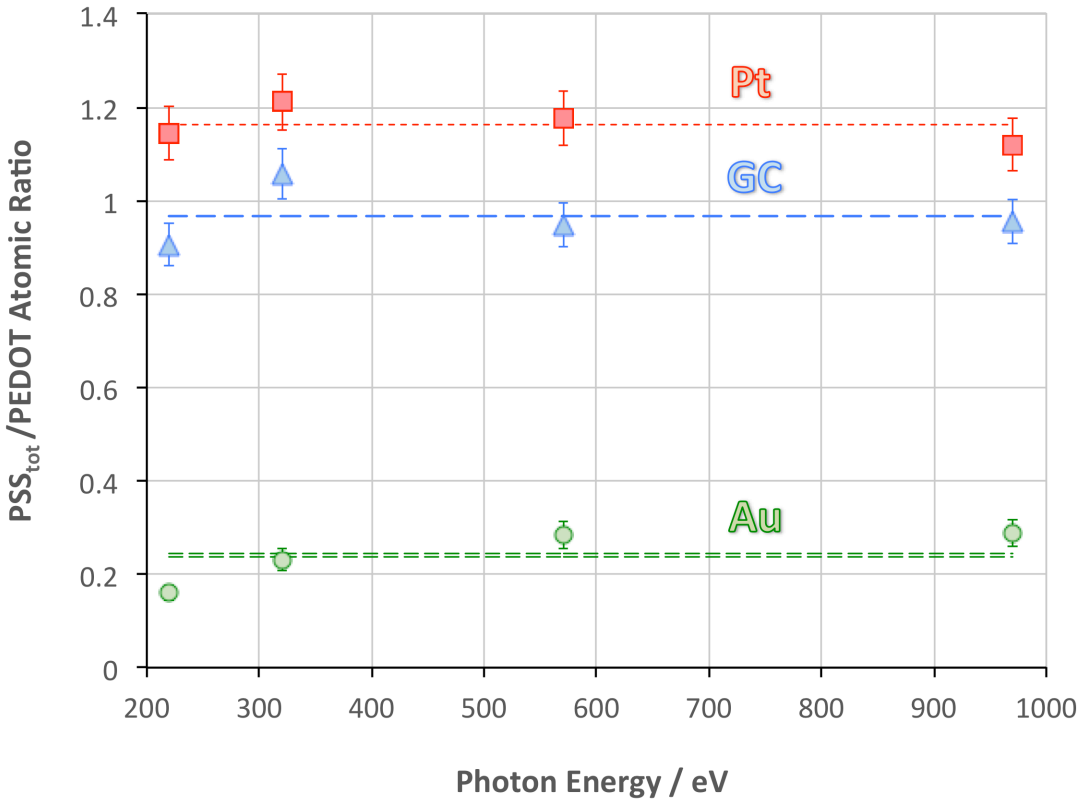

Figure 4.8. SR-XPS PSS_{tot}/PEDOT ratios for approximately 10 nm thick films of electropolymerized PEDOT(PSS) on Au, GC, and Pt measured at the Elettra Materials Science beamline. The dotted lines represent the average values of the PSS_{tot}/PEDOT ratios at 0.83 nm, 1.37 nm, 2.21 nm, and 3.12 nm inelastic mean free paths (IMFPs) for 220, 320, 570, and 970 eV photon energies (see Appendix A for the details of the calculations), or electron escape depths 3 x IMFPs of 2.49 nm, 4.11 nm, 6.63 nm, and 9.36 nm, respectively.

Calculation of NaPSS-to-PEDOT, $EDOT_n^+PSS^-$-to-PEDOT, and atomic ratios

PSS^- (PSS_{tot}) can be incorporated into the electrochemically deposited PEDOT(PSS) film as Na^+PSS^- and as $EDOT_n^+PSS^-$, ($\frac{PSS_{tot}}{PEDOT} = \frac{Na^+PSS^- + EDOT_n^+PSS^-}{PEDOT}$). For approximately 10 nm thick PEDOT(PSS) films (see Figure 4.8), the averages in PSS_{tot}/PEDOT ratios have been determined to be 1.16, 0.97, and 0.24 on Pt, GC, and Au substrate electrodes, respectively. Since the Elettra MSB can only achieve a maximum beam energy of 1000 eV, it was not possible to access the Na 1s core orbital at about 1072 eV for NaPSS on these samples at Elettra. Consequently, we electropolymerized approximately 10 nm thick films of PEDOT(PSS) onto the same electrode substrates utilizing identical electropolymerization conditions to those used at Elettra, and analyzed these samples using laboratory XPS. These multiple spot analyses yielded Na^+/PSS_{tot} ratios ($\frac{Na}{PSS_{tot}} = \frac{Na^+PSS^-}{Na^+PSS^- + EDOT_n^+PSS^-}$) (average of 3 spot analyses on each film) of 0.7, 0.2, and 0.8 on Pt, GC, and Au, respectively. The methodology used in the deduction of $Na^+PSS^-/PEDOT$, $EDOT_n^+/PEDOT$, and $EDOT_n^+/EDOT_m^0$ ratios in Table 4.3 is shown through the calculation for Pt electrode:

$$\frac{NaPSS}{PEDOT} = \frac{Na^+}{PSS_{tot}} \times \frac{PSS_{tot}}{PEDOT} = 0.7\ x\ 1.16 = 0.81\ or\ 81\ mol\%\ (Pt) \tag{4.5}$$

$$EDOT_n^+ = PSS_{tot} - Na^+PSS^- \tag{4.6}$$

$$\frac{EDOT_n^+}{PEDOT} = \frac{PSS_{tot}}{PEDOT} - \frac{Na^+PSS^-}{PEDOT} = 1.16 - 0.81 = 0.35\ or\ 35\ mol\%\ \ (Pt) \tag{4.7}$$

$$EDOT_n^+ + EDOT_m^0 = PEDOT \tag{4.8}$$

$$\frac{EDOT_m^0}{PEDOT} = 1 - \frac{EDOT_n^+}{PEDOT} = 1 - 0.35 = 0.65\ (Pt) \tag{4.9}$$

$$EDOT_n^+/EDOT_m^0 = \frac{0.35}{0.65} = 0.54\ (Pt) \tag{4.10}$$

To calculate the amounts of Na^+PSS^- in the electropolymerized PEDOT(PSS) films on Pt, GC, and Au, the $\frac{PSS_{tot}}{PEDOT}$ and $\frac{Na}{PSS_{tot}}$ ratios are multiplied. From this calculation, the Na^+PSS^--to-PEDOT ratios in the PEDOT(PSS) films on Au and GC are approximately 19 mol% but on the Pt electrode surface approximately 81 mol%. The combination of these data allowed estimation of $EDOT_n^+/PEDOT = EDOT_n^+/(EDOT_n^+ + EDOT_m^0)$ ratios in PEDOT(PSS) films on Pt, GC, and Au electrode surfaces as 0.35, 0.78, and 0.05, respectively, while it is also possible to deduce $EDOT_n^+/EDOT_m^0$ ratios in PEDOT(PSS) films (0.54 on Pt, 3.55, on GC, and 0.05 on Au). The results of the SR-XPS analysis of the buried layer of PEDOT(PSS) at the metal substrate|PEDOT(PSS) interface are summarized in Table 4.3.

Table 4.3. Concentration ratios deduced from Elettra SR-XPS and laboratory XPS data on the buried layer of electrochemically deposited, approximately 10 nm thick PEDOT(PSS) films for the Pt, GC, and Au substrate electrodes.

Concentration ratios	Substrate electrode		
	Pt	GC	Au
$PSS_{tot}/PEDOT$	1.16	0.97	0.24
$Na^+/PSS_{tot} = NaPSS/PSS_{tot}$	0.7	0.2	0.8
$NaPSS/PEDOT$	0.81	0.19	0.19
$EDOT_n^+/PEDOT = EDOT_n^+PSS^-/PEDOT$	0.35	0.78	0.05
$EDOT_n^+/EDOT_m^0$	0.54	3.55	0.05

Concentration ratios deduced from Elettra SR-XPS and laboratory XPS data on the PEDOT(PSS) films on Pt and Au electrodes in Table 4.3 are internally consistent with the proposition that these ratios correlate well with hydrophilicity of the PEDOT(PSS)-coated substrate electrode surface and their rate of the equilibration. However, the interpretation of the concentration ratios in Table 4.3 for PEDOT(PSS)-coated GC electrodes is not as straightforward. In potentiometric measurements, the PEDOT(PSS)-coated Au and GC electrodes are almost identical and significantly different from the Pt electrode (see e.g. Figure 4.2). On the other hand, the PEDOT(PSS)-coated GC electrodes appear to be more similar to the Pt electrodes in water contact angle measurements (see Table 4.2) as well as in the $\frac{PSS_{tot}}{PEDOT}$ and $\frac{EDOT_n^+}{PEDOT}$ ratios determined by SR-XPS (see Table 4.3). All things considered, these data suggest that related to the rate of the equilibration of the PEDOT(PSS) films, differences in the Na^+PSS^--to-PEDOT ratios in the electrochemically deposited PEDOT(PSS) films (~81 mol% on Pt but only ~19 mol% on both Au and GC) are the most significant. This means that the PEDOT(PSS)-coated Pt electrode surface is very hydrophilic. Comparatively, the PEDOT(PSS)-coated Au and GC electrode surfaces are quite hydrophobic comprising significantly lower concentrations of Na^+PSS^- salt (~19 mol%). Although the $EDOT_n^+PSS^-$ concentration is quite high on the GC surface (higher than on Pt) the GC/PEDOT(PSS) surface is still less hydrophilic than Pt because the concentration of Na^+PSS^- is significantly lower on the GC electrode surface (the same as on the Au electrode). With increasing thickness, the PEDOT(PSS) films become gradually more hydrophobic and the difference in their hydrophilicity on the different substrates disappears. The water sorption characteristics of the PEDOT(PSS) films, as noted in Figures 4.2-4.4, appear to be linked to the

hydrophilicity of the PEDOT(PSS) films on the utmost surface of the substrate electrodes, i.e., the presence of Na^+PSS^- and $EDOT_n^+PSS^-$ salts located on the PEDOT(PSS)-coated surfaces of Au, GC, and Pt electrodes. Last, it appears that the rate of the equilibration of the PEDOT(PSS) films on Pt, GC, and Au is dominated by their level of doping by Na^+PSS^- and is influenced to a lesser extent by $EDOT_n^+PSS^-$ doping or $EDOT_n^+/EDOT_m^0$ ratios. XPS data do not provide an answer for the reasons of the differences in the hydrophilic properties of the PEDOT(PSS)-coated Pt, Au, and GC electrodes. However, in accord with the papers of Lewenstam et. al. [21, 30], the differences in the surface chemistries of the Pt, Au, and GC electrodes and the kinetics of the electrochemical deposition of PEDOT(PSS) on these surfaces may provide the answer.

We also undertook Ar^+ sputtering of PEDOT(PSS) electropolymerized onto Au to the middle of the film, so as to ascertain if there was ion beam-induced damage of the PEDOT(PSS). As can be seen from the spectra in Figure 4.9, it is obvious that Ar^+ sputtering has preferentially sputtered/damaged the PSS^- component of PEDOT(PSS) at about 168 eV, as has been illustrated elsewhere [33], and the presence of a small shoulder at about 162 eV is symbolic of elemental sulfur that has been formed by sulfur reduction in the ion beam. This ion beam-induced damage provided the motivation for this surface study of PEDOT(PSS) using a non-destructive photon energy dependent depth profiling of PEDOT(PSS) at a synchrotron light source.

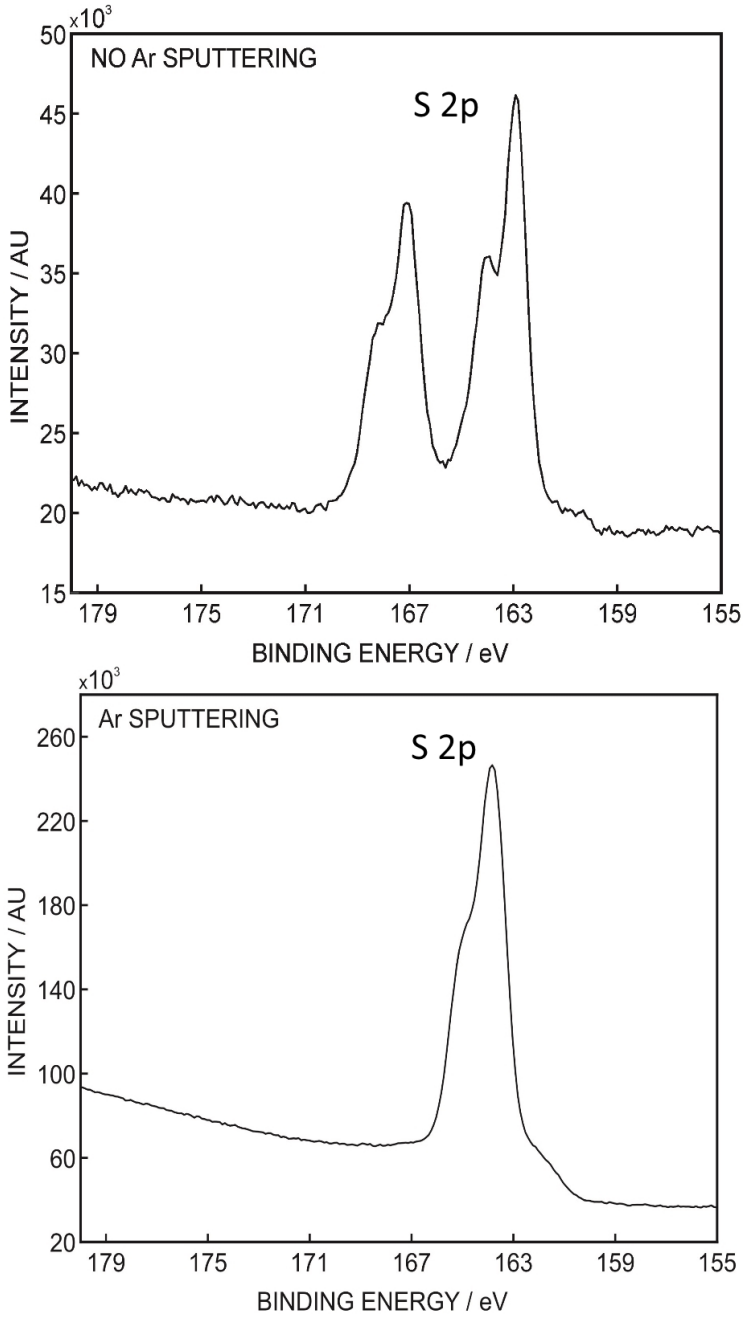

Figure 4.9. SR-XPS S 2p spectra on an Au substrate (approximate 100 nm film thickness) before and after Ar ion sputtering to a depth of approximately 5.5 nm measured at the AS SXR beamline.

CONCLUSIONS RELATED TO THE INFLUENCE OF PEDOT(PSS) FILM THICKNESS ON EQUILIBRATION TIMES

Potential vs. time traces were recorded during equilibration of Au, GC, and Pt electrodes coated with 0.1 μm, 1.0 μm, 2.0 μm, and 4.0 μm thick PEDOT(PSS) films and with fully fabricated K^+ ISEs which were built using 0.1 μm, 1.0 μm, 2.0 μm, and 4.0 μm thick PEDOT(PSS) solid contacts. Based on the potential values measured with these electrodes at their first solution contact and after 24 hour equilibration in 0.1 M KCl, it has been concluded that there are significant differences in the redox state and the hydrophobicity of the PEDOT(PSS) films.

XPS and SR-XPS surface analysis of electropolymerized PEDOT(PSS) on Au, GC, and Pt as substrate electrodes demonstrated that the electrode substrate influences the degree of oxidation together with PSS^- doping and concomitant hydrophilicity of the electropolymerized PEDOT(PSS) film. Related to the rate of equilibration of the PEDOT(PSS) films, the difference in the Na^+PSS^--to-PEDOT ratio (about ~81 mol% on Pt but only 19 mol% on both Au and GC), appears to be the most significant factor. As the thickness of the electrochemically deposited PEDOT(PSS) increases, the influence of the hydrophilicity of the buried metal|PEDOT(PSS) interface on the rate of equilibration decreases.

The contribution of activity changes in the ISM to the overall drift following its first contact with an aqueous solution has been determined by a modified sandwich membrane method. The results suggest that the most significant contribution related to the hydration of the ISM is due to potential changes at the PEDOT(PSS)|ISM interface.

CHAPTER 5

DIFFERENCES IN ELECTROCHEMICALLY DEPOSITED PEDOT(PSS) FILMS ON Au AND Pt SUBSTRATE ELECTRODES: A QUARTZ CRYSTAL MICROBALANCE STUDY

INTRODUCTION

Thus far, it has been shown that there were significant differences in the equilibration times of PEDOT(PSS)-based SC ISEs fabricated on Au and Pt as substrate electrodes [22, 34]. Additionally, the standard potentials of ISEs constructed on Pt with PEDOT(PSS) as SC were much more positive than for the electrodes on Au [34]. These findings were supported by SR-XPS analysis, which showed that the $PSS_{tot}/PEDOT$ ratio was significantly larger in PEDOT(PSS) when deposited on Pt compared to Au substrate electrodes [34]. We argued that PEDOT(PSS) on Pt is more hydrophilic than on Au based on the differences in the $PSS_{tot}/PEDOT$ ratio.

To trace the source of these differences in the PEDOT(PSS) film chemistries and the differences in the electrochemical behaviors of SC electrodes on Au and Pt substrates, PEDOT(PSS) was electrochemically deposited onto 10 MHz sensing quartz crystals of an electrochemical quartz crystal microbalance (EQCM) with Au and Pt contact electrodes. The resonant frequencies were recorded during the entire electrochemical deposition process [35]. The frequencies recorded by the EQCM during the polymerization of PEDOT(PSS) onto the electrode substrates can be related to the mass of the PEDOT(PSS) film by the Sauerbrey equation. From the deposited mass, one can calculate the thickness of the PEDOT(PSS) film. The EQCM studies suggested differences in the final thickness of the PEDOT(PSS) films deposited on Au and Pt under

the same experimental conditions. These differences in the deposited PEDOT(PSS) film thicknesses could be quantitatively confirmed by XPS etching studies. SEM analysis of PEDOT(PSS) films on Au and Pt also showed characteristic differences in agreement with the EQCM and XPS results.

EXPERIMENTAL

Chemicals

3,4-Ethylenedioxythiophene (EDOT) was purchased from Sigma Aldrich. Sodium poly(4-styrenesulfonate) (NaPSS) was purchased from Acros Organics. The aqueous solutions were prepared with 18.2 MΩcm resistivity DI water from a Millipore Milli-Q A10 system. The solution used for platinization was obtained from Technic Inc. (Cranston, RI).

Crystals, Electrodes, and Instrumentation

The 10 MHz Au-coated (A=0.205 cm^2) quartz crystals used in this experiment were purchased from International Crystal Manufacturing (ICM), (Oklahoma City, OK). To create quartz crystals with Pt electrodes, some of the Au-coated quartz crystals were electroplated with Pt. Before use, the crystals were cleaned with methanol, rinsed with DI water, and dried with nitrogen. For XPS and SEM analysis, d=3 mm Bioanalytical System, Inc. (BASi, West Lafayette, IN) Au electrodes (Model MF-1002) with and without electroplated Pt coating were used. Prior to the electrochemical deposition of Pt or PEDOT(PSS), the BASi electrodes were polished with 1.0 μm and 0.3 μm alumina slurry (Buehler, Lake Bluff, IL) and cleaned in a sonicated deionized water bath for 15 minutes.

For the electrochemical depositions of Pt and PEDOT(PSS) a Gamry Reference 600 Potentiostat/Galvanostat (Gamry Instruments, Warminster, PA) was used. In the EQCM experiment the quartz crystals were inserted into crystal holders and assembled into an ICM Teflon cell and frequencies were recorded using a Gamry eQCM 10M or a Chemical Consulting and Services, LLC Model 6000 EQCM (Williamsville, NY).

Platinization of Au-coated crystal

Pt was deposited over the Au substrate electrodes by a previously described method [36]. In short, a current density of -3 mA/cm^2 was applied to the Au substrate for 1079 seconds using a GC rod as a joint counter and reference electrode. This produced a Pt film of approximately 270 nm thickness, as calculated from the EQCM frequency change. The electroplated Pt substrate was thoroughly rinsed with DI water and dried with nitrogen.

Electrochemical deposition of PEDOT(PSS)

The 10 MHz quartz crystals with Au or Pt electrodes were inserted into a crystal holder and assembled into the Teflon cell with a Pt wire or GC rod as counter electrode and a Ag|AgCl|KCl(0.1M) electrode as reference electrode. The quartz crystal holder was attached to the oscillator and the cell was filled with an aqueous solution of 0.015 mol/dm^3 EDOT and 0.1 mol/dm^3 NaPSS. The working electrode lead of the potentiostat was connected to the crystal holder leg in contact of the gold or platinum electrode facing the EDOT/NaPSS solution. PEDOT(PSS) films were electrochemically deposited by using a current density of 0.2 mA/cm^2 for 714 seconds to create an approximately 1 μm-thick film. In the first few seconds of the galvanostatic current application, a voltage "peak" appeared on the potential time transients. The peak potential values were higher

when the deposition was performed on Au (712±8 mV) compared to Pt electrodes (683±16 mV). However, this initial potential difference gradually disappeared as the potential values on both electrodes decayed. At the end of the electrolysis, 652±20 mV and 655±7 mV were recorded with the Au and Pt electrodes, respectively.

The PEDOT(PSS) films aimed for XPS analysis were deposited with 15 s and 71 s electrolysis times over the BASi electrodes, corresponding to estimated thicknesses of 20 nm and 100 nm, respectively. PEDOT(PSS) films aimed for SEM analysis were also deposited with 15 s electrolysis time. After the electrochemical deposition of PEDOT(PSS), the CP-coated electrodes were thoroughly rinsed with DI water, dried with nitrogen, and kept in a desiccator overnight over silica orange beads.

Surface and chemical analysis of PEDOT(PSS)-coated substrates

XPS depth profile analysis was performed using a Thermo Scientific K-Alpha XPS system equipped with a monochromatic Al K_α X-ray source at 1486.6 eV. The films polymerized for 15/71 s were analyzed at 34/150 etching levels, each completed using an Ar^+ gun with 500/1000 eV for 15/5s, respectively. The higher energy was used with the thicker films in order to decrease the experimental time. After each etching cycle, the films were analyzed for S 2p and Au 4f or Pt 4f binding energies at a 40 eV pass energy, using an average of 10 scans. In Chapter 4, we argued that Ar ion sputtering induced damage of the PSS^- species in PEDOT(PSS) and consequently the technique could not be used to analyze hypothesized changes in the chemical composition of the PEDOT(PSS) films in different depths. In this section of our work, the use of Ar^+ ion etching is justified because we were only interested in the etching times necessary for the complete removal of the electrochemically deposited PEDOT(PSS) film.

For the SEM analysis, the dry PEDOT(PSS) films were sputter-coated with a Au:Pd (60:40) film of ~5 nm thickness. SEM imaging was performed in an FEI Nova NanoSEM 650 operating under high vacuum conditions. The microscope is equipped with an Everhard-Thornley detector. The working distance was adjusted to 5.0 mm. The images were recorded at a primary electron energy of 30 keV.

RESULTS AND DISCUSSION

Electrochemical deposition of PEDOT(PSS)

In our earlier studies, the significant differences in the equilibration times and standard potentials of PEDOT(PSS)-based K^+ ISEs built on Au and Pt substrate electrodes were explained by the more hydrophilic properties of PEDOT(PSS) films on Pt [34]. Here, to investigate the source of the differences in PEDOT(PSS) film chemistries deposited with the same protocol onto Au and Pt, we used EQCM to follow the change in frequency during electrochemical deposition of the polymer. Transients representing the change in frequency (Δf) during polymer film growth on Au and Pt-coated quartz crystals are shown in Figure 5.1.

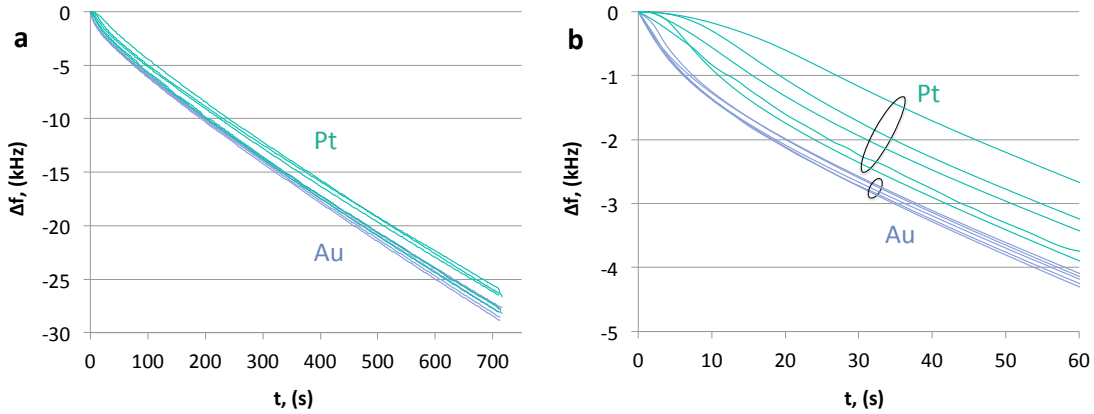

Figure 5.1. Change in EQCM crystal frequency during the galvanostatic deposition of PEDOT(PSS) onto EQCM quartz crystals with Pt (green) or Au (blue) contact electrodes. (a) Δf versus time traces recorded during the entire 714 s of galvanostatic deposition. (b) Δf versus time traces zoomed in on the first 60 s section of the traces shown in (a). The black ovals are meant to group together the Pt (top) and Au (bottom) transients, also highlighting the differences in the reproducibility of the recorded transients.

As seen in Figure 5.1a, the Δf versus time curves recorded during the electrochemical deposition of PEDOT(PSS) on Au and Pt run parallel to each other. Consequently, the total change in frequency during the 714 s electrochemical deposition of PEDOT(PSS) film is significantly less on Pt than on Au. The origin of the parallel running Δf versus time traces could be made visible by zooming in on the first 60 s of the electrochemical deposition (Figure 5.1b). Clearly, in the first 10 to 20 s, the change in frequency related to the PEDOT(PSS) deposition is significantly less on Pt compared to Au. In Figure 5.1b, it is also apparent that the polymerization of PEDOT(PSS) on Au is more reproducible than on Pt, an indication of potential differences in the electrochemically deposited Pt electrode surfaces.

The differences in the polymer growth on the two substrates are better demonstrated by plotting the rate of frequency change ($\Delta f/\Delta t$) during electrochemical deposition. As shown in Figure 5.2, in the first 10 to 20 seconds, the rate of the frequency change (the rate of polymer growth) is significantly larger on Au compared to that on Pt. After 20 s, the rate of frequency change approached the same value (~50 Hz/s).

The change in frequency (Δf) of an oscillating quartz crystal, with certain assumptions, can be used to calculate a change in mass (Δm) of deposited PEDOT(PSS) via the Sauerbrey equation (Equation 5.1), where f_0, A, ρ_q, and μ_q are constants associated with the crystal [37].

$$\Delta f = -\frac{2f_0^2 \Delta m}{A\sqrt{\rho_q \mu_q}} \tag{5.1}$$

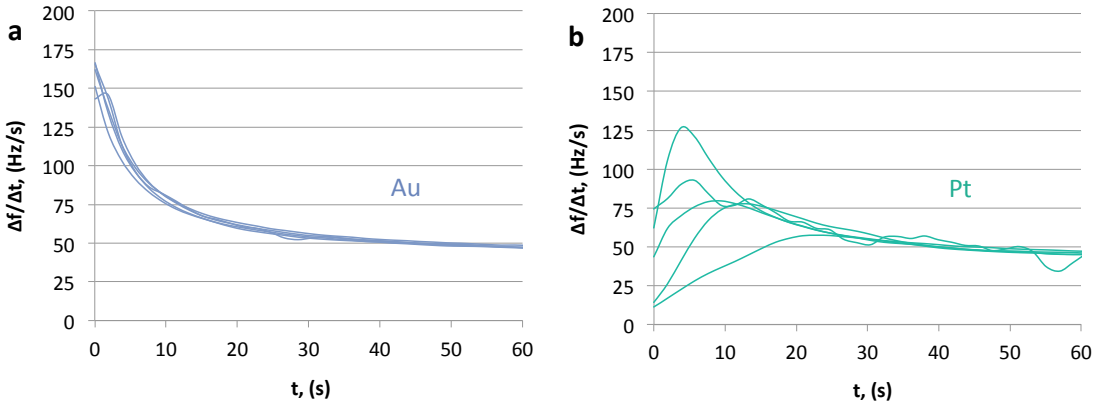

Figure 5.2. Change in the rate of PEDOT(PSS) deposition in the first 60 seconds of galvanostatic polymerization onto Au (a) or Pt (b) electrodes on quartz crystals.

The deposited mass can then be used to calculate the thickness of the PEDOT(PSS) film ($\delta_{PEDOT(PSS)}$) by assuming that PEDOT(PSS) has the same density on Au and Pt ($\rho \approx 1$ g/cm^3) [15] and using the piezoelectrically active area of the QCM

crystals (A=0.205 cm^2). The calculated average thicknesses during the initial 75 seconds of electrodeposition show that the slower polymer growth rate on Pt leads to a thinner PEDOT(PSS) film than on the Au substrate, as shown in Figure 5.3.

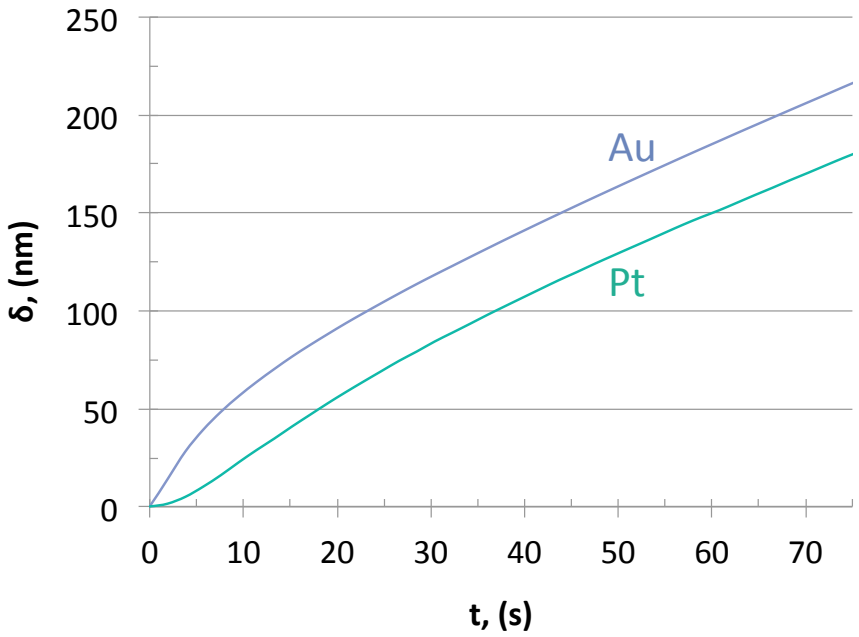

Figure 5.3. Calculated increases in the PEDOT(PSS) film thickness (δ) during the initial 75 seconds of galvanostatic polymer deposition on Au (blue) and Pt (green)-coated quartz crystals. The thicknesses shown represent the calculated average of Au and Pt, each with n=5.

Surface and chemical analysis of PEDOT(PSS)-coated substrates

To test the validity of our calculations related to the PEDOT(PSS) film thicknesses from the frequency changes recorded with the EQCM, thin PEDOT(PSS) films were grown on BASi MF-1002 Au electrodes, with and without electroplated Pt coating, with 15 s and 71 s galvanostatic electrolysis times, corresponding to 20 nm and

100 nm theoretical PEDOT(PSS) film thicknesses, respectively. These films were then analyzed by XPS depth profiling (Figure 5.4). During the XPS analysis, the PEDOT(PSS)-coated Au and Pt electrodes were sputtered by an Ar^+ gun in iterative steps. After each etch step, high resolution core level spectra of S 2p and Au 4f or Pt 4f were taken at 40 eV pass energy. As expected, in these etching experiments, a gradual decrease in the S 2p peaks in PEDOT(PSS) was observed, while the Au 4f or Pt 4f peaks increased with each etching step until they eventually reached 100% atomic ratios, indicating that PEDOT(PSS) was completely removed from the metal electrode surfaces.

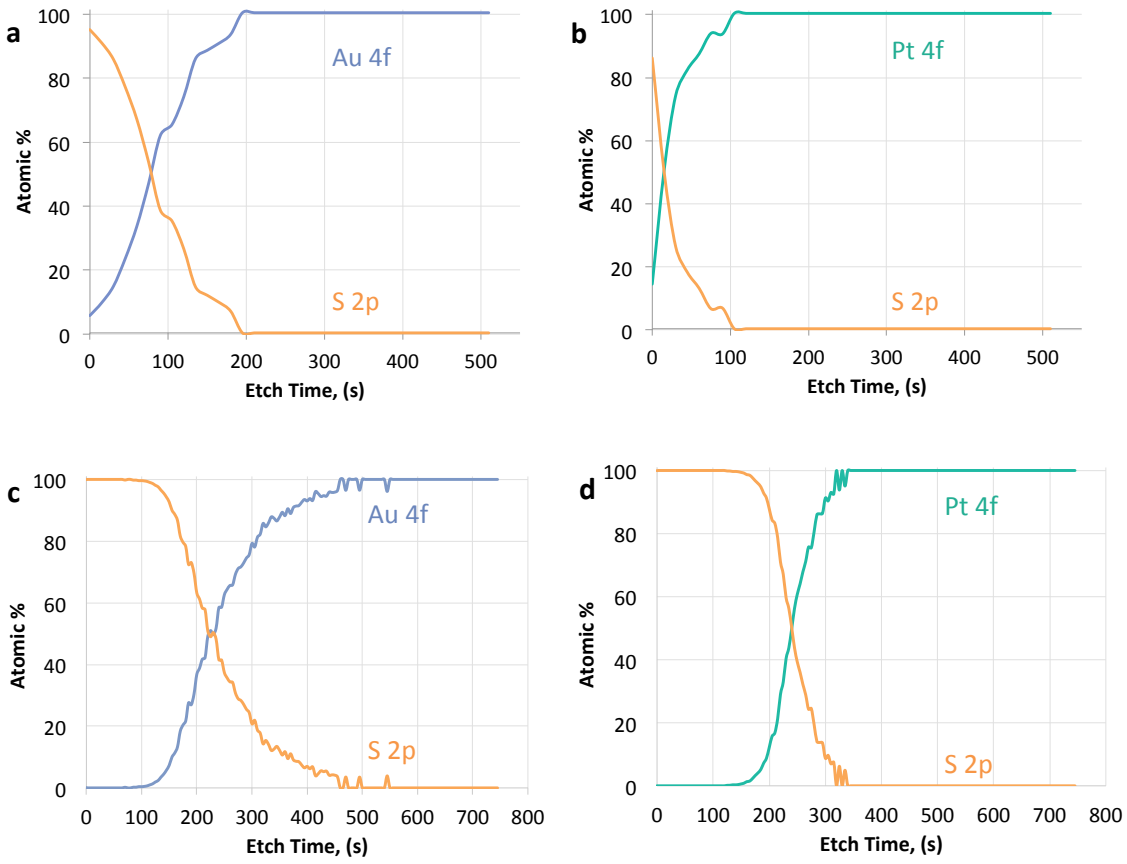

Figure 5.4. XPS depth profile analysis of PEDOT(PSS) films deposited over Au (a,c) or Pt (b,d) electrode surfaces with 15 s (a,b) and 71 s (c,d) galvanostatic polymerization. Atomic percentages of sulfur (orange lines), Pt (green lines), and Au (blue lines) are shown as a function of Ar^+ gun etching time.

For PEDOT(PSS) films which were deposited with a 15 s electrolysis time, the total etching times necessary for the complete removal of these films from Au and Pt were 195 and 105 seconds, respectively (Figure 5.4, a & b). At these etching times, the atomic ratios for Au and Pt reached 100%. For PEDOT(PSS) films which were deposited with a 71 s polymerization time, the total removal of the PEDOT(PSS) films required 460 s and 330 s of Ar^+ gun etching on Au and Pt, respectively (Figure 5.4, c & d). The ratios of these etching times are in close agreement with our estimates of the PEDOT(PSS) film thickness ratios based on our EQCM studies, as shown in Table 5.1.

Table 5.1. Layer thickness ratios for PEDOT(PSS) films on Au and Pt electrodes as determined from the frequency decreases recorded by EQCM and XPS depth profiling

Electrochemical deposition time	$\delta^{Au}_{PEDOT(PSS)}/\delta^{Pt}_{PEDOT(PSS)}$	
	EQCM	XPS
15 s	1.88	1.86
71 s	1.21	1.35

In summary, the Ar^+ gun etching and XPS analysis confirmed that PEDOT(PSS) films deposited on Pt are thinner than on Au although the parameters of the electrochemical deposition were identical. The EQCM and XPS analysis results are in agreement that with increasing electrochemical deposition time, the relative difference in the PEDOT(PSS) film thicknesses on Au and Pt gradually decreases. That is, the $\delta^{Au}_{PEDOT(PSS)}/\delta^{Pt}_{PEDOT(PSS)}$ ratio approaches 1. It is interesting to note that a similar trend was observed in water contact angle measurements on PEDOT(PSS) films [2]. While a

statistically significant difference was recorded in the contact angles over thin, 0.1 μm PEDOT(PSS) films (30±3^{o} on Pt and 35±4^{o} on Au), the difference in the water contact angles over thicker, 4 μm films faded (63±1^{o} on Pt and 63±4^{o} on Au). As discussed in Chapter 4, based on photon energy dependent SR-XPS measurements, the hydrophilicity of the PEDOT(PSS) films was related to the PSS_{tot}/PEDOT ratio, which was higher on Pt than on Au [34]. The contact angle data are in agreement with the SR-XPS findings, i.e., thin PEDOT(PSS) films are more hydrophilic on Pt than on Au. To confirm the SR-XPS results, PSS_{tot}/PEDOT ratios in this study were calculated from XPS spectra collected before the first etch cycle (i.e. etch time, t=0) in order to obtain ratios on the surface of pristine PEDOT(PSS)-coated Au and Pt electrodes. The PSS_{tot}/PEDOT ratios on Au and Pt in this study (0.43 and 0.91) closely match those obtained with SR-XPS (0.24 and 1.16) on both Au and Pt, respectively [34].

Figure 5.5 shows characteristic SEM images of thin PEDOT(PSS) films on Au and Pt substrates recorded after 15 s electrochemical deposition. The SEM image of PEDOT(PSS) on Au (Figure 5.5a) shows a few, relatively large polymer clusters while the image recorded on Pt (Figure 5.5b) shows a larger number of significantly smaller clusters. The insets in Figure 5.5 show the largest clusters formed on the Au and Pt electrode surfaces. The other clusters on Au were still quite large compared to those on Pt. The remaining clusters on Pt, however, were much smaller in size compared to its largest cluster, as shown in Figure 5.5b.

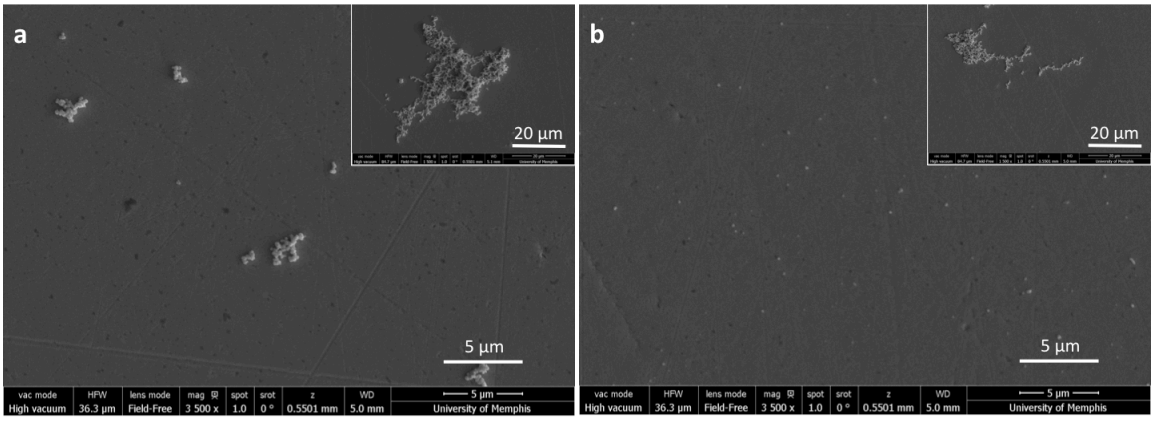

Figure 5.5. SEM images of PEDOT(PSS) films grown galvanostatically on Au (a) and Pt (b) substrates with 0.2 mA/cm^2 current density and 15 s electrolysis time. Horizontal field width (HFW) = 36.3 µm. Inset: The same films in a different area of the electrode shown with HFW = 84.7 µm.

Though the films are referred to being a certain "thickness", SEM images indicate that the electrochemical deposition results rather in randomly distributed PEDOT(PSS) clusters (with 45-220 nm cluster sizes) on Pt and significantly larger aggregates on Au electrodes. The patchy coatings of the electrode surfaces after short electrolysis time explains the relatively large Au and Pt atomic percentages measured at t=0 on Au and Pt electrode surfaces after 15 s polymerization times (Figures 5.4 a & b).

In this study, we used EQCM to demonstrate the differences in PEDOT(PSS) films deposited over Au and Pt electrode surfaces. However, our primary aim was not the quantitative determination of PEDOT(PSS) thicknesses but rather to show that the differences in the electrochemical behavior of SC K^+ ISEs could be traced back to differences in the formation of PEDOT(PSS) on Au and Pt substrate electrodes.

CONCLUSIONS RELATED TO THE DIFFERENCES IN ELECTROCHEMICALLY DEPOSITED PEDOT(PSS) FILMS ON Au AND Pt SUBSTRATE ELECTRODES

Galvanostatic deposition of PEDOT(PSS) produces different amounts of polymer on Au and Pt substrate electrodes under identical polymerization conditions. Frequency-time transients collected by EQCM during PEDOT(PSS) polymerization onto Au and Pt-coated quartz crystals showed a higher rate of polymer growth on Au during the initial 15 seconds of polymerization, after which the rates of growth on Au and Pt became similar. The differences seen by EQCM were confirmed by XPS etching studies and SEM images. XPS etching studies showed that the films deposited on Au were thicker than on Pt after both 15 s and 71 s electrodeposition times. With increasing electrodeposition time, the relative film thickness differences between Au and Pt became smaller. SEM analysis of the PEDOT(PSS)-coated Au and Pt surfaces showed that the electrochemical deposition produced randomly distributed 45 to 220 nm size PEDOT(PSS) clusters on Pt and significantly larger aggregates on Au electrodes. The differences in the initial deposition rates of PEDOT(PSS) (the rate of the polymer growth in the first 15 s) on Au and Pt suggest that these initial seconds of polymerization dictate the morphology and stoichiometry of PEDOT(PSS) on the different substrate electrode surfaces. Apparently, these differences in the morphology and chemical composition of the initial PEDOT(PSS) layers have a decisive role in the final electrochemical characteristics of SC ISEs built with PEDOT(PSS) as solid contact, as evidenced by their different equilibration times and standard potentials. Collectively, these results provide additional evidence for the newly determined importance of the substrate electrode/conductive polymer interface in the overall electrochemical characteristics of SC ISEs.

CHAPTER 6

POLY(3-OCTYLTHIOPHENE) AS SOLID CONTACT FOR ION-SELECTIVE ELECTRODES: CONTRADICTIONS AND POSSIBILITIES

INTRODUCTION

PEDOT(PSS) brings about many favorable characteristics and our studies with PEDOT(PSS) have led to better understanding of the contributions of the individual phase boundaries to the overall electrochemical response of SC ISEs [22, 34, 35]. However, the hydrophilic properties and hydrogel-like behavior of PEDOT(PSS) is a disadvantage when PEDOT(PSS) is utilized as an ion-to-electron transducer in SC ISEs. It has previously been reported that highly hydrophobic ion-to-electron transducers are beneficial in SC ISEs [11]. Due to its hydrophobic properties, POT is one of the most commonly used CPs in SC ISEs. It is considered uniquely advantageous in combination with plasticized polymer membrane-based ion-selective electrodes. However, the reports on the performance characteristics of POT-based SC ISEs are quite conflicting [38, 39] and the search for an optimal hydrophobic ion-to-electron transducer is still active. Recently, Lindfors suggested the utilization of polyazulenes as a novel SC for ISEs [11] and our lab showed the benefits of using a hydrophobic derivative of PEDOT, PEDOT-C_{14}, as SC. The advantageous properties of PEDOT-C_{14}–based SC ISEs will be discussed in Chapter 7 [40].

In this chapter, we summarize the conflicting reports on POT-based SC ISEs and show our approaches to build POT-based SC ISEs with short equilibration time, minimal potential drift and adequate sensor-to-sensor reproducibility of the standard potentials. Among the variety of performance characteristics of ISEs, we focus on these three sensor

properties because in our view these are directly influenced by the properties of the CP as well as the interfaces between the CP and the electron-conducting substrate and the membrane. The conflicting data published in the literature may originate from differences in the (i) POT film itself, (ii) substrate electrode, (iii) ion-selective membrane, and can be the consequence of an unrecognized partial or complete delamination of the ISM from its POT contact due to an aqueous film formation between the ISM and its POT contact. Since some of the papers on the POT-based SC ISEs were published before the simple test to trace the formation of an aqueous layer became available [41], this possibility is not considered in our overview.

Drop-cast vs. electrochemically deposited POT

POT can be deposited over the electron conductive substrate by drop-casting or electrochemically [42]. Drop-cast POT [43] is said to be in its undoped or neutral form. However, as it has been shown by FTIR-ATR spectroscopy, the doping level in the commercially available POT for drop-casting (average molecular weight ~ 34 kD) is not zero. FTIR-ATR spectra of POT films drop-cast over Pt-sputtered ZnSe crystals show bands of both the neutral form of POT and doping induced bands. The undoped form has low conductivity (1×10^{-6} S/cm) [10] while the oxidized doped form has high conductivity (0.4 S/cm) [42]. Lindfors reported poor day-to-day reproducibility and positively drifting potentials for drop-cast POT-coated GC electrodes (without ISM) in 0.1 M KCl [44] but negatively drifting potentials in 10^{-3} M $CaCl_2$ [10]. The positive and negative drifts were interpreted as a consequence of the gradual oxidation or reduction of the POT film, respectively. However, there were significant differences in the experimental conditions, e.g., (i) in the material and surface area of the substrate

electrodes, (ii) in the thicknesses of the POT films, (iii) in the composition of the solutions in contact of the POT-coated electrodes during the potential stability measurements, and (iv) in the illumination during the measurements, all of which could also contribute to the inconsistencies in the stability of the POT-based electrodes.

SC ISEs fabricated with POT as an internal solid contact do not show oxygen sensitivity [45, 46]. However, it is well known that POT is light sensitive, which significantly limits its application [44]. In addition, it appears that the light sensitivity is different for the drop-cast and electrochemically deposited POT films [44]. However, it is not clear how much the light sensitivity of POT contributed to the drift values reported for POT-based electrodes. It is also not clear how the drift relates to (i) the conductivity and the redox state of the polymer, (ii) the molecular mass of the drop-cast POT, e.g., 25 kD vs. 34 kD (Aldrich catalogue numbers - 682799 and 445711), and (iii) the conditions of the electrochemical deposition (galvanostatic vs cyclic voltammetry (CV)) or the incorporated counter ions [47] during the electrochemical deposition.

In summary, after more than twenty years of the pioneering works of Bobacka, et al. [16], due to the differences in the experimental conditions in the diverse studies, it is still not clear how to build robust POT-based SC ISEs with low drift and highly reproducible standard potentials. In other words, the main sources of the inconsistencies in the reported results and the main hurdles towards addressing these inconsistencies remain unclear.

POT-based ISEs on different substrate electrodes

The substrate electrode is generally not considered as a factor that might influence the performance of SC ISEs. Although in most of the studies on SC ISEs with POT as

solid contact glassy carbon (GC) is used as a substrate electrode, graphite rods [48], gold disks [46], screen-printed gold over silver [49], platinum sputtered ZnSe [10] and gold sputtered copper [38] have also been used as electrode substrate. In studying the water uptake, impedance characteristics, and potential stability of SC Ca^{2+} ISEs with POT as SC, Lindfors used Pt as substrate electrode sputtered over a ZnSe crystal for the hyphenated FTIR-ATR/impedance spectroscopy experiments but GC electrodes for the potentiometric measurements [10].

Based on our experience with PEDOT(PSS)-based SC ISEs, in our view, the selection of the substrate electrode may significantly influence the SC ISE responses. In Chapters 3 and 4, we showed that the equilibration time of solid contact sodium, potassium, and hydrogen ion-selective electrodes with PEDOT(PSS) as SC is significantly shorter with Au and GC substrates compared to Pt as substrate electrode. SR-XPS results showed that these differences are likely due to the formation of a more hydrophilic PEDOT(PSS) film on Pt substrate compared to Au. More so, EQCM experiments showed that utilizing the same parameters for electrochemical deposition leads to thinner PEDOT(PSS) films on Pt compared to Au [35]. Based on these results, the difference in the equilibration times and standard potentials have been traced back to the substrate electrode|PEDOT(PSS) interface [22, 34, 35].

POT-based ISEs with different ion-selective membranes

POT-based SC ISEs have previously been tested for the measurement of different ions (K^+ [11, 38], Ca^{2+} [10, 23, 38, 45, 46], Pb^{2+} [38, 46, 50], Ag^+ and I^- [38], Cl^- [49, 51], nitrate [48], and carbonate [39]) using a variety of sensing membranes [polyvinyl chloride (PVC) [11, 23, 39, 45, 48-51], silicone rubber (SR) [10], polyurethane (PU) [45,

49], and poly (methyl metacrylate)/poly (decyl methacrylate) (PMMA/PDMA) [38, 46]]. In other studies, the POT film loaded with an ionophore and ion-exchange sites served as the ion-selective membrane [52, 53] or POT was dissolved in the ion-selective membrane cocktail [54] which was deposited over an electron-conducting substrate (termed as single-piece ISEs) [52-54]. The drift values recorded with these electrodes range between -2.9 mV/h (in combination with Cl^--selective PVC membrane) and ~+4.0 mV/h with a carbonate-selective PVC membrane [39] and almost any value between. For example, 0.0 mV/h drift was reported for POT-based silver ISEs with a PMMA/PDMA membrane in 10^{-3} M Ag^+ ion solution [38]. Unfortunately, a survey of the drift data does not help to trace the source of the recorded drift values, which are not always monotonous and individual electrodes from the same batch may drift in opposite directions [48].

The strategies to manufacture SC ISEs with highly reproducible standard potentials cannot be separated from the efforts to improve their potential stability. Both aim towards the development of robust, maintenance-free sensors, which depending on the task, can be used without calibration or need only infrequent single point calibrations. In general, the sensor-to-sensor potential reproducibility of SC ISEs is significantly worse than for the conventional ISEs with liquid inner contact. For example, a POT-based SC Ca^{2+} ISE in combination with a SR membrane had a reported sensor-to-sensor potential reproducibility of ±6.7 mV [10]. However, the standard deviation of the potential values measured in the same solution with a POT-based Ca^{2+} ISEs using a plasticized PVC membrane (n=3) was only ±1.0 mV [23]. On the other hand, since the reported standard deviations were assessed from only three (n=3) measurements, one should treat these results with caution.

To achieve a sensor-to-sensor potential reproducibility similar to the conventional ISEs, different redox couples/centers have been implemented into the CP layer [31, 55], the ion-selective membrane [56, 57], or applied onto the electron-conducting substrate [7]. However, none of these experiments used POT-based SC ISEs as the model system. Gyurcsanyi [31] and Sutter [55] fabricated K^+ and Pb^{2+}-selective electrodes with electrochemically deposited polypyrrole as an inner contact loaded with $K_4[Fe(CN)_6]$/ $K_3[Fe(CN)_6]$ as a redox couple and achieved drift values less than 1 mV/day. Zou, et al. implemented Co(III)/Co(II) into the ion-selective membrane of an electrode with a self-assembled monolayer of 1-hexanethiol as the inner contact layer and achieved ±0.7 mV sensor-to-sensor potential reproducibility after one hour of solution contact [57]. Unfortunately, however, the impressive reproducibility was lost after 24 hours and the standard deviation of the recorded potentials increased to ±16.3 mV. Vanamo and Bobacka suggested setting the standard potential of PEDOT(PSS)-based ISEs electrochemically by short-circuiting the fully-fabricated ISEs with one another or with a reference electrode [58]. The method of Vanamo provided SC ISEs with very similar standard potentials. However, with time, the standard deviation of the potential values increased as the potentials of the disconnected electrodes gradually drifted back towards their original values.

In this study, the ambiguous drift and poor potential reproducibility of POT-based ISEs are addressed. In our view, the key is to control the interfacial potentials between the electron-conducting substrate and the conductive polymer (substrate|CP) as well as between the conductive polymer and ISM (CP|ISM). This requires a POT film with a well-defined redox potential (a constant POT/POT^{n+} ratio). To set the potential of the

POT film, it has been loaded with a 7,7,8,8-tetracyanoquinodimethane (TCNQ/$TCNQ^{\bullet -}$) redox couple. The structural change of TCNQ following a single electron reduction to $TCNQ^{\bullet -}$ is shown in Figure 6.1 [59].

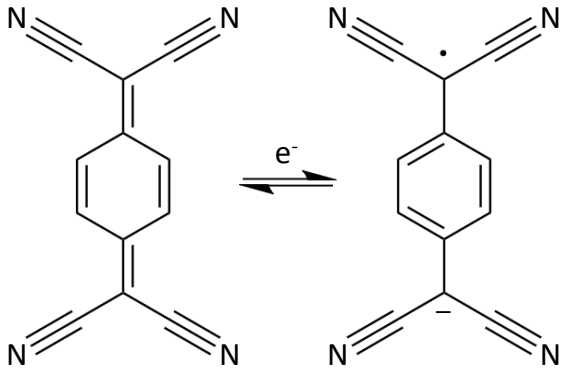

Figure 6.1. Chemical structures of TCNQ (left) and $TCNQ^{\bullet -}$ (right).

An approximately 1:1 TCNQ/$TCNQ^{\bullet -}$ ratio in the POT film has been achieved through potentiostatic control of the redox couple-loaded conductive polymer, denoted as POT+TCNQ. It is hypothesized that once the POT film has a stable, highly reproducible redox potential, it will provide stable and reproducible interfacial potentials between the POT film and the electron-conducting substrate and result in SC ISEs with improved potential stability and reproducibility. Towards this goal, the potentials of Au, GC, and Pt electrodes with drop-cast POT film coatings were recorded as function of time following the immersion of the electrodes into KCl solutions. Some of the POT films were loaded with TCNQ (POT+TCNQ) and coated with a K^+-selective membrane. The improvement in the equilibration time, potential stability, and sensor-to-sensor reproducibility, as a

consequence of both the incorporation of TCNQ in the POT film and the potentiostatic control of the TCNQ/TCNQ$^{\bullet -}$ ratio, is reported.

EXPERIMENTAL

Chemicals

Poly(vinyl chloride) (PVC, high molecular weight), bis(2-ethylhexyl) sebacate (DOS), potassium tetrakis(p-chlorophenyl)borate (KTpClPB), potassium ionophore I (Valinomycin), 7,7,8,8-tetracyanoquinodimethane (TCNQ), and poly(3-octylthiophene-2,5-diyl) (POT) (Catalogue number 445711) were purchased from Sigma Aldrich. Tetrahydrofuran (THF) and chloroform were products of Fisher Scientific. The aqueous solutions were prepared with 18.2 MΩcm resistivity DI water from Millipore Milli-Q A10 system. The potentiometric responses of the solid contact electrodes were tested using potassium chloride (KCl) standard solutions prepared by serial dilutions. KCl was purchased from Fisher Scientific. Argon and oxygen were obtained from Airgas (Airgas Inc., Radnor, PA, USA).

Electrodes and Fabrication

The Au and Pt disk electrodes (Bioanalytical System, Inc. U.S.A.) ($d_{Au/Pt}$=1.6 mm, $d_{electrode}$=6.4 mm) and Au and GC disk electrodes (MINERAL, Warsaw, Poland) ($d_{Au/GC}$=1.0 mm, $d_{electrode}$=6.3 mm) were polished with aqueous dispersions of alumina (1.0 μm (Buehler, Lake Bluff, IL) and 0.3 μm (Electron Microscopy Sciences, Hatfield, PA)) on microfiber polishing cloths. Between polishing steps, the electrodes were rinsed with DI water. Following the final polishing step, the electrodes were cleaned by sonication in DI water for 20 minutes then rinsed with DI water. The POT-coated Au, GC, and Pt electrodes were fabricated by drop-casting 0.94 μL or 0.42 μL of 10 mg/mL

solutions of POT in chloroform onto the 1.6 mm or 1.0 mm diameter electrode substrates, respectively. The same volumes were used for the deposition of the TCNQ-loaded POT films, however for this deposition, THF has been selected as solvent with 10 mg/mL POT and 5 mg/mL TCNQ concentrations because larger amounts of TCNQ could be dissolved in THF than in chloroform. The areas of the drop-cast POT and TCNQ loaded POT films were always significantly larger (between 2.2 and 3.0 times) than the areas of the conducting substrates to ensure full electrode coverage. Due to the uncertainty in the deposited areas (a consequence of the manual drop-casting), the thicknesses of the POT films also varied in a wide range (~1.5 ± 0.6 μm). The electrodes were left to dry for at least 2 hours prior to the ion-selective membrane deposition over the POT or POT+TCNQ films to create fully fabricated SC ISEs. The POT-coated or POT+TCNQ-coated electrodes were left to dry overnight in a desiccator if they were tested without ISM coating.

Membrane Cocktails

Potassium-selective SC ISEs were fabricated by drop-casting a K^+ ion-selective membrane cocktail over the POT-coated or POT+TCNQ-coated electrode surfaces. The composition of the membrane was 100 mg PVC, 200 mg DOS, 6.1 mg Valinomycin, 1.3 mg KTpClPB in 1.5 mL THF. From this membrane cocktail, 11 μL or 5 μL were dispensed over the 1.6 mm and 1.0 mm diameter electrode surfaces, respectively. The ion-selective membrane cocktail was always spread beyond the borderlines of the drop-cast POT or POT+TCNQ films, i.e., the ISM covered the entire POT or POT+TCNQ film as well as a fraction of the insulating electrode body (~5 mm diameter circular area) to

ensure proper adhesion of the ISM. The fully fabricated SC ISEs were left to dry overnight in a desiccator over silica orange beads exposed to dimmed room light.

Methods

Potential Stability Measurements

The potentials of the electrodes coated with POT and POT+TCNQ (without an ISM) were tested in air-saturated, argon-saturated, and oxygen-saturated 0.1 M KCl solutions over 24 hours versus an Orion Ag|AgCl|KCl(3M)||LiOAc(1M) double junction reference electrode (Model 900200) using a 16-channel data acquisition system (Lawson Labs Inc., Malvern, PA), which was connected to a computer equipped with L-EMF Suite 2.0 software. The potential recording started immediately after the electrodes were immersed in the solution. The fully fabricated SC ISEs were tested the same way but only in air saturated solutions, i.e., the potentials of the completely dry electrodes (just removed from the desiccator) were recorded for 24 hours during their equilibration in 0.1 M KCl solution. The potential recording started immediately after the electrodes were immersed in the solution. After the potential stability measurements, the potentiometric response of the ISEs was tested using 10^{-1} M, 10^{-2} M, and 10^{-3} M KCl solutions. When these experiments were performed under regular laboratory lighting (~242 nW measured with Newport 1830–C optical power meter equipped with a Model 818-SL detector), the reproducibility of the potential measurements (±5-30 mV), and consequently the reproducibility of the parameters of the calibration curves were unacceptable. However, when the measurements were performed at dimmed light in a dark room (26 nW), the reproducibility of the potential measurements significantly improved (±0.1-2.0 mV) and the calibration curves lead to near Nernstian responses (57.1±0.3 mV/dec).

Electrode Polarization

To minimize the drift of the fully fabricated K^+ ISEs with POT or TCNQ-loaded POT (POT+TCNQ) as solid contact, the electrodes were polarized to 285 mV, 125 mV, or 0 mV in 0.1 M KCl. The polarized potential values were selected based on the potential values measured after 24 hours of conditioning in 0.1 M KCl solution. In these experiments, the SC ISEs were used as the working electrode, a coiled Pt wire served as counter electrode, and an Orion Ag|AgCl|KCl(3M)||LiOAc(1M) double junction reference electrode completed the cell. The electrodes were polarized for 60 minutes using an Autolab (Metrohm, Utrecht, The Netherlands) potentiostat/galvanostat running General Purpose Electrochemical System (GPES) 4.9 software. The potential values for polarization were selected by successive approximation. The first polarization potential was selected based on the "stabilized" potential values measured at the end of the potential stability tests with the POT+TCNQ-based ISEs. After 60-minute polarization periods, the electrodes were disconnected from the potentiostat, rinsed with DI water, dried with argon for 2 minutes, and placed in an argon-filled desiccator over silica orange beads exposed to dimmed room light overnight. The next day, the completely dried, previously polarized electrodes were placed again into 0.1 M KCl. The potential recording started immediately after the electrodes were immersed in the solution and the potentials were recorded for 24 hours to determine the potential stability of the previously polarized electrodes. If the electrode during this second (after polarization) potential stability test still had a negative potential drift, a second polarization potential was applied at a lower potential value. The adjusted polarization potential was also applied to freshly prepared SC ISEs.

RESULTS AND DISCUSSION

Potential Stability of Au, Pt, and GC electrodes with POT and POT+TCNQ coatings

In Figure 6.2, the drift values recorded with POT- and POT+TCNQ-coated Au, GC, and Pt electrodes are summarized in a box plot format. The measurements were performed in air, oxygen, and argon-saturated 0.1 M KCl solutions for 24 hours to study the influence of the substrate electrode (Au, Pt, and GC) and the incorporation of the $TCNQ/TCNQ^{\bullet -}$ redox couple into the POT film on the potential stability of the electrodes. The drift values (mV/h) were calculated from the potential data collected during the last 14 hours of the experiment (between 10 h and 24 h).

The POT-coated Au and GC electrodes have large drift values and the values are scattered in a wide range but apparently the potential drift is not influenced by the oxygen concentration of the solution (the drift values do not show any noticeable trend between the O_2, Ar, and air-saturated KCl solutions). These results are in agreement with earlier findings [45, 46] that the ambiguous drift and poor potential reproducibility of POT-based ISEs is not related to gradual oxidation of the POT film by dissolved oxygen. Among the POT-coated electrodes, those prepared on Pt electrodes had relatively small drift and the standard deviations of the drift data were also small compared to the other electrodes. The significantly smaller drift values recorded with the POT-coated Pt electrode compared to POT-coated Au and GC electrodes implies that the substrate electrode|POT interface plays an important role on the potential stability. In agreement with results from the previous chapters, these results indicate that the substrate|CP interface is critical in the design of SC ISEs [22, 34, 35].

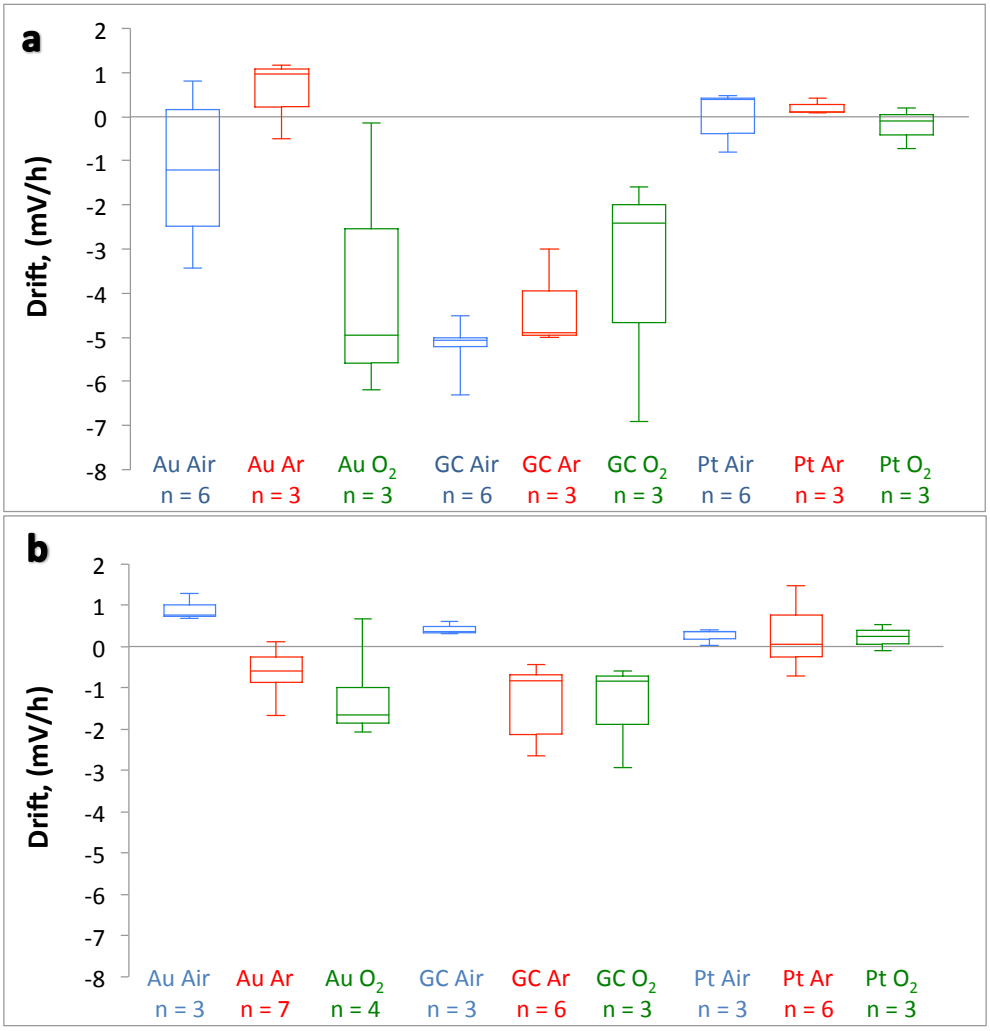

Figure 6.2. Box plots representing drift values of a) POT-coated and b) POT+TCNQ-coated Au, GC, and Pt electrodes in air, Ar, and O_2-saturated 0.1 M KCl. The drift values were calculated from the potential data collected between 10 and 24 hours of solution contact. The vertical axis of the box plot is the potential drift of the POT and POT+TCNQ-coated Au, GC, and Pt electrodes in the air, Ar, and O_2-saturated 0.1 M KCl solutions. The top and bottom whiskers represent the maximum and minimum values within the respective category while the box represents the middle 50% of the data. The horizontal line within each of the individual boxes represents the median value of the data.

As it is shown in Figure 6.2b, the incorporation of TCNQ into the POT film resulted in electrodes with significantly smaller drift in 0.1 M KCl compared to electrodes coated only with POT. The improvements are the most significant with the POT+TCNQ-coated Au and GC electrodes. To demonstrate the magnitude of the improvement in the recorded drift, in Figure 6.3 we show two representative potential-time transients recorded with a POT-coated and a POT+TCNQ-coated Au electrode in air-saturated 0.1 M KCl.

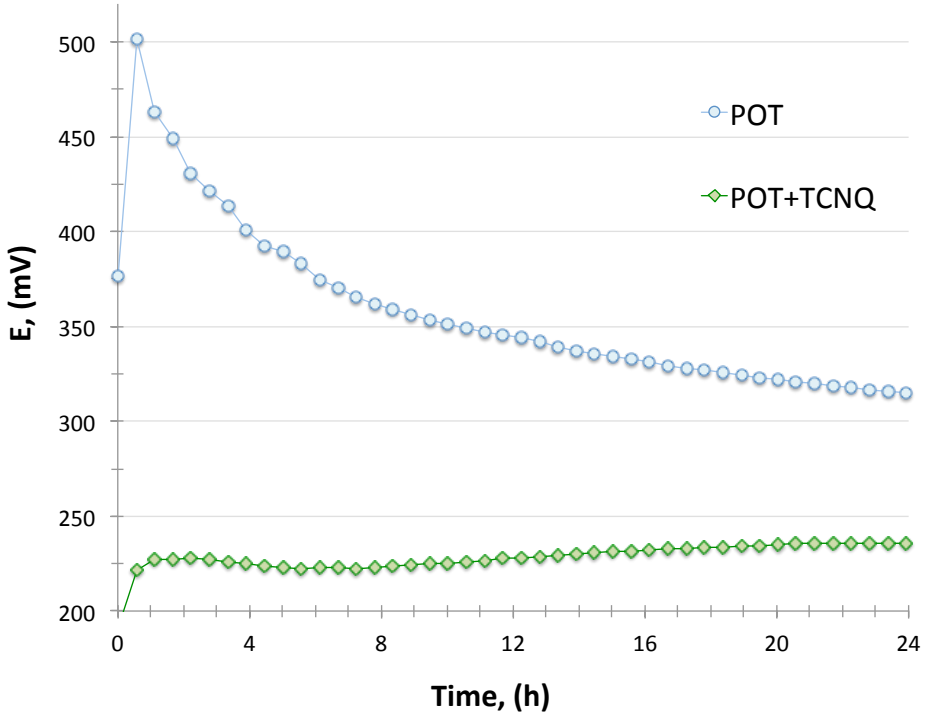

Figure 6.3. Representative examples of potential-time transients recorded with freshly prepared and dried POT-coated and POT+TCNQ-coated Au electrodes in 0.1 M KCl saturated with air.

As it is shown in Figure 6.3, the POT-coated Au electrodes have large (~ − 8 mV/h) negative drift in the first 24 hours. The negative drift indicates that the POT film becomes gradually reduced (converted further to its undoped, low conductivity form) in the aqueous KCl solution. In contrast to the POT-coated Au electrodes, the drift of the POT+TCNQ-coated electrodes is positive and significantly reduced (~ + 1 mV/h). The reduced drift suggests that the incorporation of TCNQ into the POT film sets comparatively stable redox equilibrium in the POT film, which poises the interfacial potential between the substrate electrode and the POT film.

Potassium ion-selective electrodes with POT and POT+TCNQ as solid contact

For this part of the study, the POT- or POT+TCNQ-coated Au and Pt electrodes were covered with K^+ ISMs and left to dry overnight in a desiccator. The following day, the potential vs. time transients of these fully fabricated ISEs were recorded in 0.1 M KCl for 24 hours and both the equilibration times and drift values between 10 and 24 hours were assessed. Next, the electrodes were polarized for 60 minutes to different predetermined potential values in the 0.1 M KCl, immediately removed from the solution, rinsed with DI water, dried with argon, and kept in a desiccator overnight. The potential stability measurement was then repeated the next day.

For example, since at the end of the initial equilibration (after 24 hours), the potentials of the POT+TCNQ K^+ ISEs approached ~+290 mV, they were first polarized to 285 mV (an extrapolated potential value based on the potential drift recorded after 24 h). After 60 min polarization, the electrodes were removed from the solution, rinsed with DI water, dried overnight, and the potential stability measurements were repeated the next day. The electrodes following this first polarization always had smaller drifts but the

potential of the ISEs were still drifting negatively. Therefore, using the protocol of successive approximation, the polarization of the electrodes was repeated with lower polarization potentials of 125 mV and 0 mV. In other experiments, freshly prepared electrodes were polarized to these adjusted potential values (125 mV and 0 mV) upon their initial exposure to 0.1 M KCl solution then dried overnight. The following day, their potential stability was tested for the first time. The goal of polarizing the electrodes to different potential values was to set the electrode potential close to the standard redox potential of the TCNQ/TCNQ$^{\bullet-}$ couple in the POT film ($E^0_{TCNQ/TCNQ^{\cdot-}} = 112\ mV$) where the concentration ratio of the oxidized and reduced forms of TCNQ/TCNQ$^{\bullet-}$ are close to an optimal 1:1 ratio. The role of the TCNQ/TCNQ$^{\bullet-}$ couple is to act as a redox potential buffer in the SC POT layer. Since 1:1 TCNQ/TCNQ$^{\bullet-}$ ratio offers the maximum buffer capacity, the potential drift of the POT-based sensors are expected to be the smallest with a 1:1 TCNQ/TCNQ$^{\bullet-}$ ratio. Since the redox potential of TCNQ is lower than the redox potential of POT, during polarization of the TCNQ-loaded films, it is assumed that the majority of the current is reducing TCNQ and the reduced TCNQ/TCNQ$^{\bullet-}$ couple reduces the POT film as they become in equilibrium. Conversely, during the polarization of POT ISEs without TCNQ, the POT film itself becomes further reduced. The equilibration times and the potential drifts of the electrodes recorded in 0.1 M KCl without polarization (N/A) and with polarization to different potentials are summarized in Table 6.1 and Figure 6.4.

Table 6.1. Equilibration times of POT-based ISEs without polarization and POT+TCNQ-based K^+ ISEs with polarization treatment at 125 mV reported as mean ± S.D.

	Equilibration Times ± S.D. in minutes (n)	
Electrode Substrate	**POT (N/A)**	**POT+TCNQ (125 mV)**
Au*	8±5 (11)	1.0±0.7 (6)
Pt*	16±16 (11)	1±1 (5)
GC	2±2 (10)	1.9±0.4 (6)

*Denotes statistically significant difference between POT and POT+TCNQ ISEs on an individual substrate (Au, Pt, or GC), as determined by Welch's t-test (t-test with unequal variances).

The equilibration times following implementation of TCNQ into the POT film along with polarization at 125 mV were significantly shorter on Au and Pt substrates compared to the POT-based ISEs without treatment ($p=0.0005$ and $p=0.01$, respectively). The equilibration times of ISEs built on GC substrate electrodes did not show improvement ($p=0.77$), due to the already short equilibration times achieved with POT-based ISEs without the incorporation of TCNQ and polarization.

As it is seen in Figure 6.4, despite the expectation based on Figure 6.3 the drift of the K^+ ISEs with POT and POT+TCNQ as SC without polarization are basically the same around –1.4 mV/h. The polarization of the fully fabricated ISEs with POT as solid contact did not result in improved drift values. Only the direction of the drift changed upon polarization. The drift with POT-based ISEs on Au and Pt (Au, Pt|POT|ISM) without polarization was initially negative but after polarization (60 minutes at 125 mV),

the calculated drift was positive. The change in the sign (the direction) of the drift suggests that with adequate polarization, ~0 mV/h drift may be achieved.

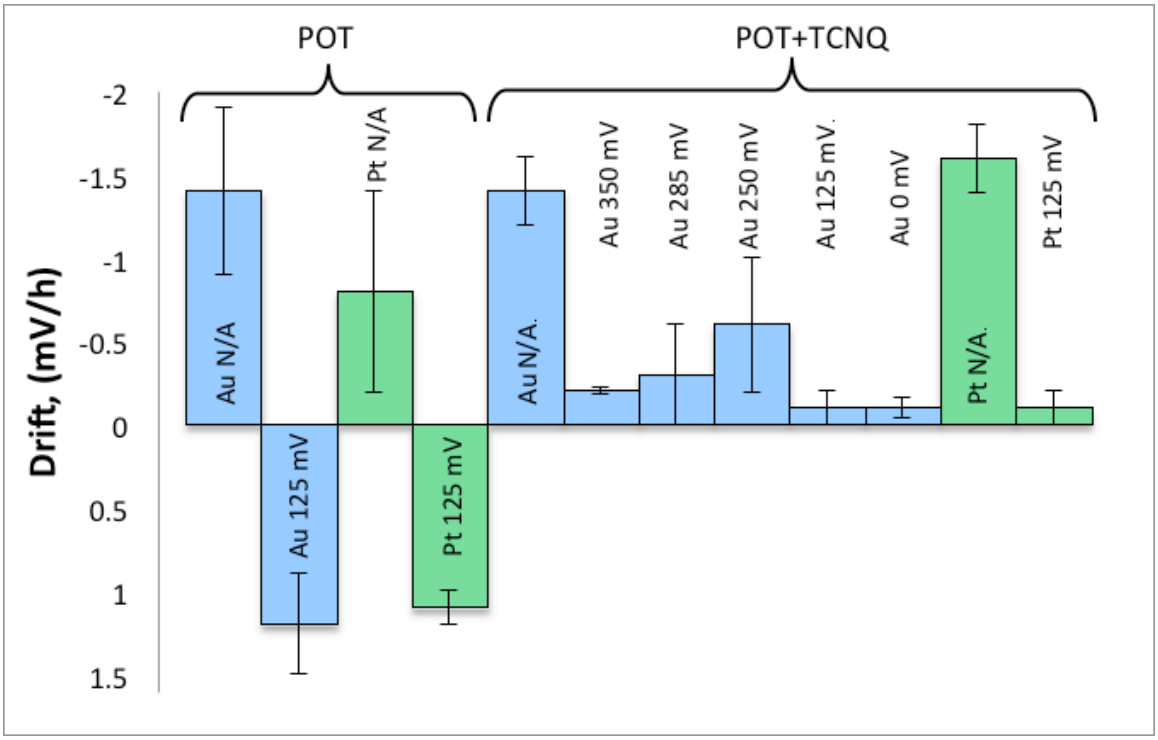

Figure 6.4. Drift values of POT- and POT+TCNQ-based K^+ ISEs on Au and Pt substrate electrodes with and without polarization. The drift values were calculated from the potential data collected between 10 and 24 hours of solution contact in 0.1 M KCl (N/A indicate drifts recorded with electrodes without potential polarization). Note: The y-axis has been inverted (up is now negative, down is positive).

In contrast to the electrodes with POT as solid contact, the polarization of the electrodes with POT+TCNQ as SC resulted in significant improvements. The drift of the K^+ ISEs both on Au and Pt substrate dropped to −0.1 mV/h when polarized to 0 mV (Au) or 125 mV (Au and Pt). The standard redox potential of TCNQ/$TCNQ^{\bullet-}$ redox couple in

the POT film $E^0_{TCNQ/TCNQ^{\cdot-}}$ has been estimated as ~112 mV from a series of cyclic voltammograms (CVs) recorded with the POT+TCNQ-coated Au electrodes in 0.1 M KCl (see Appendix B). We considered the $E^0_{TCNQ/TCNQ^{\cdot-}}$ ~112 mV only as an estimate due to the large peak separation between the oxidation and reduction peaks (~318 mV) and because it is significantly more positive than the standard potentials reported for the TCNQ/$TCNQ^{\bullet-}$ couple based on CVs recorded in acetonitrile (Appendix B) [60]. The very similar low drift values observed following the polarizations of the electrodes with POT+TCNQ as solid contact to 125 mV or 0 mV suggest that the standard potential of the TCNQ/$TCNQ^{\bullet-}$ couple in the POT film may be between these two values.

In Figure 6.5, we show representative examples of the potential-time transients recorded with SC K^+ ISEs with POT and POT+TCNQ as solid contacts without (N/A) and with polarizations to different potential values (285 mV, 125 mV, and 0 mV).

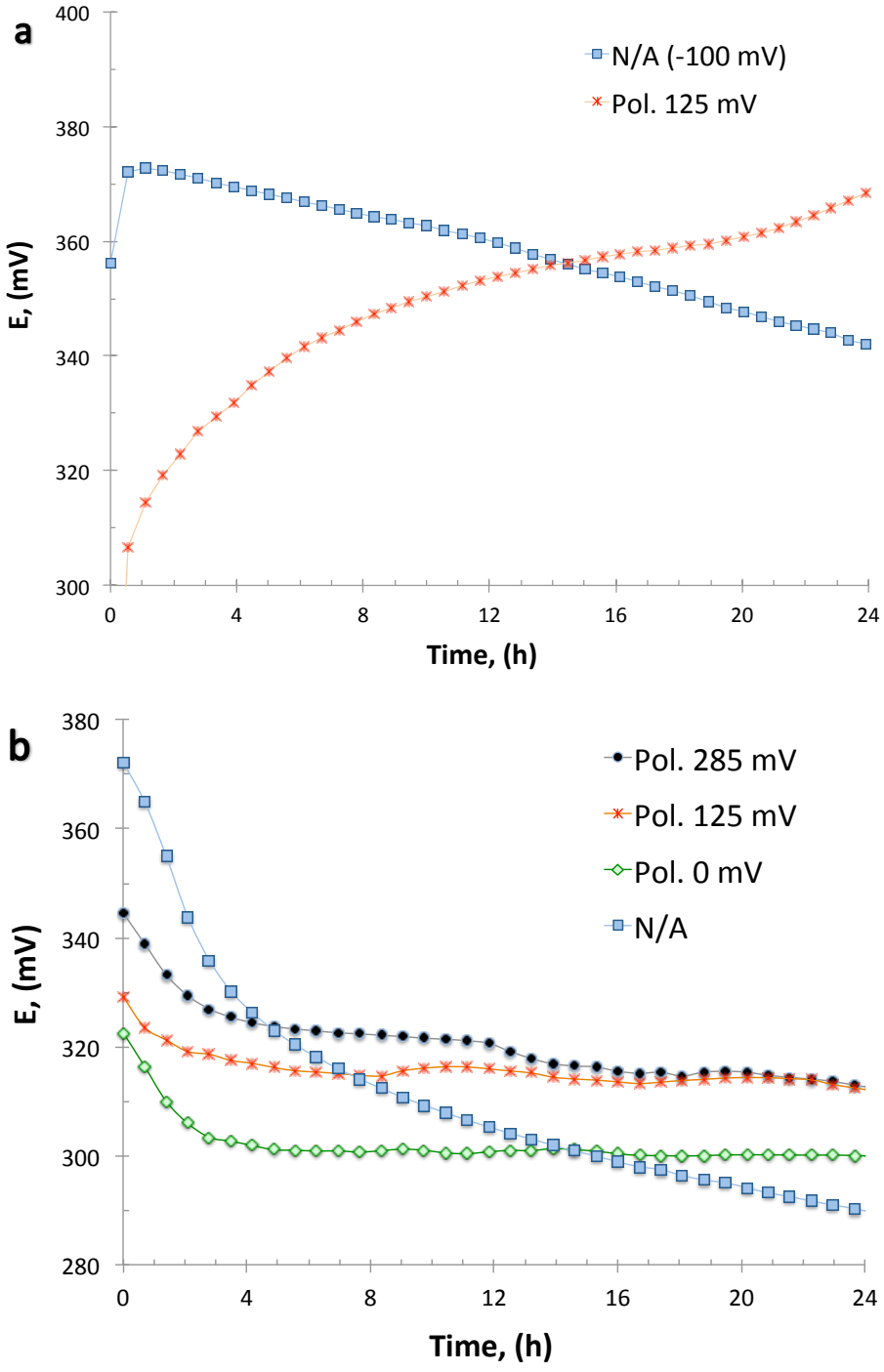

Figure 6.5. Potential-time transients of a) POT-based and b) POT+TCNQ-based ISEs on Au substrate in 0.1 M KCl over 24 hours with and without polarization (Note: Transient of POT-based ISE with no applied potential (N/A) was shifted -100 mV).

In summary, the implementation of TCNQ into the POT film along with polarization improved the equilibration time and potential stability of the SC ISEs built on both Pt and Au substrates. After ~5 hours of solution contact, the drift of the polarized POT+TCNQ-based ISEs dropped below 0.1 mV/h. Apparently, the incorporation of a redox couple into the POT film poises the potential of the POT film and the metal|POT interfacial potentials. However, the drift could not yet be reduced below −0.1 mV/h by fine-tuning the polarization potential, i.e., the TCNQ/$TCNQ^{\bullet -}$ ratio in the POT film.

Based on previous reports [58] and our successes in minimizing the equilibration time and potential drifts of POT-based SC ISEs, we assumed that the polarization of the electrodes to predefined potential values would also improve the sensor-to-sensor potential reproducibility. In Figure 6.6, the potential values recorded after 24-hour "conditioning" (measurement of the potential drifts) are shown for POT- and POT+TCNQ-based K^+ ISEs without polarization and with 60-minute polarization to 125 mV. As it is seen in Figure 6.6, the standard deviation of the measured potentials is very large for the POT-based ISEs without polarization (±36 mV). Although the incorporation of TCNQ into the POT film and the polarization of the electrodes slightly improved the sensor-to-sensor reproducibility of the potential data, the standard deviation of the potential values remained quite large. The smallest standard deviation of the potential data (± 6 mV) was measured within a single batch of POT+TCNQ-based ISEs (n = 3) following polarization to 125 mV. All results shown in Chapter 6 related to polarization of SC ISEs are based on polarization times of 60 minutes. To determine if longer polarization times would further improve the sensor electrochemical performance, POT+TCNQ-based ISEs were polarized for 2h, 4h, and 8h. It was determined that longer

polarization times did not further improve the potential reproducibility or potential stability (Appendix C).

Similar to our conclusion on the optimization of the potential drift of POT-based SC ISEs, for SC ISEs with identical standard potentials, all potential terms contributing to the standard potential of the SC ISEs must be well-defined: (i) substrate electrode|POT interfacial potential; (ii) standard potential of the POT film, i.e., constant POT/POT^{n+} ratio in the film; and (iii) POT|ISM interfacial potential. We assume that the incorporation of TCNQ into the POT film provides well-defined potentials for the POT film and for the substrate electrode|POT interface. However, in our view the interfacial potential between the POT film and the ISM is not well defined without a potential determining ion-exchange with high exchange current density. We believed that this may be achieved through the incorporation of the appropriate salt of TCNQ into the POT film [8]. To aid in the ion-exchange between the POT+TCNQ film and the K^+ ISMs, we implemented TCNQ into the POT film as potassium TCNQ salt (KTCNQ) using a method described previously [8]. In this way we were able to improve the sensor-to-sensor standard potential reproducibility from ±25 mV to ±13 mV using POT+KTCNQ-based SC and 60 min polarization of the K^+-ISE to 125 mV. Unfortunately the ±13 mV standard deviation is still too large to satisfy the requirements for a calibration-free electrode. More so, the incorporation TCNQ as K^+ salt into the POT+TCNQ film did not improve the potential stability of the electrodes. The electrodes with KTCNQ-loaded POT as SC had -0.2±0.1 mV/h drift following 60 min polarization at 125 mV. The influence of the KTCNQ concentration in the POT film on the potential stability and

sensor-to-sensor potential reproducibility of the respective electrodes was not studied in this work.

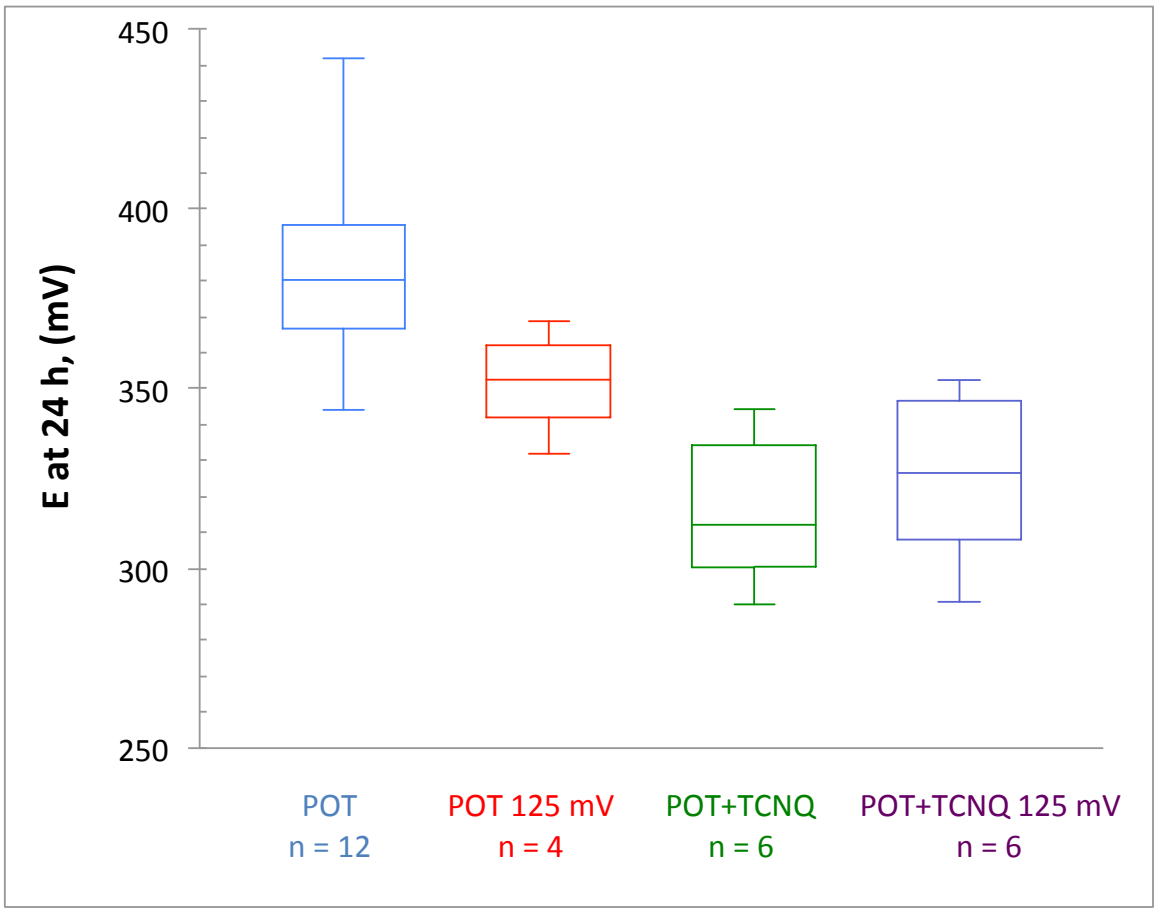

Figure 6.6. Box plots of the potential values of K^+ ISEs on Au substrate electrodes with POT and POT+TCNQ as solid contact after 24-hours exposure to 0.1 M KCl solution. POT- and POT+TCNQ-based K^+ ISEs are shown without polarization and with 60 minute polarization at 125 mV. The vertical axis of the box plot shows the potential values recorded after 24-hour "conditioning" while on the horizontal axis the composition of the different SCs and the treatment (the polarization potential) of the K^+ ISEs is indicated. The top and bottom whiskers represent the maximum and minimum potential values recorded with the respective electrodes while the box represents the middle 50% of the recorded potential data. The horizontal line within each of the individual boxes represents the median value of the data.

CONCLUSIONS RELATED TO POT-BASED SC ISES WITH AN INCORPORATED REDOX COUPLE AND POLARIZATION TREATMENT

POT has unique material characteristics to be used as an ion-to-electron transducer in SC ISEs. Despite its promising inherent features, the literature on POT-based ISEs is quite contradictory. To trace some of the contradictions, we catalogued the differences in the published works and implemented a redox couple, TCNQ/$TCNQ^{\bullet -}$, into the POT film of K^+-selective SC ISEs. The incorporation of TCNQ along with polarization of the SC ISE improved the equilibration time from ~9 minutes to ~2 minutes and improved the potential stability from -1.4 mV/h to -0.1 mV/h, in the range of the smallest drifts published with POT-based SC ISEs. We were able to use cyclic voltammetry to determine the approximate 1:1 TCNQ/$TCNQ^{\bullet -}$ ratio of the redox couple in POT+TCNQ films. It is believed that the TCNQ/$TCNQ^{\bullet -}$ couple poises the potential of the POT film and substrate|POT interfacial potential which, in summary, led to the improved potential stability. The incorporation of TCNQ into the POT film and the polarization of the ISEs hardly improved the sensor-to-sensor potential reproducibility.

Our data suggest that the material of the electron-conducting substrate (and therefore, the interfacial potential between the metal and the CP) has a significant influence on the overall potential stability of SC ISEs. However, once the CP is compounded with a redox couple, differences in the potential stability of SC ISEs built on different substrates decreased.

Based on the inconsistent literature data and our experience with the POT-based SC electrodes, despite its high hydrophobicity, POT does not appear to be an attractive CP to be used as ion-to-electron transducer in SC ISEs. The unsatisfactory performance

characteristics of the POT-based ISEs are largely due to the significant light sensitivity of POT. Small changes in the ambient light induced significant slow changes in the measured potentials. It is assumed that these non-reproducible, sluggish potential changes limited the attainable potential drifts and influenced the sensor-to-sensor potential reproducibility of the POT-based electrodes. Therefore, we shifted our focus onto a novel CP, a superhydrophobic derivative, PEDOT-C_{14}, which prior to our published results shown in Chapter 7 [40], was not used as a SC in SC ISEs.

CHAPTER 7

SOLID CONTACT pH SENSOR WITHOUT CO_2 INTERFERENCE WITH A SUPERHYDROPHOBIC PEDOT-C_{14} AS SOILD CONTACT: THE ULTIMATE "WATER LAYER" TEST

INTRODUCTION

In the search for a universally adaptable SC for ISEs, PEDOT-C_{14} stood out as a promising, hydrophobic, tetradecyl-substituted derivative of PEDOT, which is considered as the most favorable CP-based ion-to-electron transducer in SC ISEs. Beyond their ion-to-electron transducing properties, the CP layers are expected to deter the formation of an aqueous film between the SC and the ISM [61]. The presence of a water layer between the ISM and its SC can be detrimental to the performance of the SC ISE.

Although the test for the presence of an undesirable water layer appears to be simple [41], it is time consuming, and when the experimental conditions are not selected properly, it does not provide an unambiguous answer. In this paper, we propose recording the potential drifts of SC ISEs with pH sensitive membranes in samples with different CO_2 levels as the ultimate, fast test to prove the presence or absence of a water layer. When such electrodes are exposed to solutions with different levels of CO_2, the fast permeation of CO_2 across the ISM triggers changes in the pH, ionic strength, and activity coefficients in the aqueous film, if present [4, 62]. These changes are accompanied by a gradual change in the phase boundary potential on the backside of the pH membrane, and become apparent as a potential drift. However, with other membranes that do not have pH sensitivity, these changes may not be detectable [18, 62-64].

For most SC ISEs, the undesirable consequences related to the presence or the gradual formation of an aqueous film can be minimized by frequent calibrations. However, for SC pH sensors, especially in clinical diagnostics, the presence of a water layer is a serious potential source of error since the concentration of CO_2 in blood under normal physiological conditions may vary between ~20 and ~80 mmHg (2.6% and 6.6%) at 37°C. In this paper, we present data collected with electrodes utilizing PEDOT-C_{14} [65], a highly hydrophobic derivative of poly(3,4-ethylenedioxythiophene), PEDOT, as SC and compare its performance characteristics to electrodes with PEDOT(PSS) as SC as well as to production pH sensors used in the Instrumentation Laboratory GEM Premier 5000 critical care analyzer in which a buffered hydrogel layer serves as aqueous inner contact. Although Amemiya, et al. have used PEDOT-C_{14} as ion-to-electron transducer in ion-transfer stripping voltammetry [66-68], it has not been used as SC in ISEs since its appearance in 1997 [65]. The PEDOT-C_{14}-based SC ISEs have outstanding performance characteristics (response slope, equilibration time, potential stability and reproducibility, etc.) and PEDOT-C_{14}-based pH sensors have no CO_2 interference. Based on measurements in standard solutions utilized in whole blood critical care analyzers as well as in whole blood samples, in our view, PEDOT-C_{14} may appeal to become the ultimate, generally applicable SC to build miniature ISEs with the same qualities as their conventional macro electrode counterparts.

EXPERIMENTAL

Chemicals

Potassium chloride, boric acid, sodium hydroxide, acetonitrile, and the standard solutions for calibrating the combination glass electrode were purchased from Thermo

Fisher. Citric acid and potassium phosphate monobasic (KH_2PO_4) were purchased from Sigma Aldrich.

The aqueous solutions were prepared with 18.2 MΩcm resistivity DI water from Millipore Milli-Q A10 system. For testing the response of the SC ISEs in the presence of different levels of CO_2 and to calibrate the Severinghaus-type CO_2 electrode, Cal A and B solutions that are produced for the GEM® Premier family of critical care analyzers and CO_2-saturated Britton Robinson buffer solutions were used. The Cal A (pH 6.91, Na^+: 105.9 mM, K^+: 6.99 mM, Ca^{2+}: 1.78 mM, Cl^-: 47 mM and CO_2: 65.1 mmHg) and Cal B (pH 7.39, Na^+: 151.0 mM, K^+: 2 mM, Ca^{2+}: 0.79 mM, Cl^-: 89 mM and CO_2: 33.7 mmHg) solutions were provided by Instrumentation Laboratory (Bedford, MA) in gas-tight, metal-coated Mylar bags.

Procedure for the synthesis of EDOT-C_{14} (2-n-tetradecyl-2,3-dihydrothieno-[3,4-b][1,4]dioxine)

The chemical synthesis of monomer EDOT-C_{14} (2-n-tetradecyl-2,3-dihydrothieno-[3,4-b][1,4]dioxine) [65, 69] is described here, in short. To begin, 0.7777 g (5.39 mmol) of 3,4-dimethoxythiophene (97%), 0.125 g (0.539 mmol) of *p*-toluenesulfonic acid monohydrate, and 2.785 g (10.78 mmol) of 90% technical grade 1,2,-hexadecanediol (all from Sigma Aldrich) were heated under argon atmosphere in 40 mL toluene (Thermo Fisher) overnight. The reaction mixture was then mixed with ethyl acetate (Thermo Fisher) and washed twice with saturated sodium bicarbonate. Next the organic solvent was evaporated and the crude product was purified by chromatography on a silica gel-based (Thermo Fisher) column using gradient elution with 5 to 15% dichloromethane in hexane (both from Thermo Fisher) as mobile phase. The structure of

the product (0.940 g white powder, 52% yield) was confirmed by proton NMR and mass spectrometry.

Electrochemical deposition of PEDOT(PSS) and PEDOT-C_{14}(TPFPhB) films

Prior to the electrochemical deposition of PEDOT(PSS) and PEDOT-C_{14}(TPFPhB) films, the Au and GC macro electrodes were polished on wet microcloth pads using Al_2O_3-based slurry with gradually decreasing grain sizes (1.0 μm, 0.3 μm, and 0.05 μm) (Buehler, Lake Bluff, IL). After the individual polishing steps, the electrodes were rinsed and cleaned by sonication (15 min) in DI water. The Au electrodes in the flow channel of the PVC sensor card for the GEM Premier 5000 instrument were cleaned with soap solution using a soft toothbrush and thoroughly rinsed with DI water. Finally, the entire PVC card was sonicated in DI water.

The procedure for the electrochemical polymerization of PEDOT(PSS) was the same as used in Chapter 3. The PEDOT-C_{14}(TPFPhB)-based conductive polymer films were deposited over the polished/cleaned electrode surfaces, based on the works of Amemiya et. al. [66-68], by cyclic voltammetry in an acetonitrile solution of 0.01 mol/dm^3 EDOT-C_{14} and 0.03 mol/dm^3 potassium tetrakis(pentafluorophenyl) borate (KTPFPhB). KTPFPhB was purchased from Boulder Scientific. In the electrochemical cell, a platinum coil served as a quasi-reference electrode and a GC rod as a counter electrode. During the electrochemical deposition, the potential of the working electrode was cycled from −0.85 V to +1.4 V five times with a scan rate of 0.1 V/s. The potential scanning was stopped at -0.85 V, consequently at the end of the electrochemical deposition the film was in its reduced form. The cyclic voltammograms recorded during the electrochemical deposition of PEDOT-C_{14} (Figure 7.1) were very similar to the CVs

reported earlier by Wolfs et. al. [70] and by Sankaran and Reynolds [65]. After the electropolymerization, the PEDOT-C_{14}(TPFPhB)-coated electrodes were rinsed with acetonitrile and left to dry overnight in a desiccator under vacuum.

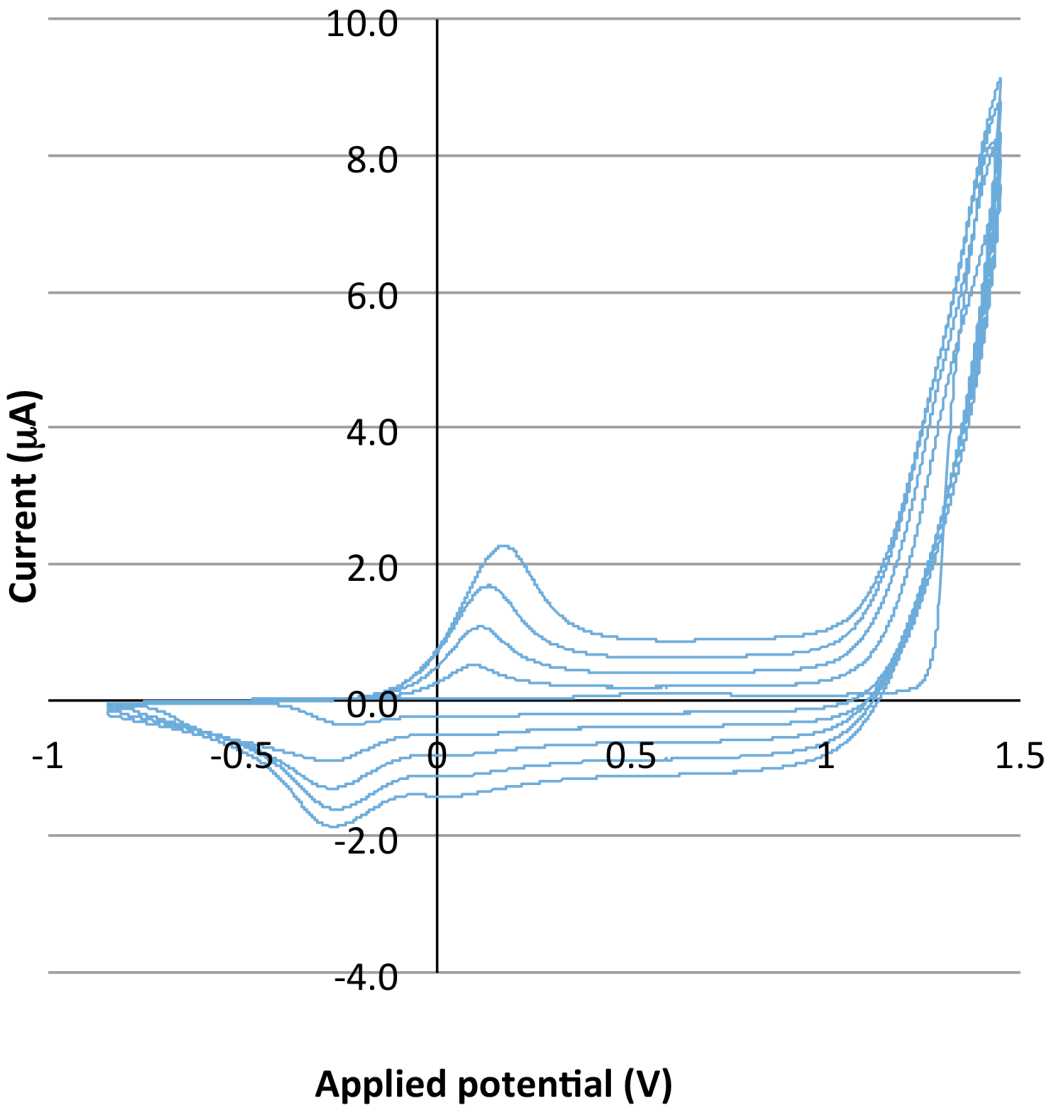

Figure 7.1. Cyclic voltammograms recorded during the electrochemical deposition of a PEDOT-C_{14}(TPFPhB) film at 0.1 V/s scan rate from 0.01 mol/dm^3 EDOT-C_{14} and 0.03 mol/dm^3 potassium tetrakis(pentafluorophenyl) borate (KTPFPhB) solution in acetonitrile.

Ion-selective membrane formulations

To prepare the ion-selective membrane cocktails, the same chemicals were used as listed in Chapter 3. The pH, K^+, and Na^+-selective membrane formulations contained 31 to 33% (w/w) PVC and 64 to 66% (w/w) DOS and were prepared with hydrogen ionophore I (3.9%), valinomycin (2.05%) and sodium ionophore X (0.8%), as well as 1.2%, 0.45%, and 0.2% KTpClPB, respectively. These membrane components (200 mg dry mass) were dissolved in 1.5 mL of THF to prepare membrane cocktails for deposition. The drop-cast volumes of the membrane cocktail were proportional to the surface areas of the electrodes: 40.0 µL for the 3.0 mm diameter electrodes, 11.5 µL for the 1.6 mm diameter electrodes and between 0.45 to 0.55 µL for the 0.24 mm electrodes in the PVC sensor card for the GEM Premier 5000 instrument. Following the complete evaporation of THF (overnight), the electrodes were ready for testing.

Electrodes

For the pH measurements, a Thermo-Fisher Model 13-620-81 combination glass electrode was used. To follow the saturation and removal of CO_2 in Britton-Robinson buffer solutions, a Severinghaus-type CO_2 electrode (Thermo Scientific 9502BNWP) was used.

The SC electrodes were built on commercially available 3 mm diameter GC and 1.6 mm diameter Au electrodes (Bioanalytical System, Inc. (BASi) model MF-2012 and MF-2014, respectively), both in a 6.4 mm outer diameter electrode body. Miniaturized SC electrodes were constructed on a PVC sensor card designed for a commercial critical care analyzer (GEM Premier 5000, Instrumentation Laboratory, Bedford, MA). The GEM Premier 5000 measures numerous critical care analytes (pH, pO_2, pCO_2, Na^+, K^+,

Ca^{2+}, Cl^-, glucose, lactate, hematocrit) directly in 150 µL of whole blood using electrochemical sensors as well as hemoglobin, hemoglobin fractions, and bilirubin using optical sensing. The PVC sensor card contains 0.24 mm diameter Ag|AgCl pins inserted within a flow channel in the plastic card on which the PVC-based ISEs are constructed for the measurement of pH and electrolytes. In this work, the Ag|AgCl pins for the SC ISEs were replaced with 0.24 mm diameter Au pins.

Instruments

Electrochemical measurements

For the electrochemical deposition of CP films, a Gamry Reference 600 Potentiostat/Galvanostat (Gamry Instruments, Warminster, PA) was utilized. For the potentiometric data acquisition, a Lawson Lab (Malvern, PA) 16-channel high input impedance data acquisition system was used in conjunction with an Orion model 900200 double junction Ag|AgCl reference electrode (Thermo Scientific, USA). The data acquisition system was connected to a computer equipped with the EMF Suite version 2.0.0.2 program. The potentiometric measurements with the macro electrodes were performed at room temperature while the electrodes in the PVC sensor card were characterized at 37°C. Most of the results summarized in this paper represent the SC electrode behavior after 24 h equilibration in a Cal B solution or in pH 5.0 Britton-Robinson buffer.

Water contact angle measurements

To assess the hydrophobicity of the different CPs, the CP films were deposited over BASi 3 mm diameter Pt (MF 1012), Au (MF 1002), and GC (MF 1000) electrodes embedded in PEEK blocks. For the WCA measurements, a VCA Optima Surface

Analysis System (AST Products, Inc., Billerica, MA) was used. The WCAs were evaluated from captured images of 0.5 μL DI water droplets on the target surface using the VCA Optima XE goniometry software. The average WCAs were calculated from 5 to 8 measurements performed on 5 to 8 completely dry CP-coated electrode surfaces.

Solutions and calibration protocols for the SC ISEs

The SC pH electrodes were calibrated in Britton-Robinson buffer solutions with pH values ranging between pH 2.4 and 12.2. To assess the level of interference caused by CO_2, the electrodes were also calibrated in: (i) blood serum-like electrolyte solutions provided by Instrumentation Laboratory with 65.1 mmHg and 33.7 mmHg CO_2 partial pressure (Cal A and B, respectively) (electrodes in the PVC sensor card) and (ii) pH ≈ 5.0 Britton-Robinson buffer solutions saturated with CO_2/N_2 gas mixtures with 8% and 20% CO_2 content as well as with 100% Ar gas via a diffusor (SC macro electrodes).

Calibration protocol for the SC pH electrodes in the GEM Premier 5000 PVC sensor card

The response characteristics of the miniature SC pH, K^+, and Na^+ electrodes in PVC sensor card of the GEM Premier 5000 were tested under continuous flow (0.1 mL/min) at 37.0°C using Cal A and Cal B as standard solutions. For the solution transport, a Gilson Minipuls 3 peristaltic pump was used. The electrodes in the flow channel were connected to an external double junction Ag|AgCl|KCl(3 mol/dm^3)| LiOAc (0.1 mol/dm^3) reference electrode by placing the outlet tubing of the flow channel into a Cal B solution-filled beaker together with the reference electrode. During the replacement of Cal A solution with Cal B solution and back to Cal A, the flow rate was increased temporarily to 10 mL/min in the flow channel.

Blood measurements

Measurements of pH in whole blood from healthy volunteers using electrodes with PEDOT(PSS) and PEDOT-C_{14}(TPFPhB) as SCs were performed at Instrumentation Laboratory (Bedford, MA) using the GEM Premier 5000 critical care analyzer. pH measurements on the GEM Premier 5000 analyzer, using the PEDOT(PSS) and PEDOT-C_{14}(TPFPhB)-based SC electrodes, were compared to pH measurements using the production pH sensor for the instrument. This production pH sensor uses an identical TDDA (Hydrogen Ionophore I)-loaded PVC-based outer membrane as the SC pH sensors. The internal layer is an aqueous hydrogel layer consisting of 50 mmol/dm^3 2-(N-morpholino)ethane sulfonic acid (MES) buffer and 50 mM of the K^+ salt of MES in a matrix of 8.7 g/L hydroxyethyl cellulose (pKa of MES buffer = 6.03 at 37°C). The MES buffer prevents pH changes at the internal interface of the pH-selective membrane caused by diffusion of CO_2 through the membrane, avoiding interference from CO_2 in the sample during pH measurement.

RESULTS AND DISCUSSION

The aim of this study was to find a CP-based SC that could appeal to become the ultimate SC for ISEs. We were primarily interested in CP-based SCs due to the unique advantages of the possibility of site-specific electrochemical deposition of CPs for building sensor arrays for simultaneous analysis of multiple ions. The target application of the new SC ISEs is electrolyte analysis of whole blood samples with specific focus on the measurement of blood pH in the presence of fluctuating CO_2 levels. To avoid potential CO_2 interference due to the formation of an aqueous layer, only highly hydrophobic CPs were considered [11, 71, 72]. Among the potential candidates, the

superhydrophobic PEDOT derivatives [70] appeared the most attractive based on our generally very positive experiences with PEDOT(PSS)-based SC ISEs [22, 34] and the works of Amemiya, et al. in which a PEDOT-C_{14} layer served as an ion-to-electron transducer for the voltammetric determination of K^+, Ca^{2+}, NH_4^+, etc. ions [67, 68, 73].

Equilibration times for PEDOT(PSS) and PEDOT-C_{14}(TPFPhB) based SC pH, K^+, and Na^+ electrodes in Cal B solution

In Chapters 3 and 4, we focused on the optimization of the equilibration time of ISEs with PEDOT(PSS) as SC [22, 34]. In Table 7.1, the equilibration times of SC pH, K^+, and Na^+ electrodes with PEDOT-C_{14}(TPFPhB) as SC are compared to our previously reported equilibration times with PEDOT(PSS) as SC. As it can be seen, all the equilibration times for the pH, K^+, and Na^+ electrodes are around or below 10 minutes. The equilibration times of PEDOT(PSS)-based SC ISEs on Pt as substrate electrode were significantly longer [22, 34].

Table 7.1. Equilibration times measured with PEDOT(PSS)- and PEDOT-C_{14}(TPFPhB)-based SC pH, K^+, and Na^+ electrodes in Cal B solution reported as mean ± S.D.

Substrate electrode	Conducting polymer	pH ± S.D. (n) [min]	K^+± S.D. (n) [min]	Na^+± S.D. (n) [min]
GC	PEDOT-C_{14}(TPFPhB)	8.2±3.9 (5)	6.3±2.6 (5)	11±4.4 (5)
	PEDOT(PSS) [22]	6.2±1.4 (5)	6.5±2.8 (27)	5.4±2.2 (5)
Au	PEDOT-C_{14}(TPFPhB)	6.4±3.7 (23)	6.4±3.8 (17)	10.1±4.6 (13)
	PEDOT(PSS) [22]	8.7±2.8 (18)	7.2±3.4 (35)	12.5±4.4 (25)

Calibration of the solid contact pH electrodes

SC pH sensors aimed for blood pH measurement must have no interference from fluctuating CO_2 levels in blood. CO_2 can easily diffuse through plasticized PVC membranes and change the pH of an aqueous solution on the backside of the membrane, if present. This pH change can induce a systematic error in the pH measurement and has been exploited in differential CO_2 sensors [74-76]. Considering the importance and the challenges of pH measurements with SC ISEs, it surprising that only about 5% of all papers on SC ISEs are related to SC pH sensors.

The pH sensors with the same ion-selective membrane but PEDOT(PSS) or PEDOT-C_{14}(TPFPhB) as SC had identical response slopes (57.7±0.2 mV/pH) in Britton-Robinson buffer [77] in the pH range from pH 3 to pH 11. Similarly, the SC K^+ and Na^+ electrodes with PEDOT(PSS) or PEDOT-C_{14}(TPFPhB) as SC had Nerstian responses (60.0±0.4 mV/decade slope) between 10^{-1} and 10^{-5} mol/dm^3 with a few tenths of mV (~0.3 mV) residual mean standard deviation around the fitted lines of the calibration curves. The standard deviations of the standard potentials of pH, Na^+, and K^+ electrodes built on Au, GC, and Pt with PEDOT-C_{14}(TPFPhB) as SC ranged between 3.7 and 10.6 mV with no statistically significant difference between the different ISEs (H^+, Na^+, and K^+ electrodes) or the electrodes built on the different electron-conducting substrates (Au, GC and Pt). For the same electrodes with PEDOT(PSS) as SC, the standard deviations of the standard potentials ranged between 4.5 and 31.9 mV.

Responses of SC pH sensors in solutions with different levels of CO_2

Potential vs. time transients recorded during the calibration of the SC pH sensors in the PVC sensor card of the GEM Premier 5000 analyzer with PEDOT(PSS) and

PEDOT-C_{14}(TPFPhB) as SC using Cal A and Cal B as standard solutions are shown in Figure 7.2.

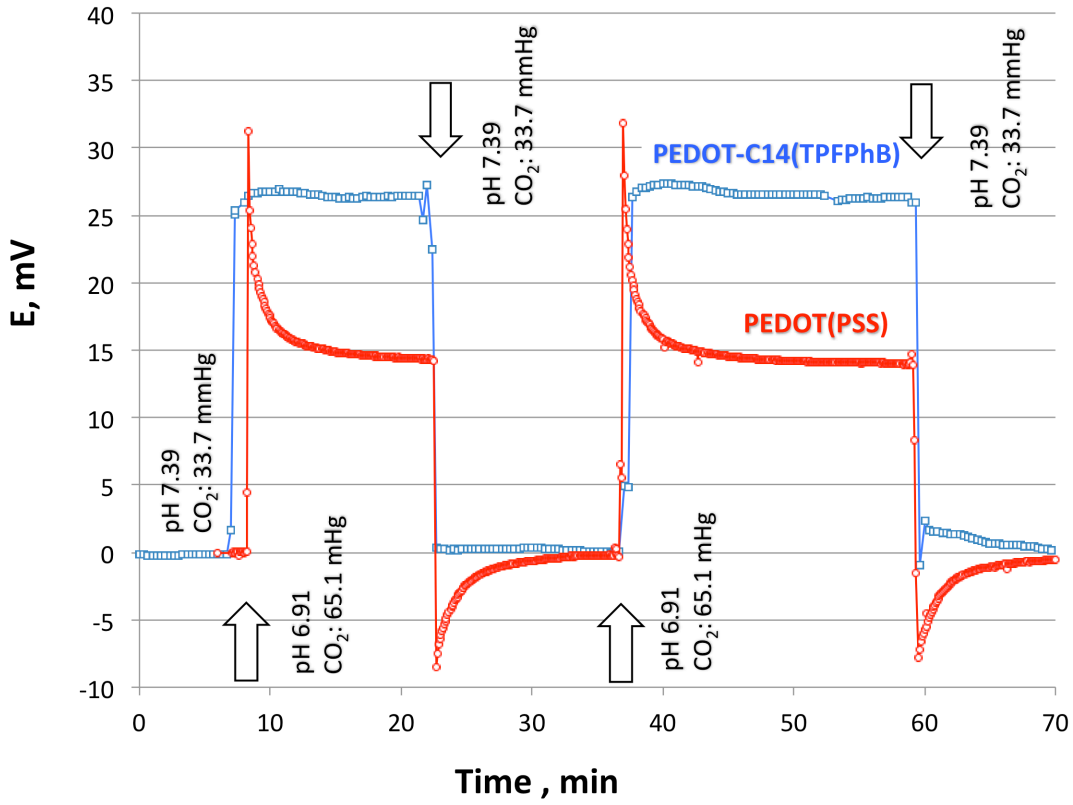

Figure 7.2. The calibration of SC pH ISEs with PEDOT(PSS) and PEDOT-C_{14}(TPFPhB) as SC in the PVC sensor card of the GEM Premier 5000 analyzer under flow through conditions using Cal A (pH 6.91 and pCO_2 65.1 mmHg) and Cal B (pH 7.39 and pCO_2 33.7 mmHg) as standard solutions. For better comparison, the starting potentials of the electrodes in Cal B solution were shifted to 0 mV. After the replacement of the Cal A solution with Cal B solution or the other way around the solutions were stopped in the sensor cards.

As seen in Figure 7.2, the pH electrode with PEDOT-C_{14}(TPFPhB) as SC has a very fast response with 57-58 mV/pH response slope and stable potential in both Cal A and Cal B solutions. However, the potential of the pH electrode with PEDOT(PSS) as SC decays slowly following the quick potential change corresponding to the pH changes in the solution upon the replacement of Cal A with Cal B solution and back. Using the steady state potential values, after about 10 minutes of equilibration, response slopes of 40-42 mV/pH were calculated for pH ISEs with PEDOT(PSS) as SC. If the calibration is performed with Cal A and Cal B standards without CO_2, the response slopes of the pH electrodes with PEDOT(PSS) or PEDOT-C_{14}(TPFPhB) as SCs were almost identical; 57.6±0.3 and 58.1±0.1 mV/pH, respectively (data not shown).

The large interference experienced with the PEDOT(PSS)-based pH sensors suggests that there is a water layer between the PEDOT(PSS) and the ISM, or as Veder, et al. [19, 78] pointed out, PEDOT(PSS) behaves like a hydrophilic aqueous hydrogel. The slow drift experienced with the PEDOT(PSS)-based pH sensors in solutions with different CO_2 content is due to pH changes in this hydrogel-like layer, on the back side of the H^+-selective membrane, as a consequence of CO_2 transport from the sample solution through this membrane. With PEDOT-C_{14}(TPFPhB) as SC, the lack of CO_2 interference verifies that due to the high hydrophobicity of PEDOT-C_{14} and its counter ion, a water layer did not form and in contrast to PEDOT(PSS), the PEDOT-C_{14}(TPFPhB) film does not behave as a hydrogel but rather as a genuine SC.

Based on reports that even 100% CO_2 saturated solutions had only minor effect on the potential of PEDOT(PSS)-coated GC electrodes [18] and PEDOT(PSS)-based SC K^+ electrodes [18, 79], the significant interference of CO_2 on PEDOT(PSS)-based pH

sensors, as shown in Figure 7.2, may appear contradictory to earlier findings. However, this is not the case. The significant CO_2 interference in our experiments is due to the hydrogel-like behavior of PEDOT(PSS) and the pH sensitivity of the membrane. As CO_2 diffuses through the pH ISM, it dissolves in the hydrogel-like PEDOT(PSS) and thus changes the pH on the backside of the pH sensitive ISM, which reveals as a drifting potential. With K^+-selective membranes, the CO_2 uptake-related pH change on the back side of the membrane does not induce significant interference due to the pH insensitivity of the K^+-selective membrane ($logK_{K^+,H^+}^{pot} \approx -4$) and because CO_2 has only a minor effect on the potential of the PEDOT(PSS) film itself [18]. In agreement with this expectation, as we show in Figure 7.3, the response properties of K^+ (and Na^+, which is not shown) ISEs with PEDOT(PSS) and PEDOT-C_{14}(TPFPhB) as SC were identical in calibration protocols using Cal A and Cal B solutions with different levels of CO_2.

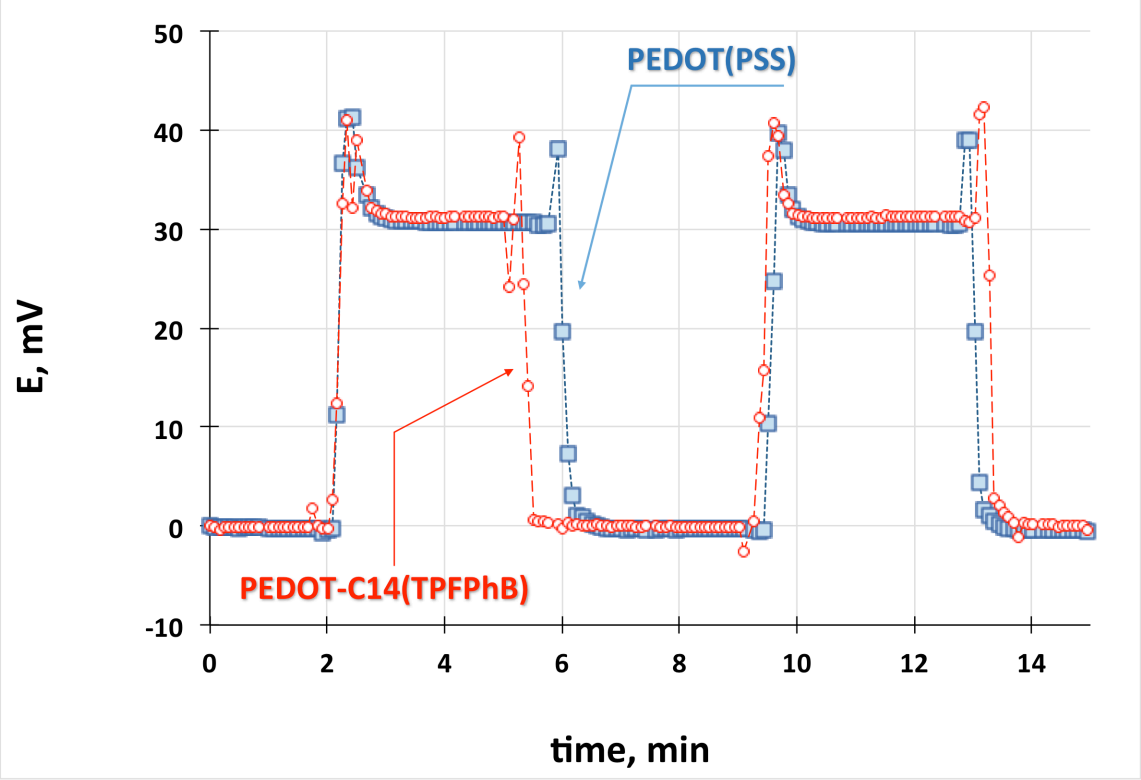

Figure 7.3. The calibration of SC K^+-ISEs with PEDOT(PSS) and PEDOT-C_{14}(TPFPhB) as SC under flow through conditions using Cal A (K^+ 6.99 mmol/dm^3, pCO_2 65.1 mmHg) and Cal B (K^+ 2.00 mmol/dm^3, pCO_2 33.7 mmHg) as standard solutions. For better comparison, the starting potentials of the electrodes were shifted to 0 mV in Cal B standard solution.

The ultimate "water layer" test:

The experiments shown in Figures 7.2 and 7.3 were designed to assess the CO_2 interference on SC electrodes with different SCs and sensing membranes. However, the results also point to the possibility of utilizing similar experiments as the ultimate "water layer" test with fast and unambiguous results. Based on the data shown in Figure 7.2, we recommend recording the potential drifts of SC electrodes with pH sensitive membranes in samples with different CO_2 levels to prove the presence or absence of a water layer beneath the ISM. Although the conventional test for the presence of an undesirable water layer appears to be simple [41], it is time consuming and when the experimental conditions are not selected properly, it does not provide an unambiguous answer. In the conventional test, the potential of a SC ISE is recorded in a primary ion solution and then as the SC ISE is switched to a solution containing only interfering ion and finally back again to the primary ion solution. It is assumed that drift of the electrode following these solution changes is related to ionic fluxes across the ISM and the concomitant change in the concentrations in the water layer, located on the backside of the ISM. However, in experiments with highly discriminated ions and sensors with thick and rigid membranes, ionic fluxes are negligible or extremely slow. Such minor fluxes induce measurable concentration changes in the water layer only after very long times and these changes are not expected to induce significant changes in the membrane potential due to the selectivity of the membrane. Consequently, the drifts (or the lack of drift) recorded during these experiments could be biased by other factors (e.g., temperature fluctuations, ions leaching from the reference electrode, etc.), which may obscure the interpretation of the potential changes (or the lack of the potential changes) experienced in the

conventional water layer test. The results in Figure 7.3 demonstrate a case when the absence of CO_2 interference does not mean the absence of a water layer. Since the highly discriminated H^+ ions hardly influence the potential of the K^+-selective membrane, the CO_2 transport-related pH change in the water layer does not generate a measurable drift.

Conventional water layer test with PEDOT(PSS)-based SC K^+ electrode

To demonstrate the challenges in the interpretation of the transients recorded in the conventional water layer test, in Figure 7.4 we show the results of a conventional water layer test with a PEDOT(PSS)-based K^+ electrode. The conventional water layer test assumes very long (up to 24 hours) equilibrations both in the primary and in the interfering ion solutions. If the duration of the experiment is significantly reduced (see Fig. 7.4 inset-1), it may prevent the recognition of long-term drifts. Similarly, the ion-transport related drifts might not be recognizable in full-scale presentation of the transients, without adequate potential resolution, as shown in inset-2, and lead to incorrect interpretation. However, in very long experiments, the small drifts like in inset-2 might be obscured by other factors (e.g., temperature fluctuations, ions leaching from the reference electrode, etc.) and lead to misinterpretation of the results.

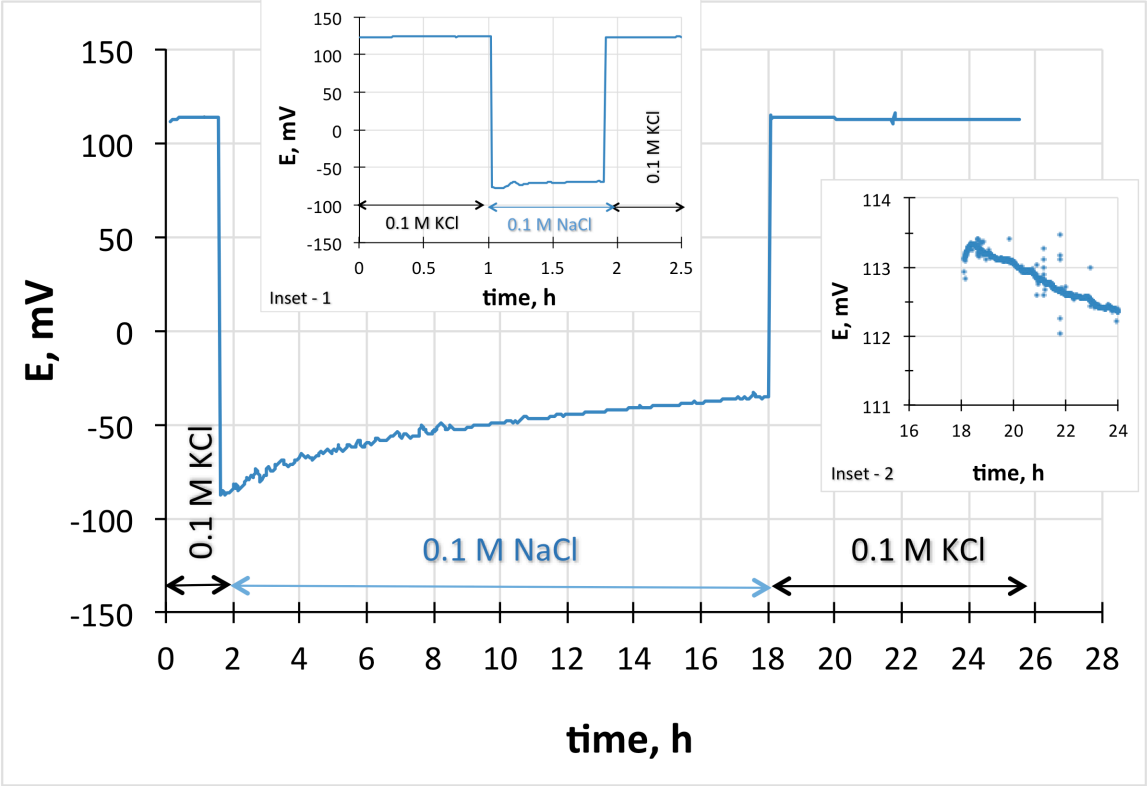

Figure 7.4. "Conventional" water layer test performed with a PEDOT(PSS)-based SC K^+ electrode. A fully equilibrated K^+ electrode (in 0.1 mol/dm^3 KCl) at 1.8 hours in the figure was brought in contact with 0.1 mol/dm^3 NaCl. After 18 hours, the bathing solution was switched back to 0.1 mol/dm^3 KCl. Inset-1: The same test performed in 2.5 hours. Inset-2: The data points collected between 18 and 24 hours plotted on a zoomed in potential scale.

Upon replacing the primary ion solution (0.1 mol/dm^3 KCl) with the interfering ion solution (0.1 mol/dm^3 NaCl), a significant potential overshoot is recorded, but when the solution sequence was reversed, an apparent steady state was reached instantaneously without any potential overshoot. Such responses are commonly seen in the literature [80] but in our view, does not provide an unambiguous answer to the original question of the experiment on the presence of a water layer between the sensing membrane and its SC. Inset-1 of Figure 7.4 shows that if the duration of the test is too short, the recorded transients may lead to an erroneous conclusion. Inset-2 of Figure 7.4 shows that without adequate potential resolution, the ion-transport related drift might not be recognizable and lead to incorrect interpretation. On the other hand, the transients in Figure 7.2 prove the presence of the undesirable water layer between the sensing membrane and the PEDOT(PSS) film.

CO_2 interference of pH sensors with PEDOT(PSS) and PEDOT-C_{14}(TPFPhB) as solid contacts

To assess the CO_2 interference beyond physiologically relevant CO_2 fluctuations, the pH sensors with PEDOT(PSS) and PEDOT-C_{14}(TPFPhB) as SC were placed in a pH≈5 Britton-Robinson buffer which was saturated with 8% (61 mmHg) and 20% (152 mmHg) pCO_2-containing CO_2/N_2 gas mixtures. To follow the saturation process, a Severinghaus CO_2 electrode and a Thermo-Fisher combination glass electrode were used. The potential transients recorded in this experiment are shown in Figure 7.5.

Similar to Figure 7.2, increasing CO_2 levels induce significant interference in the potential of the pH sensor with PEDOT(PSS) as SC while the potential of the pH sensor with PEDOT-C_{14}(TPFPhB) as SC is not influenced. Upon increasing the CO_2

concentration in the buffer, the potential of the PEDOT(PSS)-based SC pH sensor becomes more negative indicating that the pH on the back side of the membrane became more acidic. The ~9 mV and ~12 mV potential changes which have been recorded during the saturation of the solution with 8% and 20% CO_2 correspond to ~0.15 and ~0.2 pH change in the hydrogel-like PEDOT(PSS) film on the back side of the pH membrane, respectively. The potential of the pH sensor with PEDOT-C_{14}(TPFPhB) as SC is not influenced by the different CO_2 levels, even at 152 mmHg pCO_2. The pH of the buffer solution remained practically constant throughout the experiment ($\Delta pH < 0.02$), i.e., considering the potential change related to a change in pH was not necessary.

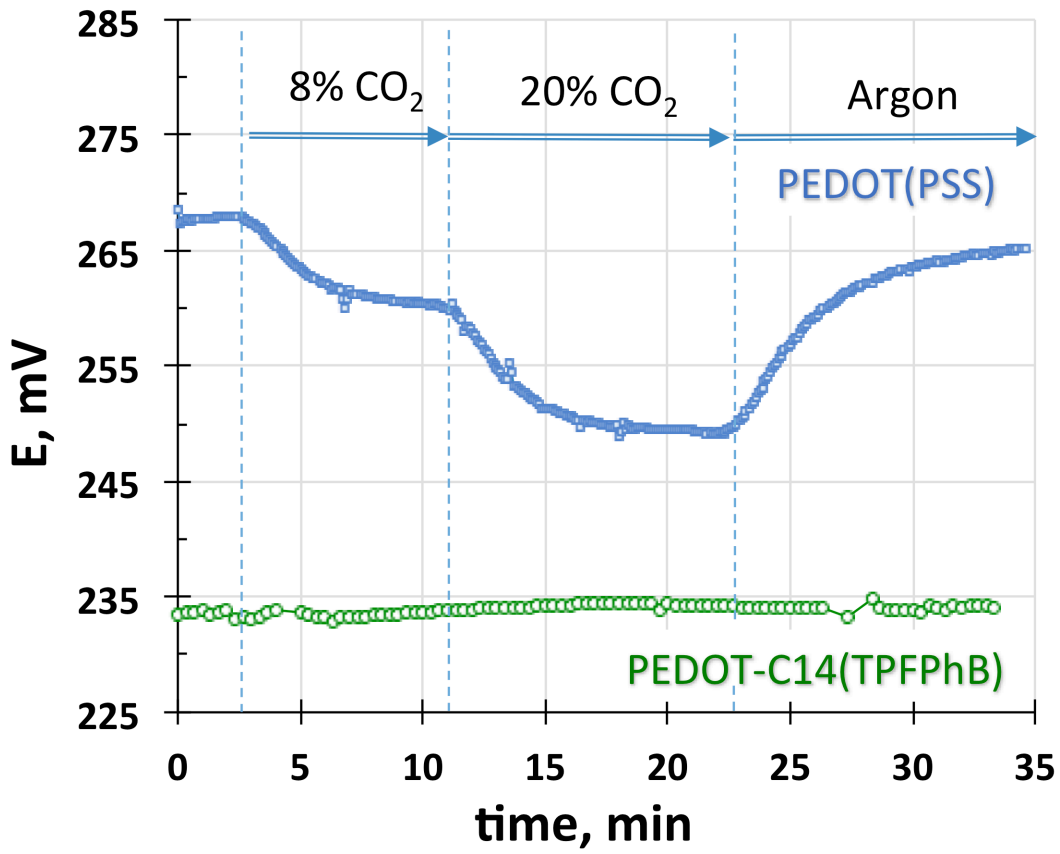

Figure 7.5. Potential transients of pH electrodes built with PEDOT(PSS) and PEDOT-C_{14}(TPFPhB) as SC during the saturation of a 0.1 mol/dm^3 Britton-Robinson buffer solution with 8% CO_2 and 20% CO_2-containing CO_2/N_2 gas mixtures as well as with argon.

Repeatability and long term stability of pH sensors with PEDOT-C_{14}(TPFPhB) as solid contact

The most commonly mentioned deficiency of SC ISEs is their poor potential stability and inadequate repeatability. Both of these sensor characteristics are key in clinical applications. The repeatability of the different sensors must meet specific criteria to be used in critical care diagnostics for measuring ion concentrations in biological samples with narrow physiologically relevant concentration ranges [81]. The repeatability of the pH sensors with PEDOT-C_{14}(TPFPhB) as SC was determined by a repeated two-point calibration using the Cal A and Cal B standard solutions in the thermostated flow cell. An example of such measurement is shown in Figure 7.6.

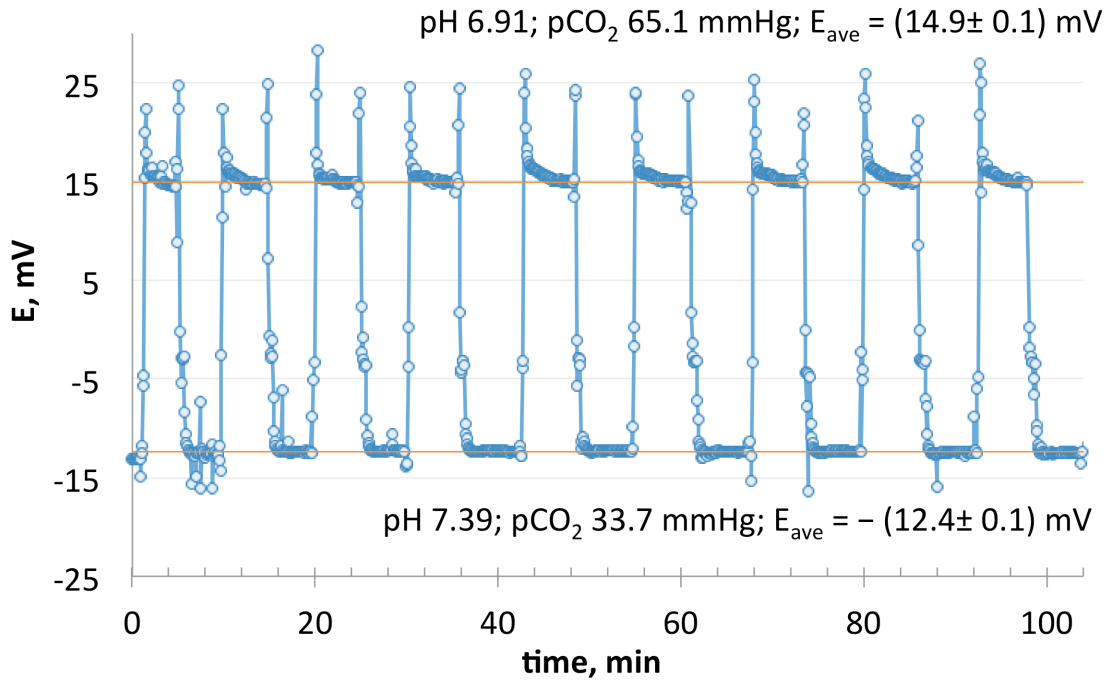

Figure 7.6. The repeatability measurement with a PEDOT-C_{14}(TPFPhB)-based SC pH sensor under thermostated (37.0°C) flow-through conditions (0.1 mL/min) using blood serum-like electrolyte solutions as standards. During the replacement of Cal A solution with Cal B solution and back to Cal A, the flow rate was increased temporarily to 10 mL/min in the flow channel.

The repeatability (the standard deviation of the potential values measured in the same solution) of the PEDOT-C_{14}(TPFPhB)-based SC pH sensor in both Cal A and Cal B solutions was better than ±0.1 mV which translates to better than ±0.002 pH units uncertainty in the pH measurement, which meets the requirements of blood pH measurements [81]. According to the 2002 IUPAC document on the measurement of pH [82], the target uncertainty of a pH measurement with a glass electrode is between 0.02 and 0.03 pH units. This outstanding repeatability of the PEDOT-C_{14}(TPFPhB)-based SC pH sensor is due to its excellent potential stability. Figure 7.7 shows the results of a 31-day long sequence of measurements in which the PEDOT-C_{14}(TPFPhB)-based SC pH sensors were calibrated every day in the flow channel using the Cal A and Cal B standard solutions. The pH electrode potential was recorded in Cal B solution following the daily calibrations.

The potential stability of PEDOT-C_{14}(TPFPhB)-based K^+ ISEs on Au between 10-24 hours was -0.20±0.4 mV/h. Since the potentials of the ISEs were measured for 31 days, the long-term stability of the PEDOT-C_{14}(TPFPhB)-based electrodes could also be estimated by fitting a line to the recorded potential values between day 3 and day 31. The overall drift throughout of these measurements was 0.02±0.03 mV/day (n=5) for the SC pH sensors and 0.1±0.1 mV/day for the SC K^+ ISEs. The drift of PEDOT(PSS)-based pH and K^+ electrodes was significantly larger than with the PEDOT-C_{14}(TPFPhB)-based electrodes; 1.4±0.2 mV/day (n=4) and 0.9±0.5 mV/day (n=3), respectively.

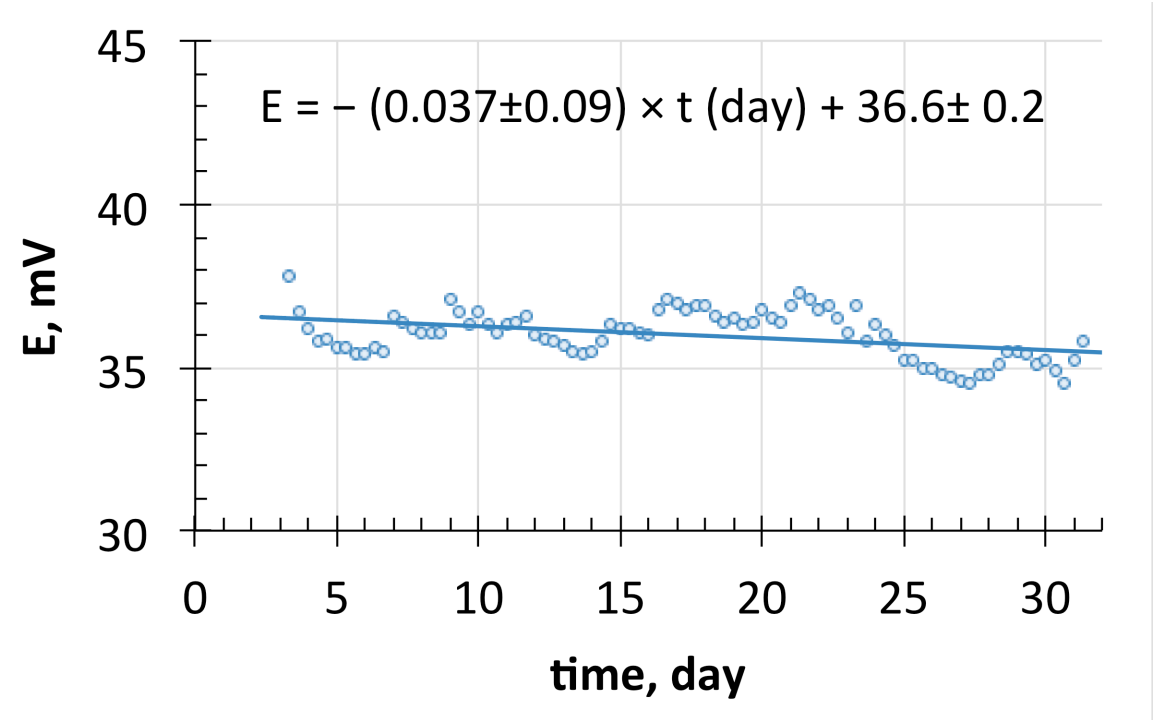

Figure 7.7. Long term potential stability of a pH sensor with PEDOT-C_{14}(TPFPhB) as SC. The data points represent potential values recorded in Cal B solution after the daily calibration of the electrode under flow-through conditions in Cal A and Cal B solutions. The slope of the line fitted to the recorded potential data is reported as long-term drift of the SC pH sensor.

Based on comments by Lindfors, et. al. [11, 71], it is assumed that the distinctive properties of the PEDOT-C_{14}(TPFPhB)-based electrodes are related to the unique hydrophobicity of this SC material. The WCA measured on the PEDOT-C_{14}(TPFPhB) film (136±5°, n=12) suggests that it is significantly more hydrophobic compared to PEDOT(PSS) or polyazulene-based films with reported WCA values of 51±7° (n=16) and 98±11° [11, 71], respectively. The WCA values measured on PEDOT-C_{14}(TPFPhB) films in this work are, however, slightly smaller than data reported by Wolfs et. al. [70] (~ 160°) for the PEDOT-C_{10} and PEDOT-C_{12} derivative-based films, with hexafluorophosphate as counter ion. However, Wolfs et. al. [70] emphasized that surface water-repellent properties (assessed by WCA) of the different PEDOT derivatives depend not only on the chemical composition (polymer and doping) but also on the surface morphology and roughness, which depend on the polymer deposition method and solvent.

Assessment of the light sensitivity of ISEs with PEDOT(PSS) and PEDOT-C_{14}(TPFPhB) as solid contacts

Compared to PEDOT(PSS) [44], an additional advantage of the PEDOT-C_{14}(TPFPhB)-based SC is that it has no light sensitivity. The results of an experiment in which PEDOT(PSS) and PEDOT-C_{14}(TPFPhB)-based macro pH sensors were illuminated with ~300 nW light (normal laboratory lighting) is shown in Figure 7.8.

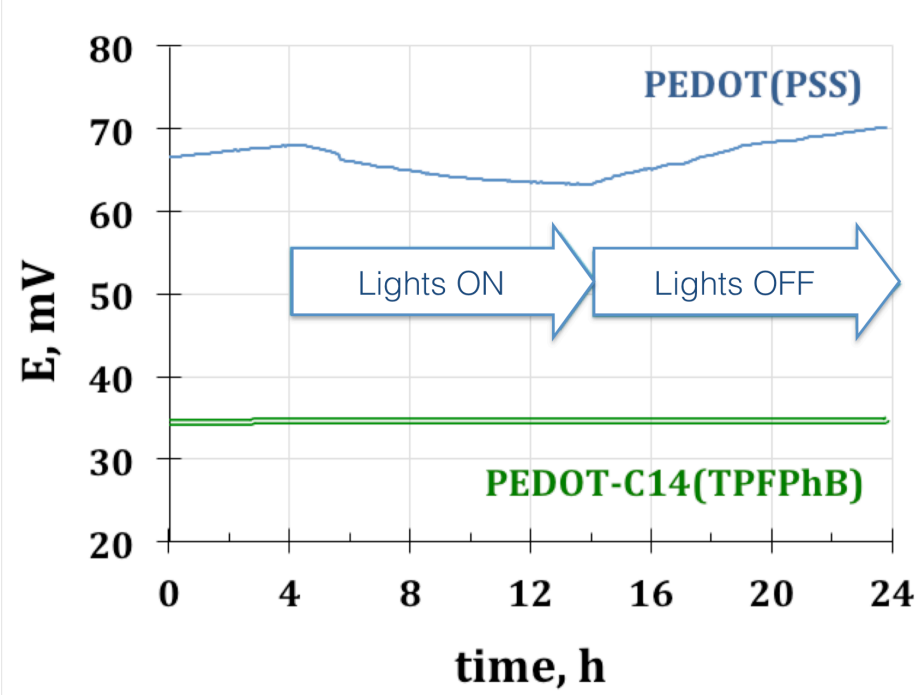

Figure 7.8. Light sensitivity of SC pH ISEs built with PEDOT(PSS) and PEDOT-C_{14}(TPFPhB) as SC. The source of light was the main light in the laboratory with intensity 250 – 400 nW. The potential of the SC ISEs was shifted for better comparison.

The responses of PEDOT(PSS) and PEDOT-C_{14}(TPFPhB)-based pH sensors in an Instrumentation Laboratory GEM Premier 5000 critical care analyzer

Responses of SC pH sensors using PEDOT(PSS) and PEDOT-C_{14}(TPFPhB) constructed on the PVC sensor card of the GEM Premier 5000 analyzer were compared to the standard production pH sensor for the analyzer which contains an aqueous internal hydrogel layer with 50 mmol/dm^3 MES buffer to prevent interference from pCO_2 in the sample. The pCO_2 content of samples of Cal B solution were adjusted from ~33 mmHg up to ~90 mmHg by equilibrating aliquots of Cal B solution with gas mixtures containing 5% and 10% CO_2. These samples were assayed for pH on analyzers equipped with the SC-based pH sensors and the standard production pH sensor. Figure 7.9 shows the

difference in the measured pH between the production sensor and three SC PEDOT(PSS)-based (Figure 7.9A) and four SC PEDOT-C_{14}(TPFPhB)-based (Figure 7.9B) pH sensors as a function of the pCO_2 concentration.

Figure 7.9A shows that the PEDOT(PSS)-based SC pH sensor has a systematic, proportional bias with increasing pCO_2 toward alkaline pH values as a consequence of interference from pCO_2 which shifts the pH of the internal electrolyte layer toward more acidic values. Slopes of the PEDOT(PSS)-based pH sensors measured in Cal A (pH=6.91, pCO_2=65.1 mmHg) and Cal B (pH=7.39, pCO_2=33.7 mmHg) were: 49.1, 49.4, and 50.2 mV/pH, and as expected, sensors with the lowest slope show the largest pH bias. Figure 7.9B shows the same experiment conducted using four PEDOT-C_{14}(TPFPhB)-based SC pH sensors. In this case, the change in pH measured by the SC pH sensors relative to the production pH sensor is negligible; indicative of no interference with the PEDOT-C_{14}(TPFPhB) pH sensors from diffusion of CO_2 through the outer pH sensing membrane. Slopes of the PEDOT-C_{14}(TPFPhB)-based SC pH sensors were consistent among sensors: 59.0, 60.0, 60.1 and 60.2 mV/pH (theoretical slope = 61.6 mV/pH at 37°C).

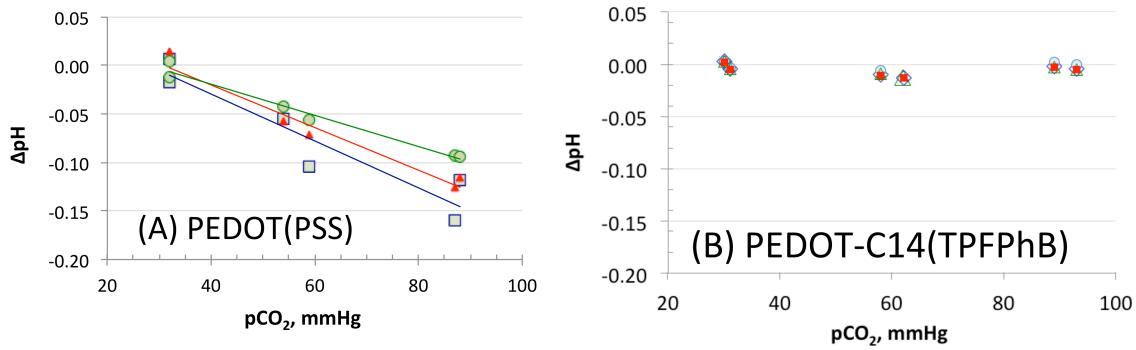

Figure 7.9. Differences in the pH values (ΔpH) measured in a GEM Premier 5000 critical care analyzer with a production pH sensor and SC pH sensors based on PEDOT(PSS) (n=3) (A) and PEDOT-C_{14}(TPFPhB) (n=4) (B) as a function of pCO_2. Samples of GEM Premier 5000 Cal B solutions were adjusted to pCO_2 concentrations from ~33 to ~90 mmHg and assayed as samples on the analyzers.

A SC pH sensor based on PEDOT-C_{14}(TPFPhB) was also used to measure the pH of whole blood samples and the results were compared to pH values measured with a production pH sensor for the GEM Premier 5000. First, the pCO_2 concentration of a pooled blood sample was set to 74 mmHg and then exposed to air over a period of about 30 minutes. During this 30 minute period, intermittent pH measurements were made using both the PEDOT-C_{14}(TPFPhB)-based and the production pH sensors and the pCO_2 values were assayed with the GEM Premier 5000 analyzer. As shown in Figure 7.10, as the pCO_2 level in the sample was decreasing, the corresponding pH value was increasing due to loss of CO_2. At the end of the experiment, the pCO_2 level was 54 mmHg. No statistically significant difference was found between the slopes of the pH vs time lines recorded with the two pH sensors ($p=0.875$), confirming the lack of CO_2 interference for the SC pH sensor based on PEDOT-C_{14}(TPFPhB). The origin of the constant offset of

0.07 pH units seen between the two types of sensors is not clear. However, it is important to point out that the measurements with the production pH sensor were performed in a commercial GEM 5000 instrument but with the PEDOT-C_{14}-based pH sensor in a test bed (a modified commercial instrument).

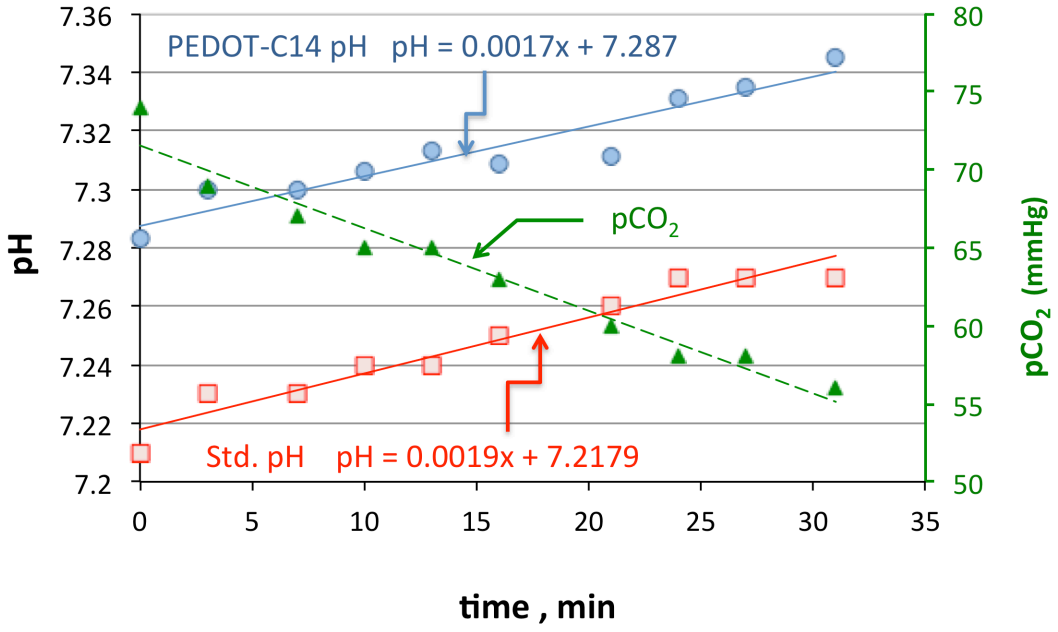

Figure 7.10. Measurements of blood pH using the GEM Premier 5000 analyzer with a SC pH sensor based on PEDOT-C_{14}(TPFPhB) and a standard production pH sensor. pCO_2 in the blood sample was first adjusted to 74 mmHg and was then decreased by exposing the sample to air. The resulting pH values were measured using both sensors as a function of time. The pCO_2 values measured during the experiment are plotted on the second y-axis.

CONCLUSIONS RELATED TO SC pH SENSORS WITH SUPERHYDROPHOBIC PEDOT-C_{14} AS SC

Ion-selective electrodes with the superhydrophobic PEDOT-C_{14}(TPFPhB) as SC have outstanding performance characteristics (theoretical response slopes, ~10 min equilibration time, 0.02±0.03 mV/day long-term potential stability, and ±0.002 pH unit reproducibility, etc.) and most importantly, PEDOT-C_{14}-based SC pH sensors have no CO_2 interference. The PEDOT-C_{14}(TPFPhB)-based K^+, Na^+, and pH electrodes have the same responses as the conventional electrodes used in commercial instruments in critical care diagnostics but have the additional advantage of site-specific electrochemical deposition of the PEDOT-C_{14}-based SCs. The superhydrophobic property of PEDOT-C_{14} is a significant benefit compared to other conductive polymer-based SCs. The possibility of site-specific electrochemical deposition is a considerable advantage compared to carbon-based SCs, which are generally deposited by drop-casting. The long term potential stability of the pH sensor with PEDOT-C_{14}(TPFPhB) as SC matches the potential stability of electrodes with colloid-imprinted mesoporous carbon, which were reported to have the best potential stability (drift ~ 31 μV/day) among SC ISEs [9].

CHAPTER 8

CONCLUSIONS

SC ISEs fabricated with a conductive polymer as ion-to-electron transducer are attractive for a variety of advantages, e.g., i) possibility for microfabrication due to ease site-specific deposition of the CP, ii) simple, robust, maintenance free design, iii) excellent detection limit, etc. However, after decades of research, SC ISEs have yet to make their way out of research laboratories and into commercial products due to their subpar electrochemical characteristics, specifically long equilibration times, inferior potential stability, and insufficient sensor-to-sensor standard potential reproducibility. The unsatisfactory performance of these SC ISEs is believed to be related to i) the chemical instability of the CP layer, i.e., gradual change in its redox state, ii) blocked interface between the CP and its highly plasticized liquid membrane coating, iii) the delamination of the liquid membrane from its SC and formation of a water layer between the CP and ISM as a consequence of insufficient hydrophobicity of the CP layer. To address these issues, CPs with varying degrees of hydrophibicity (PEDOT(PSS), POT, and PEDOT-C_{14}(TPFPhB)) have been studied on Au, Pt, and GC substrate electrodes with and without the incorporation of TCNQ into the CP film to control its redox potential. These CP-coated Au, Pt, and GC electrodes were tested directly as well as with an additional ion-selective membrane coating, i.e., as fully assembled K^+, Na^+, and H^+ SC ISEs.

SC ISEs fabricated with PEDOT(PSS) as SC exhibit short equilibration times on Au and GC substrates (<15 min) but long equilibration times on Pt (77 min). The differences between the ISEs fabricated on different substrates was also apparent in the

absolute values of the measured potential; the measured potentials for the PEDOT(PSS)-based ISEs on Pt were significantly more positive than on Au as substrate electrodes. These results suggest that the substrate electrode|CP interface plays a significant role in the electrochemical behavior of the fully fabricated SC ISE. These differences were traced back to higher PSS_{tot}/PEDOT ratio on Pt compared to Au, which has been deduced from SR-XPS data. Due to the higher PSS_{tot}/PEDOT ratio, PEDOT(PSS) is more hydrophilic on Pt compared to Au, which has been confirmed by WCA measurements. EQCM measurements showed that the electrochemically deposited PEDOT(PSS) is a thinner film on Pt compared to Au electrodes despite that identical conditions were used for the deposition. The difference in the PEDOT(PSS) film thickness on Pt and Au electrodes were confirmed by XPS etching studies. SEM images showed differences in the surface morphologies of PEDOT(PSS) films electropolymerized on the two different electrode substrates.

Based on recommendations from literature, we also studied SC ISEs with more hydrophobic CP layers, i.e., using POT and PEDOT-C_{14}(TPFPhB) as SC. SC ISEs fabricated with POT as SC have short equilibration times (< 15 min) but large drifts and inadequate sensor-to-sensor potential reproducibility. Upon the implementation of a redox mediator (TCNQ/$TCNQ^{\bullet-}$) into the POT film (POT+TCNQ) in combination with the potentiostatic optimization of the TCNQ/$TCNQ^{\bullet-}$ ratio for maximum redox buffer capacity, the potential stability of the POT-based ISEs was significantly improved to -0.1 mV/h. However, the poor reproducibility of the standard potentials and the significant light sensitivity of the POT-based ISEs could not be overcome through the incorporation of the TCNQ/$TCNQ^{\bullet-}$ couple.

PEDOT-C_{14} as a CP has all the advantages as an ion-to-electron transducer as PEDOT and it is more hydrophobic than POT. In the frame of this work, it has been used for the first time as SC in ISE sensors. Based on the performance characteristics of the PEDOT-C_{14}-based SC electrodes, it appears to be an ideal SC. PEDOT-C_{14}-based electrodes have short equilibration time, negligible potential drift, no CO_2 interference and are insensitive to light. The superhydrophobic PEDOT-C_{14}-based SC works well in combination with different ISMs (K^+, Na^+ and pH).

CHAPTER 9

RECOMMENDATIONS FOR FUTURE WORK

Based on the promising performance characteristics of PEDOT-C_{14}(TPFPhB)-based SC ISEs, this superhydrophobic CP should be the focus for future works towards minimal calibration or calibration-free SC ISEs. Although it has been shown that the PEDOT-C_{14}-based ISEs exhibit many impressive properties, the sensor-to-sensor reproducibility of the standard potentials of these sensors is not acceptable for calibration-free ISEs. Therefore, future work could focus on the exploration of the sources leading to the unacceptable sensor-to-sensor reproducibility of the standard potentials. Our work with PEDOT-C_{14} followed one particular method for polymerization that results in a reduced CP film following polymerization. It would be interesting to study the influence of electrochemical polarization on the redox state of the PEDOT-C_{14}-based film and on the performance characteristics (e.g. the potential reproducibility) of PEDOT-C_{14}-based SC ISEs.

Another possible route to improve the sensor-to-sensor potential reproducibility would be to implement an appropriate redox couple into the PEDOT-C_{14} film. A hydrophobic redox couple may be best because it would not likely leach out of the superhydrophobic PEDOT-C_{14} film. The possibility of the simultaneous electrochemical deposition of the redox couple and the PEDOT-C_{14} film would be a significant benefit. To maximize the buffer capacity of the SC film, a redox couple with a standard potential near that of the ideal redox state of PEDOT-C_{14}, as mentioned above, should be investigated.

It would be interesting to systematically study the performance characteristics of SC ISEs with PEDOT, PEDOT-C_4, PEDOT-C_8 and PEDOT-C_{14} CP films deposited electrochemically in the presence of various hydrophobic counter anions (TPB^-, $TpClPB^-$, $TPFPhB^-$, etc.). This would provide further information on the benefits of a hydrophobic CP as well as on the influence of the counter anion on the hydrophobicity of the CP films.

We are convinced that through the utilization of hyphenated techniques like QCM-potentiometry-impedance spectroscopy and FTIR-ATR-potentiometry-impedance spectroscopy as well as surface analytical techniques like XPS, SR-XPS, and SEM, the ultimate CP material for SC ISEs will be discovered.

REFERENCES

[1] J. Bobacka, Conducting polymer-based solid-state ion-selective electrodes, Electroanalysis, 18 (2006) 7-18.

[2] M.D. Kraft, I.F. Btaiche, G.S. Sacks, K.K. Kudsk, Treatment of electrolyte disorders in adult patients in the intensive care unit, Am. J. Health-Syst. Pharm., 62 (2005) 1663-1682.

[3] E. Lindner, B.D. Pendley, A tutorial on the application of ion-selective electrode potentiometry: An analytical method with unique qualities, unexplored opportunities and potential pitfalls; Tutorial, Anal. Chim. Acta, 762 (2013) 1-13.

[4] E. Lindner, R.E. Gyurcsanyi, Quality control criteria for solid-contact, solvent polymeric membrane ion-selective electrodes, J. Solid State Electrochem., 13 (2009) 51-68.

[5] R.W. Cattrall, H. Freiser, Coated wire ion-selective electrodes, Anal. Chem., 43 (1971) 1905-1906.

[6] A. Michalska, All-solid-state ion-selective and all-solid-state reference electrodes, Electroanalysis, 24 (2012) 1253-1265.

[7] O. Enger, F. Nuesch, M. Fibbioli, L. Echegoyen, E. Pretsch, F. Diederich, Photocurrent generation at a fullerene self-assembled monolayer-modified gold electrode cast with a polyurethane membrane, J. Mater. Chem., 10 (2000) 2231-2233.

[8] B. Paczosa-Bator, M. Pięk, R. Piech, Application of nanostructured TCNQ to potentiometric ion-selective K^+ and Na^+ Electrodes, Anal. Chem., 87 (2015) 1718-1725.

[9] J. Hu, X.U. Zou, A. Stein, P. Buhlmann, Ion-selective electrodes with colloid-imprinted mesoporous carbon as solid contact, Anal. Chem., 86 (2014) 7111-7118.

[10] T. Lindfors, L. Hofler, G. Jagerszki, R.E. Gyurcsanyi, Hyphenated FT-IR attenuated total reflection and electrochemical impedance spectroscopy, Anal. Chem., 83 (2011) 4902-4908.

[11] N. He, R.E. Gyurcsanyi, T. Lindfors, Electropolymerized hydrophobic polyazulene as solid-contacts in potassium-selective electrodes, Analyst, 141 (2016) 2990-2997.

[12] J.W. Schultze, H. Karabulut, Application potential of conducting polymers, Electrochim. Acta, 50 (2005) 1739-1745.

[13] B.L. Groenendaal, F. Jonas, D. Freitag, H. Pielartzik, J.R. Reynolds, Poly(3,4-ethylenedioxythiophene) and its derivatives: Past, present, and future, Adv. Mater., 12 (2000) 481-494.

[14] M. Vazquez, P. Danielsson, J. Bobacka, A. Lewenstam, A. Ivaska, Solution-cast films of poly(3,4-ethylenedioxythiophene) as ion-to-electron transducers in all-solid-state ion-selective electrodes, Sens. Actuators, B, 97 (2004) 182-189.

[15] M. Wagner, G. Lisak, A. Ivaska, J. Bobacka, Durable PEDOT:PSS films obtained from modified water-based inks for electrochemical sensors, Sens. Actuators, B, 181 (2013) 694-701.

[16] J. Bobacka, All solid-state poly(vinyl chloride) membrane ion-selective electrodes with poly(3-octylthiophene) solid internal contact, Analyst, 119 (1994) 1985-1991.

[17] J. Bobacka, Potential stability of all-solid-state ion-selective electrodes using conducting polymers as ion-to-electron transducers, Anal. Chem., 71 (1999) 4932-4937.

[18] M. Vazquez, J. Bobacka, A. Ivaska, A. Lewenstam, Influence of oxygen and carbon dioxide on the electrochemical stability of poly(3,4-ethylenedioxythiophene) used as ion-to-electron transducer in all-solid-state ion-selective electrodes, Sens. Actuators, B, 82 (2002) 7-13.

[19] J.P. Veder, R. De Marco, G. Clarke, S.P. Jiang, K. Prince, E. Pretsch, E. Bakker, Water uptake in the hydrophilic poly(3,4-ethylenedioxythiophene):poly(styrene sulfonate) solid-contact of all-solid-state polymeric ion-selective electrodes, Analyst, 136 (2011) 3252-3258.

[20] T. Lindfors, F. Sundfors, L. Hofler, R.E. Gyurcsanyi, FTIR-ATR study of water uptake and diffusion through ion-selective membranes based on plasticized poly(vinyl chloride), Electroanalysis, 21 (2009) 1914-1922.

[21] J. Bobacka, Z.Q. Gao, A. Ivaska, A. Lewenstam, Mechanism of ionic and redox sensitivity of p-type conducting polymers: Part 2. Experimental study of polypyrrole, J. Electroanal. Chem., 368 (1994) 33-41.

[22] M. Guzinski, J.M. Jarvis, B.D. Pendley, E. Lindner, Equilibration time of solid contact ion-selective electrodes, Anal. Chem., 87 (2015) 6654-6659.

[23] T. Lindfors, F. Sundfors, L. Hofler, R.E. Gyurcsanyi, The water uptake of plasticized poly(vinyl chloride) solid-contact calcium-selective electrodes, Electroanalysis, 23 (2011) 2156-2163.

[24] F. Sundfors, L. Hofler, R.E. Gyurcsanyi, T. Lindfors, Influence of poly(3-octylthiophene) on the water transport through methacrylic-acrylic based polymer membrane, Electroanalysis, 23 (2011) 1769-1772.

[25] N. He, T. Lindfors, Determination of water uptake of polymeric ion-selective membranes with the coulometric Karl Fischer and FTIR-attenuated total reflection techniques, Anal. Chem., 85 (2013) 1006-1012.

[26] Z.A. Boeva, T. Lindfors, Few-layer graphene and polyaniline composite as ion-to-electron transducer in silicone rubber solid-contact ion-selective electrodes, Sens. Actuators, B, 224 (2016) 624-631.

[27] Y.M. Mi, E. Bakker, Determination of complex formation constants of lipophilic neutral ionophores in solvent polymeric membranes with segmented sandwich membranes, Anal. Chem., 71 (1999) 5279-5287.

[28] M.P. Seah, W.A. Dench, Quantitative electron spectroscopy of surfaces: A standard data base for electron inelastic mean free paths in solids, Surf. Interface Anal., 1 (1979) 2-11.

[29] Z. Li, X.Z. Li, M. Rothmaier, D.J. Harrison, Comparison of numerical modeling of water uptake in poly(vinyl chloride)-based ion-selective membranes with experiment, Anal. Chem., 68 (1996) 1726-1734.

[30] A. Lewenstam, J. Bobacka, A. Ivaska, Mechanism of ionic and redox sensitivity of p-type conducting polymers: Part 1. Theory, J. Electroanal. Chem., 368 (1994) 23-31.

[31] R.E. Gyurcsanyi, N. Rangisetty, S. Clifton, B.D. Pendley, E. Lindner, Microfabricated ISEs: critical comparison of inherently conducting polymer and hydrogel based inner contacts, Talanta, 63 (2004) 89-99.

[32] G. Greczynski, T. Kugler, M. Keil, W. Osikowicz, M. Fahlman, W.R. Salaneck, Photo-electron spectroscopy of thin films of PEDOT-PSS conjugated polymer blend: a mini-review and some new results, Electron Spectrosc. Relat. Phenom., 121 (2001) 1-17.

[33] J.H. Hwang, F. Amy, A. Kahn, Spectroscopic study on sputtered PEDOT(PSS): Role of surface PSS layer, Org. Electron., 7 (2006) 387-396.

[34] M. Guzinski, J.M. Jarvis, F. Perez, B.D. Pendley, E. Lindner, R. De Marco, G.A. Crespo, R.G. Acres, R. Walker, J. Bishop, PEDOT(PSS) as solid contact for ion-selective electrodes: the influence of the PEDOT(PSS) film thickness on the equilibration times, Anal. Chem., 89 (2017) 3508-3516.

[35] J.M. Jarvis, M. Guzinski, F. Perez, B.D. Pendley, E. Lindner, Differences in electrochemically deposited PEDOT(PSS) films on Au and Pt substrate electrodes: a quartz crystal microbalance study, Electroanalysis, 29 (2017).

[36] M. Baumgärtner, C. Raub, The electrodeposition of platinum and platinum alloys, Platinum Met. Rev., 32 (1988) 188-197.

[37] G. Sauerbrey, Verwendung von schwingquarzen zur wägung dünner schichten und zur mikrowägung, Z. Physik, 155 (1959) 206-222.

[38] K. Chumbimuni-Torres, N. Rubinova, A. Radu, L. Kubota, E. Bakker, Solid contact potentiometric sensors for trace level measurements, Anal. Chem., 78 (2006) 1318-1322.

[39] D. Yuan, A. Anthis, M. Afshar, N. Pankratova, M. Cuartero, G. Crespo, E. Bakker, All-solid-state potentiometric sensors with a multi-walled carbon nanotube inner transducing layer for anion detection in environmental samples, Anal. Chem., 87 (2015) 8640-8645.

[40] M. Guzinski, J.M. Jarvis, P. D'Orazio, A. Izadyar, B.D. Pendley, E. Lindner, Solid contact pH sensor without CO_2 interference with a superhydrophobic PEDOT-C_{14} as solid contact: the ultimate "water layer" test, Anal. Chem., 89 (2017) 8468-8475.

[41] M. Fibbioli, W.E. Morf, M. Badertscher, N.F. de Rooij, E. Pretsch, Potential drifts of solid-contacted ion-selective electrodes due to zero-current ion fluxes through the sensor membrane, Electroanalysis, 12 (2000) 1286-1292.

[42] J. Bobacka, M. Grzeszczuk, A. Ivaska, Electrochemical study of poly(3-octylthiophene) film electrodes I. Electrolyte effects on the voltammetric characteristics of the polymer. Three states of the polymer film, Synth. Met., 44 (1991) 9-19.

[43] T. Chen, X. Wu, R. Rieke, Regiocontrolled synthesis of poly(3-alkylthiophenes) mediated by Rieke zinc: their characterization and solid-state properties, J. Am. Chem. Soc., 117 (1994) 233-244.

[44] T. Lindfors, Light sensitivity and potential stability of electrically conducting polymers commonly used in solid contact ion-selective electrodes, J. Solid State Electrochem., 13 (2009) 77-89.

[45] J. Sutter, E. Pretsch, Response behavior of poly(vinyl chloride)- and polyurethane-based Ca^{2+}-selective membrane electrodes with polypyrrole- and poly(3-octylthiophene)-mediated internal solid contact, Electroanalysis, 18 (2005) 19-25.

[46] J. Sutter, A. Radu, S. Peper, E. Bakker, E. Pretsch, Solid-contact polymeric membrane electrodes with detection limits in the subnanomolar range, Anal. Chim. Acta, 523 (2004) 53-59.

[47] M. Ates, T. Karazehir, F. Arican, N. Eren, Comparison of electrolyte effects for poly(3,4-ethylenedioxythiophene) and poly(3-octylthiophene) by electrochemical impedance spectroscopy and polymerization parameters with morphological analyses on coated films, J. Coat. Technol. Res., 10 (2013) 317-330.

[48] G. Khripoun, E. Volkova, A. Liseenkov, K. Mikhelson, Nitrate-selective solid-contact electrodes with poly(3-octylthiophene) and poly(aniline) as ion-to-electron transducers buffered with electron-ion-exchanging resin, Electroanalysis, 18 (2006) 1322-1328.

[49] R. Paciorek, P. van der Wal, N. de Rooij, M. Maj-Zurawska, Optimization of the composition of interfaces in miniature planar chloride electrodes, Electroanalysis, 15 (2003) 1314-1318.

[50] A. Michalska, M. Wojciechowski, E. Bulska, K. Maksymiuk, Experimental study on stability of different solid contact arrangements of ion-selective electrodes, Talanta, 82 (2010) 151-157.

[51] P. Sjoberg-Eerola, J. Nylund, J. Bobacka, A. Ivaska, Soluble semiconducting poly(3-octylthiophene) as a solid-contact material in all-solid-state chloride sensors, Sens. Actuators, B, 134 (2008) 878-886.

[52] M. Vasquez, J. Bobacka, A. Ivaska, Potentiometric sensors for Ag^+ based on poly(3-octylthiophene) (POT), J. Solid State Electrochem., 9 (2005) 865-873.

[53] J. Bobacka, A. Ivaska, A. Lewenstam, Plasticizer-free all-solid-state potassium-selective electrode based on poly(3-octylthiophene) and valinomycin, Anal. Chim. Acta, 385 (1999) 195-202.

[54] Z. Mousavi, A. Teter, A. Lewenstam, M. Maj-Zurawska, A. Ivaska, J. Bobacka, Comparison of multi-walled carbon nanotubes and poly(3-octylthiophene) as ion-to-electron transducers in all-solid-state potassium ion-selective electrodes, Electroanalysis, 23 (2011) 1352-1358.

[55] J. Sutter, E. Lindner, R.E. Gyurcsányi, E. Pretsch, A polypyrrole-based solid-contact Pb^{2+}-selective PVC-membrane electrode with a nanomolar detection limit, Anal. Bioanal. Chem., 380 (2004) 7-14.

[56] X. Zou, J. Cheong, B. Taitt, P. Bühlmann, Solid contact ion-selective electrodes with a well-controlled Co(II)/Co(III) redox buffer layer, Anal. Chem., 85 (2013) 9350-9355.

[57] X. Zou, X. Zhen, J. Cheong, P. Bühlmann, Calibration-free ionophore-based ion-selective electrodes with a Co(II)/Co(III) redox couple-based solid contact, Anal. Chem., 86 (2014) 8687-8692.

[58] U. Vanamo, J. Bobacka, Instrument-free control of the standard potential of potentiometric solid-contact ion-selective electrodes by short-circuiting with a conventional reference electrode, Anal. Chem., 86 (2014) 10540-10545.

[59] M. Begoña, R. Pou-Amérigo, R. Viruela, E. Ortí, A theoretical study of neutral and reduced tetracyano-p-quinodimethane (TCNQ), J. Mol. Struct.: THEOCHEM, 709 (2004) 97-102.

[60] T.H. Le, A. Nafady, X. Qu, A.M. Bond, L.L. Martin, Redox and acid–base chemistry of 7,7,8,8-tetracyanoquinodimethane, 7,7,8, 8-tetracyanoquinodimethane

radical anion, 7,7,8,8- tetracyanoquinodimethane dianion, and dihydro-7,7,8,8-tetracyanoquinodimethane in acetonitrile, Anal. Chem., 84 (2012) 2343-2350.

[61] N. He, S. Papp, T. Lindfors, L. Höfler, R.-M. Latonen, R.E. Gyurcsányi, Pre-polarized hydrophobic conducting polymer solid-contact ion-selective electrodes with improved potential reproducibility, Anal. Chem., 89 (2017) 2598-2605.

[62] E. Grygolowicz-Pawlak, K. Plachecka, Z. Brzozka, E. Malinowska, Further studies on the role of redox-active monolayer as intermediate phase of solid-state sensors, Sens. Actuators, B, 123 (2007) 480-487.

[63] S. Anastasova-Ivanova, U. Mattinen, A. Radu, J. Bobacka, A. Lewenstam, J. Migdalski, M. Danielewski, D. Diamond, Development of miniature all-solid-state potentiometric sensing system, Sens. Actuators, B, 146 (2010) 199-205.

[64] F. Sundfors, R. Bereczki, J. Bobacka, K. Toth, A. Ivaska, R.E. Gyurcsanyi, Microcavity based solid-contact ion-selective microelectrodes, Electroanalysis, 18 (2006) 1372-1378.

[65] B. Sankaran, J.R. Reynolds, High-contrast electrochromic polymers from alkyl-derivatized poly(3,4-ethylenedioxythiophenes), Macromolecules, 30 (1997) 2582-2588.

[66] R. Ishimatsu, A. Izadyar, B. Kabagambe, Y. Kim, J. Kim, S. Amemiya, Electrochemical mechanism of ion-ionophore recognition at plasticized polymer membrane/water interfaces, J. Am. Chem. Soc., 133 (2011) 16300-16308.

[67] A. Izadyar, Y. Kim, M.M. Ward, S. Amemiya, Double-polymer-modified pencil lead for stripping voltammetry of perchlorate in drinking water, J. Chem. Educ., 89 (2012) 1323-1326.

[68] B. Kabagambe, A. Izadyar, S. Amemiya, Stripping voltammetry of nanomolar potassium and ammonium ions using a valinomycin-doped double-polymer electrode, Anal. Chem., 84 (2012) 7979-7986.

[69] D.W. Breiby, E.J. Samuelsen, L. Groenendaal, B. Struth, Smectic structures in electrochemically prepared poly(3,4-ethylenedioxythiophene) films, J. Polym. Sci., Part B: Polym. Phys., 41 (2003) 945-952.

[70] M. Wolfs, T. Darmanin, F. Guittard, Versatile superhydrophobic surfaces from a bioinspired approach, Macromolecules, 44 (2011) 9286-9294.

[71] N. He, L. Hofler, R.-M. Latonen, T. Lindfors, Influence of hydrophobization of the polyazulene ion-to-electron transducer on the potential stability of calcium-selective solid-contact electrodes, Sens. Actuators, B, 207 (2015) 918-925.

[72] J.M. Jarvis, M. Guzinski, B.D. Pendley, E. Lindner, Poly(3-octylthiophene) as solid contact for ion-selective electrodes: contradictions and possibilities, J. Solid State Electrochem., 20 (2016) 3033-3041.

[73] B. Kabagambe, M.B. Garada, R. Ishimatsu, S. Amemiya, Subnanomolar detection limit of stripping voltammetric Ca^{2+}-selective electrode: effects of analyte charge and sample contamination, Anal. Chem., 86 (2014) 7939-7946.

[74] H.S. Yim, G.S. Cha, M.E. Meyerhoff, Differential ion-selective membrane electrode-based potentiometric gas-sensing cells with enhanced gas sensitivity, Anal. Chim. Acta, 237 (1990) 115-125.

[75] M.E. Meyerhoff, New in vitro analytical approaches for clinical-chemistry measurements in critical care, Clin. Chem., 36 (1990) 1567-1572.

[76] E. Lindner, R.P. Buck, Calibration of a planar differential CO_2 probe, Fresenius J. Anal. Chem., 364 (1999) 22-27.

[77] D. Perrin, Buffers for pH and metal ion control, Springer Netherlands 2012.

[78] J. Veder, K. Patel, M. Sohail, S. Jiang, M. James, R. De Marco, An electrochemical impedance spectroscopy/neutron reflectometry study of water uptake in the poly(3,4-ethylenedioxythiophene):poly(styrene sulfonate)/polymethyl methacrylate-polydecyl methacrylate copolymer solid-contact ion-selective electrode, Electroanalysis, 24 (2012) 140-145.

[79] Z. Mousavi, J. Bobacka, A. Lewenstam, A. Ivaska, Poly(3,4-ethylenedioxythiophene) (PEDOT) doped with carbon nanotubes as ion-to-electron transducer in polymer membrane-based potassium ion-selective electrodes, J. Electroanal. Chem., 633 (2009) 246-252.

[80] C.-Z. Lai, M.A. Fierke, A. Stein, P. Buhlmann, Ion-selective electrodes with three-dimensionally ordered macroporous carbon as solid contact, Anal. Chem., 79 (2007) 4621-4626.

[81] A. Lewenstam, Routines and challenges in clinical application of electrochemical ion-sensors, Electroanalysis, 26 (2014) 1171-1181.

[82] R.P. Buck, S. Rondinini, A.K. Covington, F.G.K. Baucke, C.M.A. Brett, M.F. Camoes, M.J.T. Milton, T. Mussini, R. Naumann, K.W. Pratt, P. Spitzer, G.S. Wilson, Measurement of pH. Definition, standards, and procedures Pure Appl. Chem., 74 (2002) 2169-2200.

[83] J. Bobacka, A. Ivaska, M. Grzeszczuk, Electrochemical study of poly(3-octylthiophene) film electrodes II. Reversible redox/conductivity state switching. Impedence study, Synth. Met., 44 (1991) 21-34.

APPENDIX A

CALCULATION OF INELASTIC MEAN FREE PATH OF PHOTOELECTRONS IN SR-XPS

The inelastic mean free paths (IMFPs) of organic soft matter is given by:

$$IMFP_i = 49\left(\frac{1}{(E_k)^2}\right) + 0.11\sqrt{E_k} \quad \text{(A.1)}$$

where E_k is kinetic energy of the photoelectrons in eV from the core level atomic orbital. Since the binding energies of the PEDOT and PSS^- S 2p components of the SR-XPS spectra differ only by a few eV, we have utilized the mid-point binding energy of 166 eV in calculations of the IMFPs in the SR-XPS photon energy dependent depth profiling experiments (see Table A.1).

Table A.1. IMFPs as a function of photon energy calculated using Equation 4 together with an average S 2p binding energy of 166 eV for the PEDOT and PSS^- components at approximately 164 and 168 eV, respectively.

Photon energy / eV	220	320	570	970	1487
Kinetic energy / eV	54	154	404	804	1321
IMFP / nm	0.83	1.37	2.21	3.12	4.00

APPENDIX B

DETERMINATION OF TCNQ STANDARD POTENTIAL IN POT FILM

Redox activity of the POT and POT+TCNQ-coated Au electrodes (discussed in Chapter 6) were studied by cyclic voltammetry. As seen in Figure B.1, with the incorporation of TCNQ into the POT film, an oxidation and a reduction peak emerged (at 0.3 V and -0.2 V, respectively) in the original CV of the POT film.

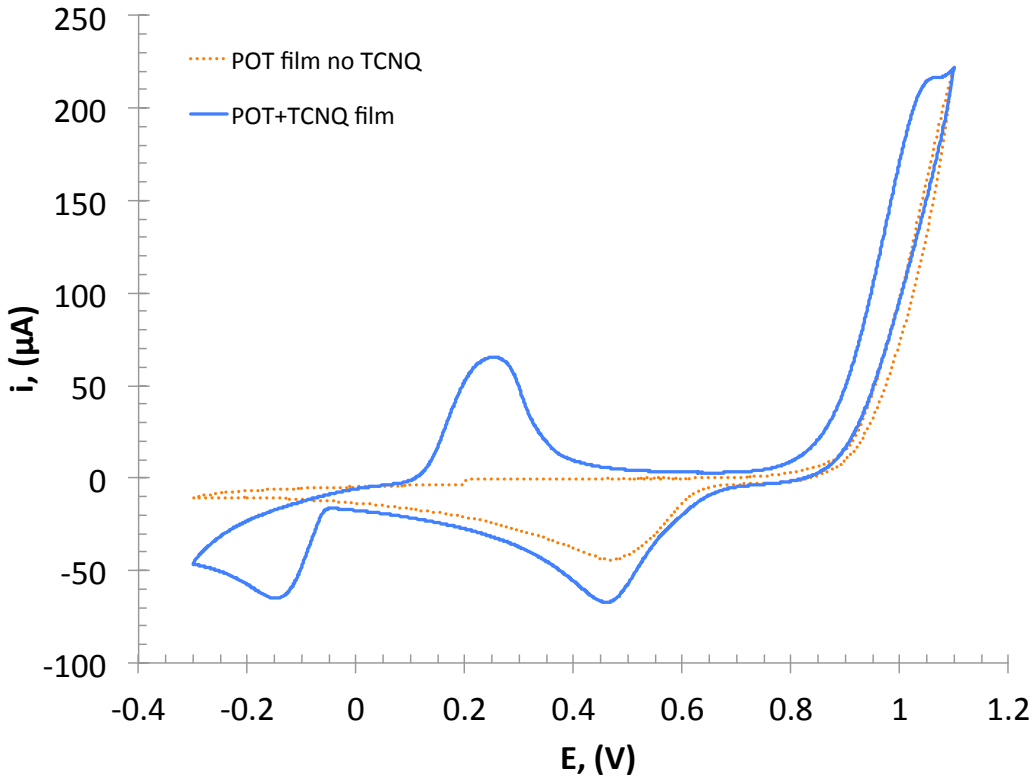

Figure B.1. Cyclic voltammogram of a POT-coated (dotted orange curve) and POT+TNCQ-coated (solid blue curve) Au electrode in 0.1 M KCl.

Next, to characterize the one-electron reaction of the TCNQ/ $TCNQ^{\bullet -}$ redox couple within the POT film, the voltage range was scanned from -0.3 V to +0.3 V.

Although we are interested in the TCNQ/TCNQ$^{\bullet-}$ redox activity, we recognize that the full reduction of TCNQ involves a 2-electron transfer. To understand the redox activity of TCNQ/TCNQ$^{\bullet-}$ in the POT film, we compared to the TCNQ/TCNQ$^{\bullet-}$/TCNQ^{2-} activity in solution. Figure B.2 shows the cyclic voltammograms collected for both the one-electron reaction of TCNQ/TCNQ$^{\bullet-}$ inside of the POT film in 0.1 M KCl and the two-electron transfer in an acetonitrile solution of 1 mM TCNQ and 0.1 M $LiClO_4$ using a bare Pt electrode.

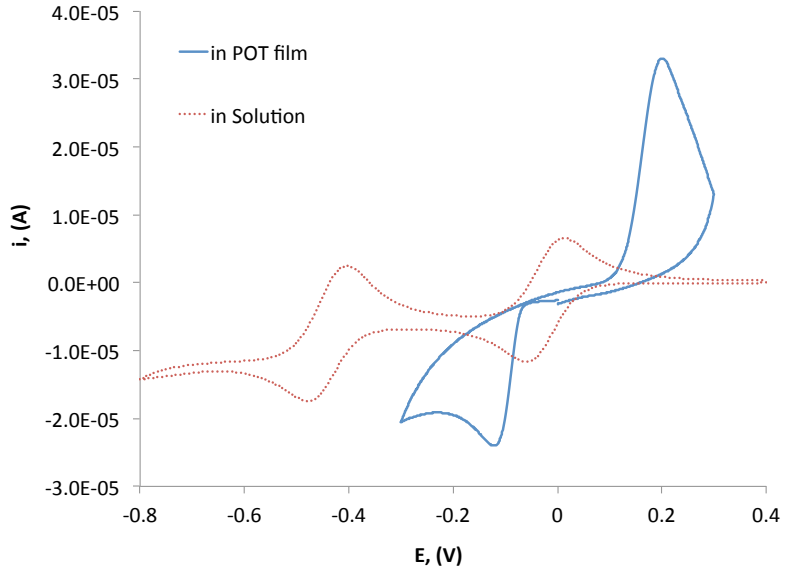

Figure B.2. Cyclic voltammograms recorded with a POT+TCNQ-coated Au electrode in 0.1 M KCl (solid blue curve) and a Pt electrode in an acetonitrile solution containing 1 mM TCNQ and 0.1 M $LiClO_4$ (dotted red curve).

When comparing the redox activity of TCNQ in the POT film and in acetonitrile solution in Figure B.2, there is a noticeable potential shift in the first one-electron reaction (TCNQ/TCNQ$^{\bullet-}$). TCNQ within the POT film shows oxidation and reduction

peaks at +0.19 V and -0.11 V, respectively, giving a large peak separation of 300 mV, which may be related to the resistance of the neutral POT film [83]. TCNQ in solution, however, shows the first electron transfer at +0.012 V and -0.059 V, with a peak separation of only 71 mV. Due to the large peak separation of the redox couple within the POT film, determining the standard redox potential is not trivial.

In attempts to determine the standard redox potential of TCNQ in the POT film, the potential of the POT+TCNQ film, and therefore the TCNQ/ $TCNQ^{\bullet-}$ ratio, was manipulated by an applied potential. Based on the scan of TCNQ in the POT film in Figure B.2, the standard potential of TCNQ was estimated as $\frac{E_{ox}+E_{red}}{2} = 0.0375$ V. Since at the standard potential, the TCNQ/$TCNQ^{\bullet-}$ ratio is 1 and our goal is to set the TCNQ/$TCNQ^{\bullet-}$ ratio close to 1, we applied the estimated standard potential to the POT+TCNQ-coated electrode for 5 minutes. Immediately following the potential application, CVs were obtained with a i) positive polarity scan and ii) negative polarity scan with the starting potential being 0.0375 V, the previously applied potential value. The positive polarity scan will show an oxidation peak, representing the oxidation of $TCNQ^{\bullet-}$ to TCNQ. The peak height corresponds to the concentration of species that were in the reduced form ($TCNQ^{\bullet-}$) following the polarization potential application. Conversely, the negative polarity scan will show the reduction peak of TCNQ to $TCNQ^{\bullet-}$ and the peak height will be indicative of the concentration of TCNQ that was in its oxidized state following polarization and prior to the scan. The CV scans obtained after applying the estimated standard potential (0.0375 V) to the POT+TCNQ-coated Au electrodes are shown in Figure B.3.

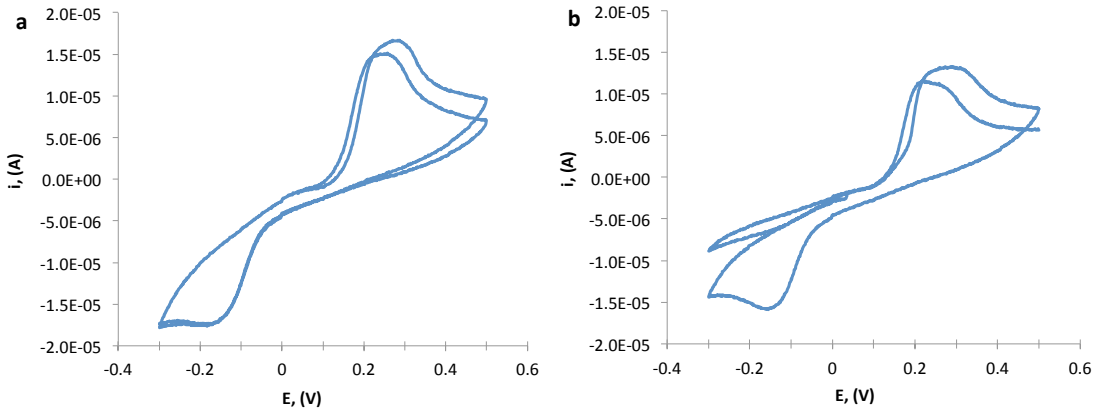

Figure B.3. Cyclic voltammograms obtained after polarizing the POT+TCNQ-coated Au electrode to 0.0375 V for 5 minutes in 0.1 M KCl solution with an initial a) positive polarity and b) negative polarity scan.

The oxidation peak in the positive polarity scan (Figure B.3a) does not grow appreciably (i.e. does not double, as expected with a ~1:1 ratio of TCNQ/$TCNQ^{\bullet -}$) from the first to the second scan, which indicates that the concentration of the redox species being oxidized is very similar in both scans and thus it is not likely that only half of the species were reduced at the fixed potential of 0.0375 V but rather that most all of the species were in the reduced form at this potential. This interpretation matches that from the negative polarity scan shown in the CV on the right. The first scan does not show any reduction peak but the second scan does. This suggests that TCNQ was already in reduced form and thus when the potential was scanned to the reduction potential, no species were available to be reduced. During the latter part of the first scan in Figure B.3b, the potential was scanned positively to 0.3 V. TCNQ is oxidized at ~0.2 V so the species was then altered to its oxidized form. When scanned negatively for the second time (second scan), a reduction peak is seen because there are oxidized species readily

available to be reduced. Overall, this suggests that the held potential of 0.0375 V reduces most of the TCNQ species to $TCNQ^{\bullet -}$. Thus, to obtain a true 1:1 ratio of oxidized and reduced TCNQ in the POT film, the applied potential must be more positive.

The same process was repeated for POT+TCNQ-coated Au electrodes polarized to 0.112 V (112 mV) for 5 minutes. After the application of 0.112 V to the POT+TCNQ-coated electrodes, the positive and negative polarity scans showed that roughly half of the species was in its oxidized form (Figure B.4a). This can be seen by the growth of the oxidation peak at 0.2 V from 1.8 µA to 3.8 µA. Similarly, the reduction peak seen in Figure B.4b around -0.1 V increases from -1.9 µA to -3.1 µA from the first to the second cycle.

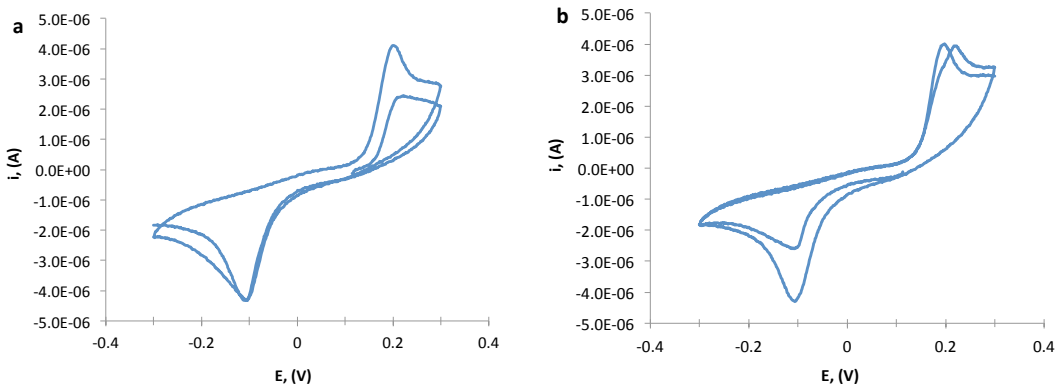

Figure B.4. Cyclic voltammograms obtained after polarizing the POT+TCNQ-coated Au electrode to 0.112 V for 5 minutes in 0.1 M KCl solution with an initial a) positive polarity and b) negative polarity scan.

It is apparent that even after the second scan, all current peak heights (i_p) are much less in Figure B.4 when compared to Figure B.3. This suggests that the concentration of TCNQ has decreased during the experiment. This could be the

consequence of TCNQ leaching from the POT film into aqueous solution during the experiment. To confirm this assumption, the concentration of TCNQ in a freshly prepared POT+TCNQ-coated Au electrode film was monitored over 24 hours with cycles being completed every 10 minutes for the first hour and every hour afterwards for the following 3 hours and finally at 24 hours (Figure B.5). The results indicate that the peak height and thus the concentration of TCNQ does decrease over time. To prevent leaching during polarization, the POT+TCNQ ISEs were polarized only after ISM deposition.

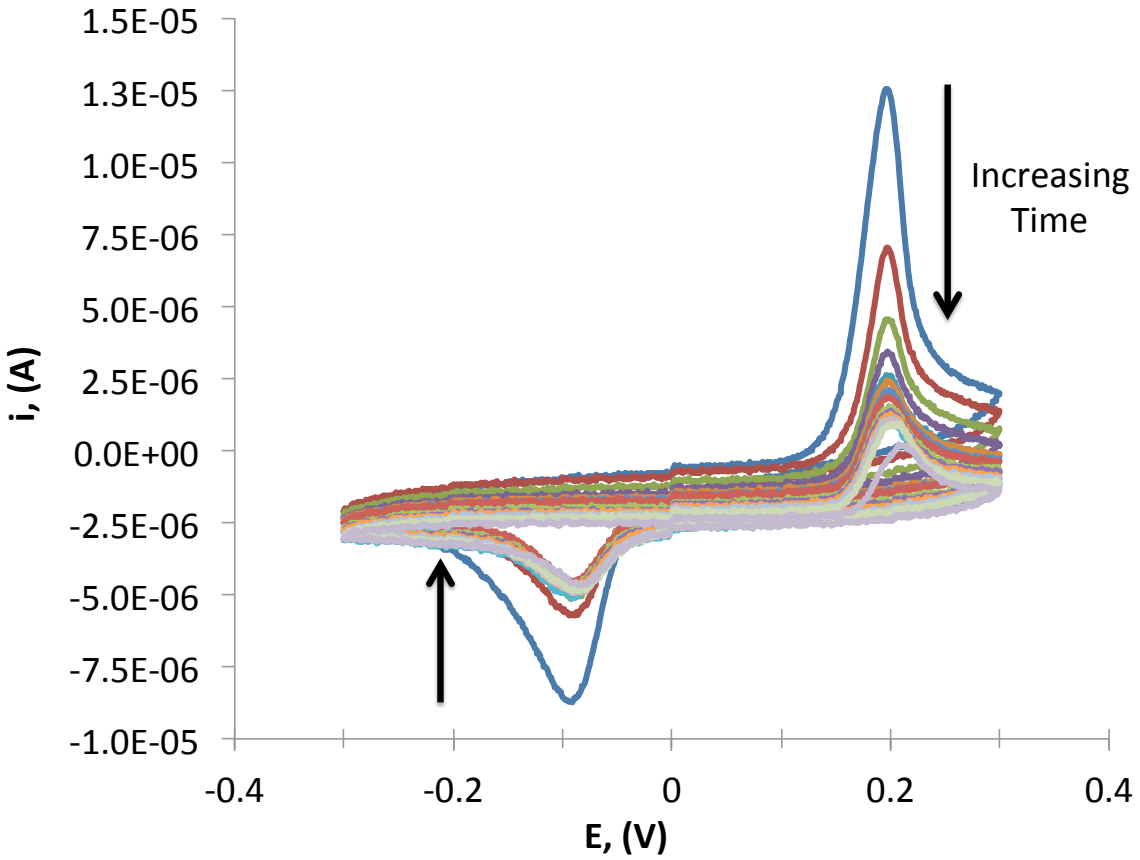

Figure B.5. Cyclic voltammograms recorded with a POT+TCNQ-coated Au electrode in 0.1 M KCl solution during 24 hours of continuous solution contact to prove that TCNQ is gradually leaching from the POT film. The arrows indicate increasing soaking times from t=0 through 24 hours.

APPENDIX C

OPTIMIZATION OF POLARIZATION PARAMETERS

To optimize the polarization time, fully fabricated K^+ ISEs with a TCNQ-loaded POT film as solid contact (see Chapter 6) were polarized in 0.1 M KCl to 125 mV versus an Ag|AgCl|KCl(3M)||LiOAc(1M) reference electrode for 1h, 2h, 4h, or 8 h. Immediately following polarization, the open circuit potential (OCP) was measured versus the same reference electrode in the same 0.1 M KCl solution. The potential stabilities and standard potential reproducibilities of the polarized ISEs are displayed in Table C.1.

Table C.1. Potential stability and sensor-to-sensor standard potential reproducibility of POT+TCNQ-based K^+ ISEs measured immediately after polarization times of 1h, 2h, 4h, and 8h at 125 mV versus a reference electrode. The values are displayed as the mean ± S.D.

Polarization Time	n	Drift, (mV/h)	E^0 at 24 h (mV)
1h	8	0.6 ±0.5	214±25
2h	6	1.0±0.4	263±28
4h	4	0.4±0.3	220±35
8h	4	0.4±0.3	244±19

A one-way ANOVA was used to determine that there was no statistically significant difference between the drift values of ISEs polarized at 1h, 2h, 4h, or 8h ($p=0.3$). Using a Bartlett's Test for equal variance, it was determined that there was no statistically significant difference between the variances of ISEs polarized for 1h, 2h, 4h,

or 8h ($p=0.8$). Based on the statistical analysis of the results presented in Table C.1, the optimal polarization time was determined to be 1h since longer polarization times provided no additional benefit.

It can be seen that when comparing the potential drift of POT+TCNQ-based ISEs with 1h polarization in Table C.1, the drift is larger than the values reported in Chapter 6 (-0.1 ± 0.1 mV/h). The difference is likely due to the storage conditions after polarization. The values presented in Table C.1 correspond to ISEs measured immediately following polarization. In contrast, the ISEs in Chapter 6 were polarized for one hour, dried with argon, and stored in a desiccator overnight. The OCP was not measured until the following day. It is apparent that this storage (wet vs. dry) has an effect on the potential stability of the SC ISE. Based on these results, the final recommendation to obtain the smallest potential drift for POT+TCNQ-based ISEs is to polarize the ISE to 125 mV for 1 hour and store dry (i.e. dry with argon and store in a desiccator overnight).